地理科学学院博士研究生刘心怡 2024 年博士学位论文答辩及科研成果公示

2024 年 5 月地理科学学院理学学院理学专业博士研究生刘心怡完成博士学位论文答辩，答辩委员会一致同意该研究生通过博士学位论文答辩，建议授予理学博士学位。该生在读期间发表论文及佐证材料公示如下：

学号	姓名	专业	论文名称	刊物名称	发表情况	期刊类别	发表时间	是否达到学术论文发表要求
20206019006	刘心怡	地理学	Exploring sandy vegetation sensitivities to water storage in China's arid and semi-arid regions	Ecological Indicators	见刊	SCI	2022	是
			Exploring grassland ecosystem water use efficiency using indicators of precipitation and soil moisture across the Mongolian Plateau	Ecological Indicators	见刊	SCI	2022	是
			Spatio-temporal patterns and control mechanism of the ecosystem carbon use efficiency across the Mongolian Plateau	Science of the Total Environment	见刊	SCI	2023	是

主持项目名称	项目类型	主要参与人	是否主持	项目起止期限	项目简介
基于叶绿素荧光遥感的内蒙古植被生长对气候变化的响应(CXJJB21020)	内蒙古师范大学研究生科研创新基金项目	炎丽、元志辉、叶志刚、卜灵心、塔娜	是	2021.11.9 - 2022.11.9	本项目结合多源卫星遥感观测数据，利用多种技术手段，探讨内蒙古植被生长与水资源供应之间的关系，以分析植被生长对气候变化的具体响应。

张瑞祥

2024 年 5 月 3 日

Exploring sandy vegetation sensitivities to water storage in China's arid and semi-arid regions

Xinyi Liu [a], Quan Lai [a,b,*], Shan Yin [a,b], Yuhai Bao [a,b], Song Qing [a,b], Li Mei [a], Lingxin Bu [a]

[a] *College of Geographical Science, Inner Mongolia Normal University, Hohhot 010022, China*
[b] *Inner Mongolia Key Laboratory of Remote Sensing and Geographic Information Systems, Inner Mongolia, Normal University, Hohhot 010022, China*

ARTICLE INFO

ABSTRACT

Hulunbuir, Otindag, Horqin and Mu Us are the four greater sandy lands in China. They are typical ecologically fragile areas with limited ability to resist interference and are susceptible to changes in the external environment. With climate change in recent decades, these areas have experienced severe land desertification and decreased groundwater levels. The ecological environment is at risk of further deterioration, and continuous vegetation restoration and management should be adapted to the local climate and maintain the water balance with natural precipitation. This paper combines multi-source satellite observations to explore the relationship between vegetation growth and water supply. The results show four main points. (1) Although the vegetation growth in Otindag and Horqin had degraded before 2010, it improved after 2010. The vegetation growth and soil moisture (SM) of the four sandy lands both generally increased from 2003 to 2016. The SM of the Horqin increased significantly (84% anomaly $> 1.4 \times 10^{-2}$ cm^3/cm^3). Other than the Hulunbuir, the other sandy lands show a downward trend in terrestrial water storage (TWS), especially the Mu Us declined the most (97% anomaly < -40 mm). (2) Solar-induced chlorophyll fluorescence (SIF) has specific advantages in characterizing the sandy vegetation productivity and water composition changes compared to vegetation index (EVI) or gross primary productivity (GPP). (3) The regional pattern of the vegetation-moisture relationship is mainly affected by the precipitation-driven SM and depends on the types of underlying vegetation functions. (4) Both SM and TWS have approximately one-month persistence in the four sandy lands, especially the Mu Us has the longest persistence (0.94 months and 1.1 months). The persistence in the early period is generally longer than that in the late period, implying that the resilience of water components after the mutation year is stronger than before it. This study provides a scientific basis for the management and restoration of sandy lands. It is recommended that different vegetation restoration and protection strategies should be developed for specific sandy land moisture conditions in arid/semi-arid regions of northern China, which includes the improvement of water use efficiency to maintain soil moisture and the reduction of excessive groundwater uses.

1. Introduction

The four greater sandy lands account for 2% of China's land area. As the second ecological security barrier in northern China, the sandy lands have extremely important ecological functions (Dai et al., 2019; Liao et al., 2019). In recent decades, China has implemented a series of ecological restoration projects in these regions, including the "Three-North Shelterbelt Project", the "Grain for Green Project", and the "Beijing and Tianjin sandstorm source controlling project" (Cheng et al., 2021; Wang et al., 2020d; Wu et al., 2021; Zhang et al., 2012). Although the regional ecological environment has been partially improved

through these efforts, the desertification expansion of the four sandy lands is still significant. This continuing expansion mainly resulted from climate change and intensified human destruction (Cheng et al., 2021; Fan et al., 2020; Jia et al., 2020; Liao et al., 2019). A steady increase in global warming is due to the effects of greenhouse gas emissions. Combined with irregular changes in rainfall patterns, water evaporates from the ground more rapidly and causes drought stress. Drought stress can severely alter physiological, biochemical and molecular processes, thereby affecting plant growth and development (Fahad et al., 2021a; b; c; d; Fahad et al., 2019; Hasanuzzaman et al., 2019). In addition, the increase in population and frequent unreasonable human activities

includes overgrazing, over-cultivation, over-use of water resources and extensive mining (Wu et al., 2021; Yu et al., 2017; Zhou et al., 2015). Land reclamation is still going on in some areas, and these areas will need continuous monitoring and management (Ma et al., 2019; Xie et al., 2020; Zhang et al., 2012). Understanding the internal mechanisms between vegetation growth and water composition is significant for the effective protection and restoration of vegetation on the four sandy lands and the region's sustainable development. This study may also provide recommendations for reducing the cost of policy measures and improving responses to the complexities of climate change more effectively.

With the development of remote sensing technology, many studies have shown that EVI is a good indicator of canopy structural variations and can effectively characterize vegetation growth (Cao et al., 2015; Hashimoto et al., 2012; Kong et al., 2019; Sims et al., 2006). However, compared with the traditional vegetation index (EVI and Normalized Difference Vegetation Index, NDVI), SIF is known to be an effective probe for vegetation photosynthesis, and SIF can estimate vegetation productivity more directly and effectively (Bacour et al., 2019; Cheng et al., 2013; Damm et al., 2015; Duveiller and Cescatti 2016; Hu and Mo 2020). SIF has unique technical advantages for monitoring the vegetation growth conditions and the surrounding environment changes (Frankenberg et al., 2014; Guanter et al., 2014; Joiner et al., 2013; Köhler et al., 2018). For example, many academics have compared SIF retrievals on different vegetation types, including cropland, forest, grassland, and wetland (Bandopadhyay et al., 2019; Jeong et al., 2017; Mohammed et al., 2019; Qiu et al., 2019; Wang et al., 2020d). However, it is unclear whether SIF data can characterize the sandy vegetation growth and water composition changes. To effectively evaluate SIF, this paper uses EVI, GPP and SIF to jointly represent the vegetation growth conditions of the four sandy lands.

Land desertification is inseparable from changes in water composition (Ji et al., 2006; Kairis et al., 2013; Li et al., 2014; Yang et al., 2017). Therefore, the scale and method of vegetation restoration on sandy land should be adapted to the local climate and maintain the water balance with natural precipitation (Fan et al., 2020; Wang et al., 2016; Yu et al., 2018). Unreasonable use of water resources has always been a serious problem faced by the four sandy lands, and it has attracted the attention of the government and scholars. Previous studies have mainly investigated soil moisture and the groundwater's temporal and spatial changes in different sandy areas (Cheng et al., 2021; Wang et al., 2020d; Wu et al., 2021; Yang et al., 2018). Other scholars have analyzed vegetation water use efficiency for specific pioneer species, including *Pinus sylvestris, Mongolian pine,* and *Caragana microphylla* (Jia et al., 2020; Song et al., 2015; Su et al., 2014; Yu et al., 2017). In addition, most academics are analyzing the impacts of multiple factors on surface soil water content and groundwater, including temperature, precipitation, vegetation restoration projects, and mining (Cheng et al., 2020; Cheng et al., 2018; Musa et al., 2019; Yu et al., 2018). However, there are few studies on the response and sensitivity analysis of the vegetation and water component factors in the four sandy lands. Su et al. (2022) proposed a groundwater weighted fusion model by combining Gravity Recovery and Climate Experiment (GRACE) TWS data and hydrological models, which can effectively improve the accuracy of groundwater storage estimates in the arid region of Northwest China. Therefore, this study uses the SM and the TWS data to explore the relationship between vegetation growth and water compositions of the four sandy lands as follows: (1) comparing the changing trend of vegetation growth conditions and water compositions in the different sandy lands during 2003–2016; (2) analyzing the vegetation-moisture correlations in different sandy lands in the periods of 2003–2009 and 2010–2016; (3) exploring the vegetation sensitivity to water storage components; and (4) examining the resilience of water components in different sandy lands. The results of this study can provide a scientific basis for the management and restoration of sandy lands.

2. Material and methods

2.1. Study areas

China's four greater sandy lands of Hulunbuir, Horqin, Otindag and Mu Us are located in the ecotone between the agricultural and animal husbandry regions of the north (Fig. 1). Hulunbuir Sandy Land is situated in the hinterland of Hulunbuir Grassland. The study area is 47,600 km^2, including three sand belts with an area of about 7,400 km^2. It has a typical sandy forest and grassland landscape, and the central and western parts have typical grassland vegetation (Fig. 2(a)). The Otindag Sandy Land is located in the south-central part of the Xilin Gol Grassland. The total area is 42,900 km^2, including typical grassland, desert grassland and sandy vegetation (Fig. 2(b)). The Horqin covers an area of 63,300 km^2, making it the largest sandy land in China. It is located on the alluvial plain of the mainstream and tributaries of the lower reaches of the Xiliao River. This area is a transitional area between forest grassland and arid steppe (Fig. 2(c)). The Mu Us Sandy Land is located in the southeast of the Ordos Plateau with an area of 38,600 km^2. The southwestern edge of this sandy land belongs to the desert steppe belt and the typical grassland belt transitioning to the desert, while the middle and east are mostly distributed with sandy vegetation (Fig. 2(d)). All four are areas with severe land desertification and sensitivity to global climate changes, and they represent significant vegetation ecological construction areas in China (Zhou et al., 2015).

2.2. Data

2.2.1. The land cover type data

The distribution boundaries of the four sandy lands are delineated based on the 1:100,000 desert (sand) distribution dataset for China (http://westdc.westgis.ac.cn) and the land cover dataset from the Resource and Environmental Science Data Center of the Chinese Academy of Sciences (http://www.resdc.cn/DataList.aspx) (Fig. 1). We chose the 1 km dataset of Inner Mongolia in 2010 to define the vegetation distribution in the study areas (Fig. 2).

2.2.2. Three vegetation growth metrics

In this study, three sets of satellite-derived records represent the vegetation growth conditions, including MOD13A3 monthly 1 km EVI records, MOD17A2H eight-day 500 m GPP records, and GOSIF eight-day 0.05°×0.05° SIF records. MODIS data products were downloaded from https://lpdaacsvc.cr.usgs.gov/appeears/task/area. GOSIF records were obtained from https://globalecology.unh.edu//data.html.

2.2.3. The water storage components data

Two series of satellite records are used in this study to represent the water storage components, including surface SM records and overall TWS records. The fifth-generation ECMWF reanalysis (ERA-5) SM product provides a monthly 0.25°×0.25° resolution with precise accuracy and performance (See Annex 1 for the comparison of soil moisture products) (Cheng et al., 2019; Zhang et al., 2018b). We chose the 0–7 cm volumetric soil moisture to characterize the surface water content changes in the study areas (Zhang et al., 2018b), which is available at https://cds.climate.copernicus.eu/cdsapp/dataset/.

The monthly TWS data were obtained from the Gravity Recovery and Climate Experiment (GRACE) satellite (https://grace.jpl.nasa.gov/data/get-data/jpl_global_mascons/), with a spatial resolution of 0.5°×0.5° from January 2003 to December 2016. We used the original TWS data to be downscaled into a monthly 0.25°×0.25° TWS time series to match the spatial resolution of SM data.

2.2.4. The meteorological data

Considering the influence of snow cover in winter, by analyzing the monthly 2 m air temperature data of ERA-5 (Wang et al., 2019), the growing season from April to October is used to evaluate the dynamic
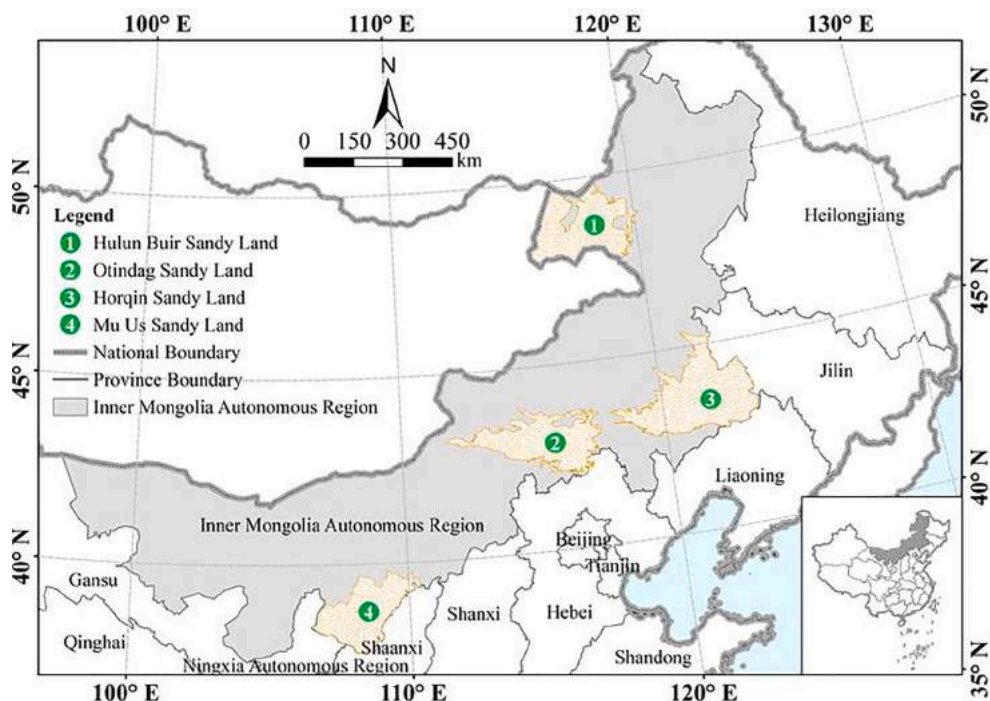
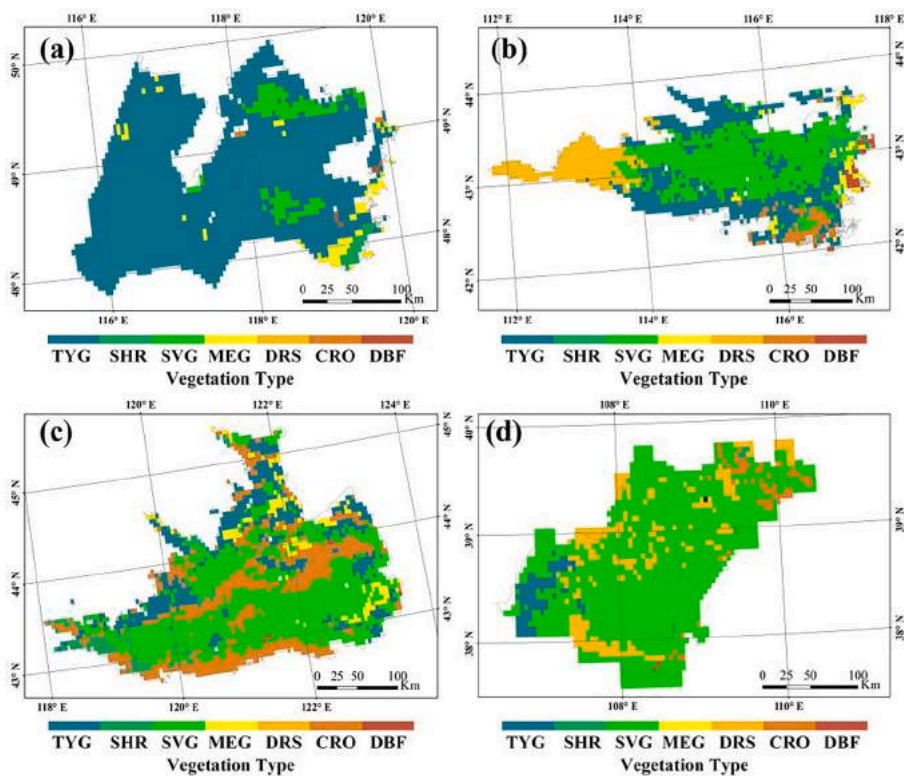**Fig. 1.** Locations of the four greater sandy lands.

Fig. 2. Vegetation type distributions of (a) Hulunbuir Sandy Land, (b) Otindag Sandy Land, (c) Horqin Sandy Land, and (d) Mu Us Sandy Land. (TYG: Typical Grassland; SHR: Shrub; SVG: Sandy Vegetation; MEG: Meadow Grassland; DRS: Desert Steppe; CRO: Cropland; DBF: Broadleaf Forest).

changes in vegetation growth (Bao et al., 2014). The precipitation data came from the China Meteorological Data Service Center (http://data.cma.cn/) and the Resource and Environmental Science Data Center of the Chinese Academy of Sciences (http://www.resdc.cn/). They were processed by the Inverse Distance Weighted (IDW) spatial interpolation method to obtain a monthly continuous precipitation dataset. For consistency, all datasets finally generated the long-term series (2003–2016) with a monthly 0.25°to match the GRACE data. GRACE processing provides a regional average time series, but largely retains the inter-annual variation of the finer time series.

2.3. Methods

The local climate changes heterogeneously because of differences in spatial and temporal ranges between vegetation growth conditions and water storage components. Therefore, the same amount of water shortage in one location or period may have a significantly different impact on biomes than in another (Ji and Peters 2003; Vicente-Serrano et al., 2013). Therefore, we utilize the z-score standardization method for the time series. This process normalizes the time series according to its monthly standard deviation, which can effectively remove the influence of climatic factors from the original time series. We use z-score standard time series data to calculate the average anomalies for all datasets. The mean anomalies could obviously reflect the vegetation growth trends during 2003–2016.

In order to explore the vegetation-moisture relationship, we also use the corresponding de-trended z-score time series data to compute the partial correlations between EVI and TWS ($R_{EVI-TWS}$), EVI and SM (R_{EVI-SM}), GPP and TWS ($R_{GPP-TWS}$), GPP and SM (R_{GPP-SM}), SIF and TWS ($R_{SIF-TWS}$), and SIF and SM (R_{SIF-SM}) during the growing season before and after 2010. The de-trending process does not affect the spatial pattern of the correlation between vegetation and moisture, but it can usually estimate the correlation more conservatively. Furthermore, it considers that the vegetation growth in semi-arid areas is greatly restricted by water. Therefore, we utilize air temperature as a control variable to compute the partial correlation coefficient to remove its influence on vegetation growth (Sun et al., 2019; Zheng et al., 2006; Zhou et al., 2015). Similarly, the partial correlation coefficient between SM and TWS (R_{SM-TWS}) is also considered.

To clearly illustrate the inter-annual and long-term change trends of vegetation growth conditions and water storage components, the 13-month temporal smoothing approach can effectively remove the higher temporal frequency seasonal variations (A et al., 2016). For each 13-month window, the sum of the constant term and the linear trend is assigned to the center point (the seventh month) to generate a smooth time series.

To further evaluate the memory effect and persistence in water compositions, we utilize the corresponding de-trended z-score time series data to calculate the autocorrelation function between SM and TWS. When the correlation coefficient of the autocorrelation function is reduced to 1/e, the characteristic time point is defined as the lag time of each time series data.

3. Results

3.1. Abnormal climate change year

The Mann-Kendall mutation test analysis using the precipitation data of Inner Mongolia from 2003 to 2016 shows that there is a mutation point in the study areas from late 2010 to 2011 (Fig. 3). Inner Mongolia entered the wet period from the dry period. Therefore, we determined 2010 as the abnormal climate year and analyzed the vegetation-moisture relationship in the study areas in the early period (2003–2009) and the later period (2010–2016).

3.2. Spatial variation of vegetation growth conditions and the water storage components in the four sandy lands

Figure 4 shows the average anomalies of EVI, GPP, SIF, SM and TWS for the four sandy lands from 2003 to 2016, which indicate a solid spatial agreement among EVI, SIF and GPP observations in the four sandy lands. SIF and GPP results illustrate higher similarity and better spatial continuity, while the EVI result shows notable speckling. From the perspective of various vegetation indicators, the improved area of the four sandy lands is much larger than the degraded area, which shows that the vegetation of the four sandy lands has been improving overall from 2003 to 2016. In addition, the SM and TWS results show
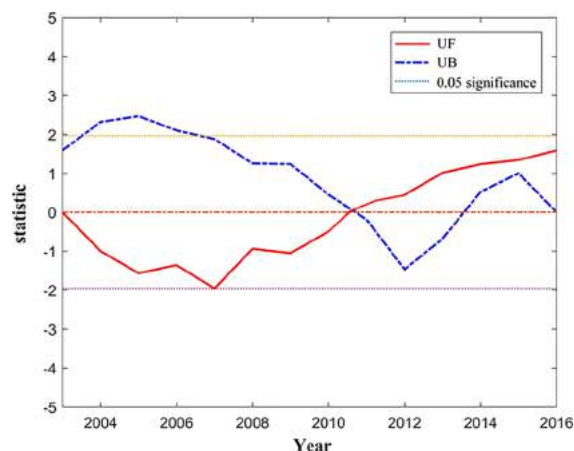

Fig. 3. Mann-Kendall mutation test using precipitation data from 2003 to 2016 in Inner Mongolia.

continuous spatial distribution changes and strong regularity. Specifically, the result reveals that the vegetation growth in most of the Hulunbuir sandy land has continued to improve (Fig. 4(b)-(c)). Both surface moisture and groundwater in the Hulunbuir Sandy Land have an increasing trend from 2003 to 2016 (Fig. 4(d)-(e)). While the reduced areas are mainly distributed northwest of the sandy land, the spatial variation of SM increases in a step-wise distribution from northwest to southeast (Fig. 4(d)). In terms of the Otindag Sandy Land, the EVI result shows a downward trend in most areas (Fig. 4(f)), while the GPP and SIF results show the opposite trend (Fig. 4(g)-(h)). Surface SM in most areas has shown a continuous increase (Fig. 4(i)), and SM increases in the east are higher than in the west. In comparison, the overall TWS has continued to decrease (Fig. 4(j)). Vegetation growth in Horqin Sandy Land presents a trend of continuous improvement (Fig. 4(k)-(m)). The soil moisture in Horqin increased significantly (84% anomaly $> 1.4 \times 10^{-2}$ cm^3/cm^3) compared with the other three sandy lands, but TWS continued to decline in most regions (Fig. 4(n)-(o)). The Mu Us Sandy Land has the strongest spatial distribution regularity. The vegetation growth has shown a continuous improvement over the majority of the analyzed domain (Fig. 4(p)-(r)). The SM result shows a downward trend, while it shows the opposite trend in TWS (Fig. 4(s) and (t)). The amount of groundwater in the Mu Us Sandy Land has declined the most (97% anomaly < -40 mm).

3.3. Vegetation-moisture correlations of the four sandy lands

Figures 5 to 8 show the vegetation-moisture partial correlation coefficients calculated using growing season EVI, GPP, SIF, SM and TWS records of the four sandy lands during 2003–2009 and 2010–2016. All the vegetation metrics have similar significant correlation areas (P < 0.05) with moisture conditions from 2003 to 2016, although the significant correlation areas of SIF and GPP are obviously greater than that of EVI. There are also the same spatial patterns for R_{GPP-SM}, $R_{GPP-TWS}$, R_{SIF-SM} and $R_{SIF-TWS}$ as those using EVI, but with slightly larger magnitudes. These results indicate that the GPP and SIF observations are superior for characterizing vegetation growth. In addition, all vegetation growth indicators show strong correspondence with surface SM and a relatively weak correlation with TWS over the majority of the four sandy lands. Similarly, the vegetation growth of the four sandy lands illustrates different responses to the SM and TWS observables.

From the partial correlation analysis of Hulunbuir Sandy Land, it can be seen that the growth of vegetation is significantly positively correlated with surface SM. The areas with the highest correlation (R > 0.6) are located in the southeast of the sandy land before 2010 (Fig. 5(a), (e) and (i)) and in the northeast after 2010 (Fig. 5(f) and (j)). Vegetation growth in the eastern portion of the sandy land is significantly correlated
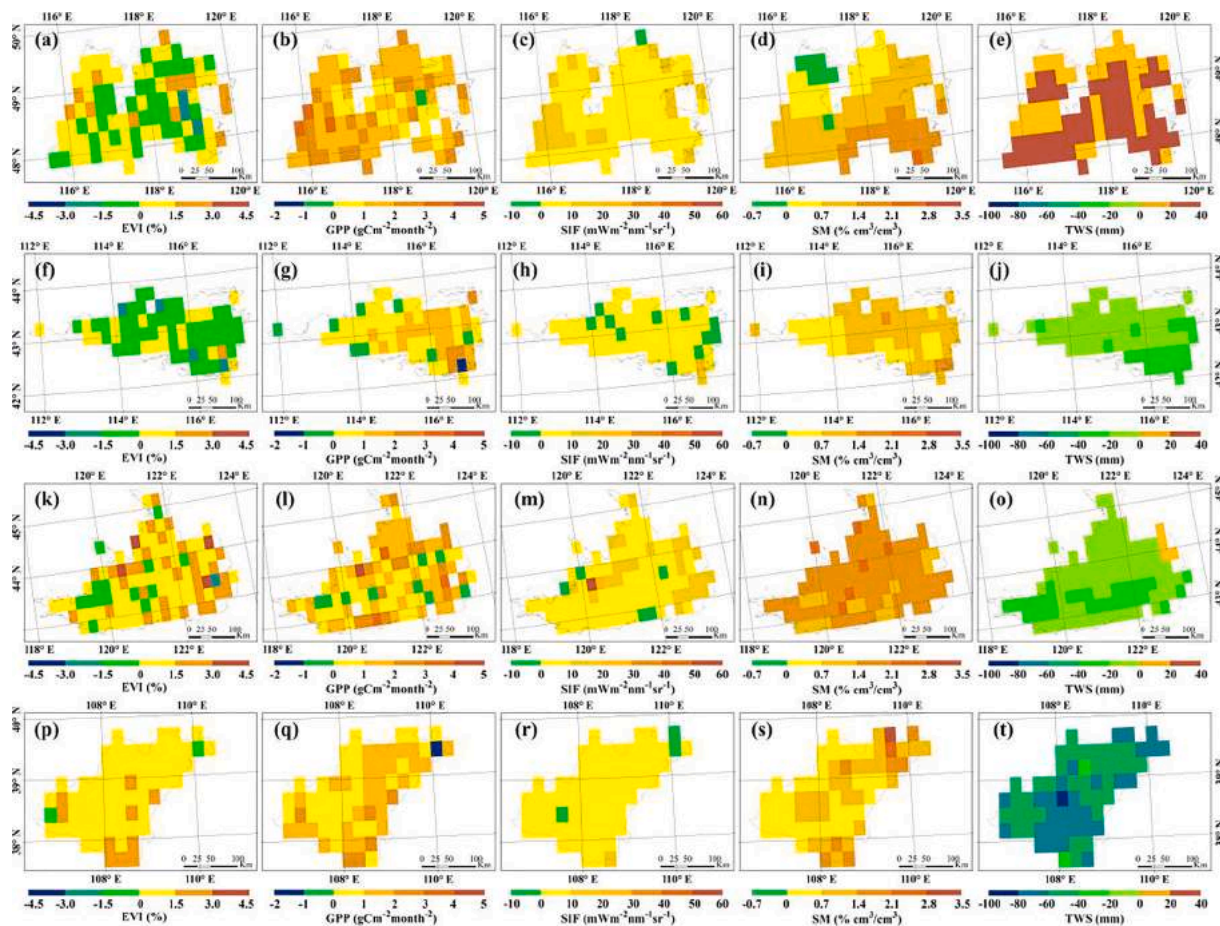
Fig. 4. The average anomalies of (a) (f) (k) (p) EVI in %, (b) (g) (l) (q) GPP in gCm^{-2}month^{-1};(c) (h) (m) (r) SIF in mWm^{-2}nm^{-1}sr^{-1};(d) (i) (n) (s) SM in % cm^3/cm^3, and (e) (j) (o) (t) TWS in mm of four sandy lands.

with overall TWS, and the correlation in the western part has improved in the later period (Fig. 5(g), (h), (k) and (l)).

From Fig. 6, we find that there is an obvious east–west difference in the vegetation-moisture relationship of Otindag Sandy Land. The vegetation growth shows a significant positive correlation with SM and an insignificant negative correlation with TWS in most of the analyzed domain. The correlation between vegetation growth and SM in the western sandy land is strongest at the initial stage (Fig. 6(a) and (i)), which is the same area where the correlation declined rapidly in the later period (Fig. 6(b), (f) and (j)). However, the vegetation-moisture relationship in the eastern region is relatively stable (Fig. 6(b), (f) and (j)), and the correlation with TWS has improved in the later period (Fig. 6(d), (h) and (l)).

For the Horqin Sandy Land, all vegetation indicators are significantly positively correlated with SM (Fig. 7). The correlation in the later stage is higher than that in the earlier stage, and it is notablystrongest in the southern cropland of the sandy land (Fig. 7(f) and (j)). The data show consistent responses to changes in SM and TWS prior to 2010. The spatial pattern of the correlation changes between vegetation growth and TWS is consistent with the northwest-southeast step-wise distribution of the precipitation variation, and the correlation in the southeast is higher than that in the northwest (Fig. 7(c), (g) and (k)). Through the 2003–2016 period, vegetation indicators are significantly positively correlated with TWS in most areas before 2010, while the correlation is sharply reduced or even becomes insignificant negative in the later stage (Fig. 7(d), (h) and (l)).

The Mu Us Sandy Land has a vegetation-moisture relationship similar to that of the Otindag Sandy Land. Over most of the analyzed domain, vegetation growth significantly correlates with SM, while the correlation with TWS is still insignificant (Fig. 8). The SIF result shows the strongest correspondence with surface moisture compared to EVI and GPP, including almost all the areas with the highest correlation (Fig. 8(i)). Although the correlation between the northwest and south-west of the sandy land has decreased, the correlation is still strong (R > 0.4) (Fig. 8(j)).

Indeed, the SM and TWS variations will affect vegetation growth, but vegetation sensitivities to SM and TWS are different, so it is useful to explore the relationship between SM and TWS. From the partial correlation analysis of the four sandy lands, it is obvious that SM and TWS have significant positive correlations in three of the sandy lands, but not for the Otindag Sandy Land. In the early stage, the entire Hulunbuir sandy land correlation increased from southwest to northeast, with the highest correlation in the northeast (Fig. 9(a)). In the later period, the correlation increased in the southwest and decreased in the southeast (Fig. 9(b)). Although there is an insignificant correlation between SM and TWS in Otindag Sandy Land overall, the correlation in the eastern region has improved in the later period (Fig. 9(d)). The Mu Us Sandy Land correlation also increases in the eastern part of the area after 2010 (Fig. 9(h)). Similarly, the correlations during the entire period are strongest in the southeast and either weaker or insignificant in the northwest (Fig. 9(e)-(f)), which is consistent with the annual precipitation gradient of the entire Horqin Sandy Land. These results indicate that the moisture conditions of almost all of the four sandy lands have improved in the later stage, and plants can directly obtain the shallow depth SM variations, which dominate the entire TWS variability.
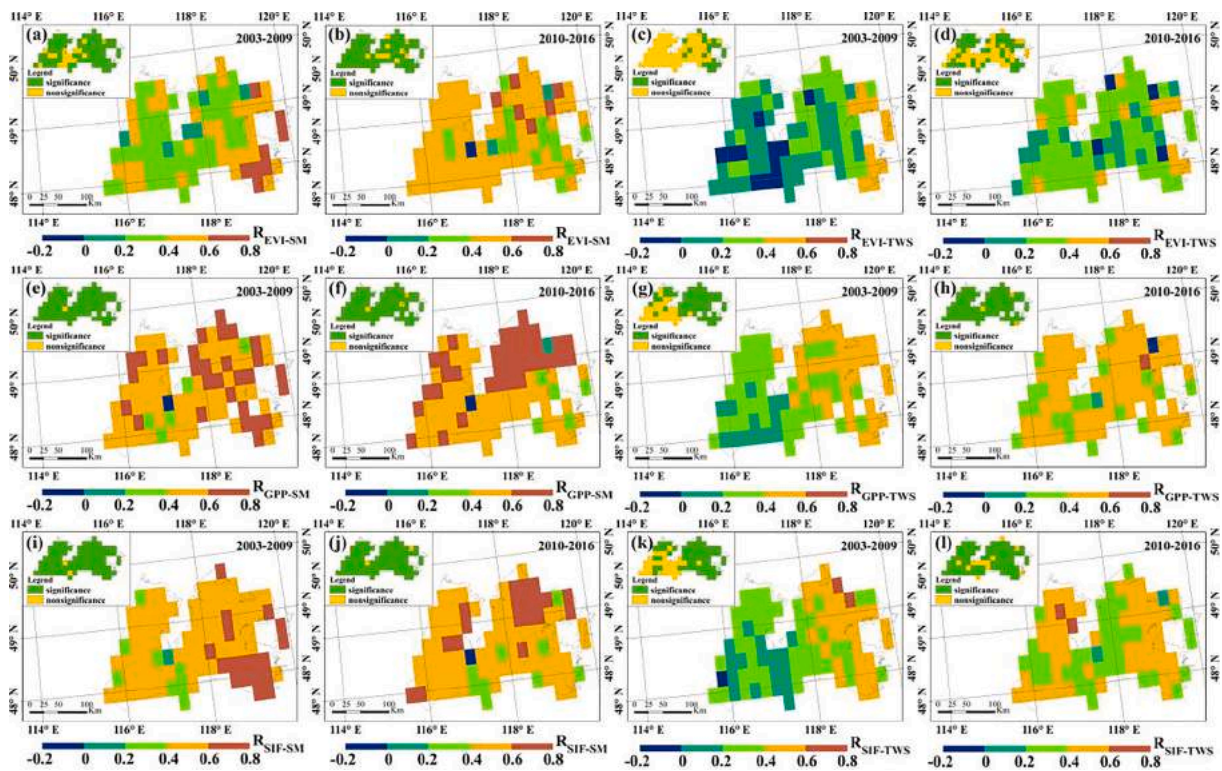
Fig. 5. Partial correlation coefficients for (a) (b) EVI and SM (R_{EVI-SM}), (c) (d) EVI and TWS ($R_{EVI-TWS}$), (e) (f) GPP and SM (R_{GPP-SM}), (g) (h) GPP and TWS ($R_{GPP-TWS}$), (i) (j) SIF and SM (R_{SIF-SM}), (k) (l) SIF and TWS ($R_{SIF-TWS}$) for growing seasons during 2003–2009 and 2010–2016 in the Hulunbuir Sandy Land.
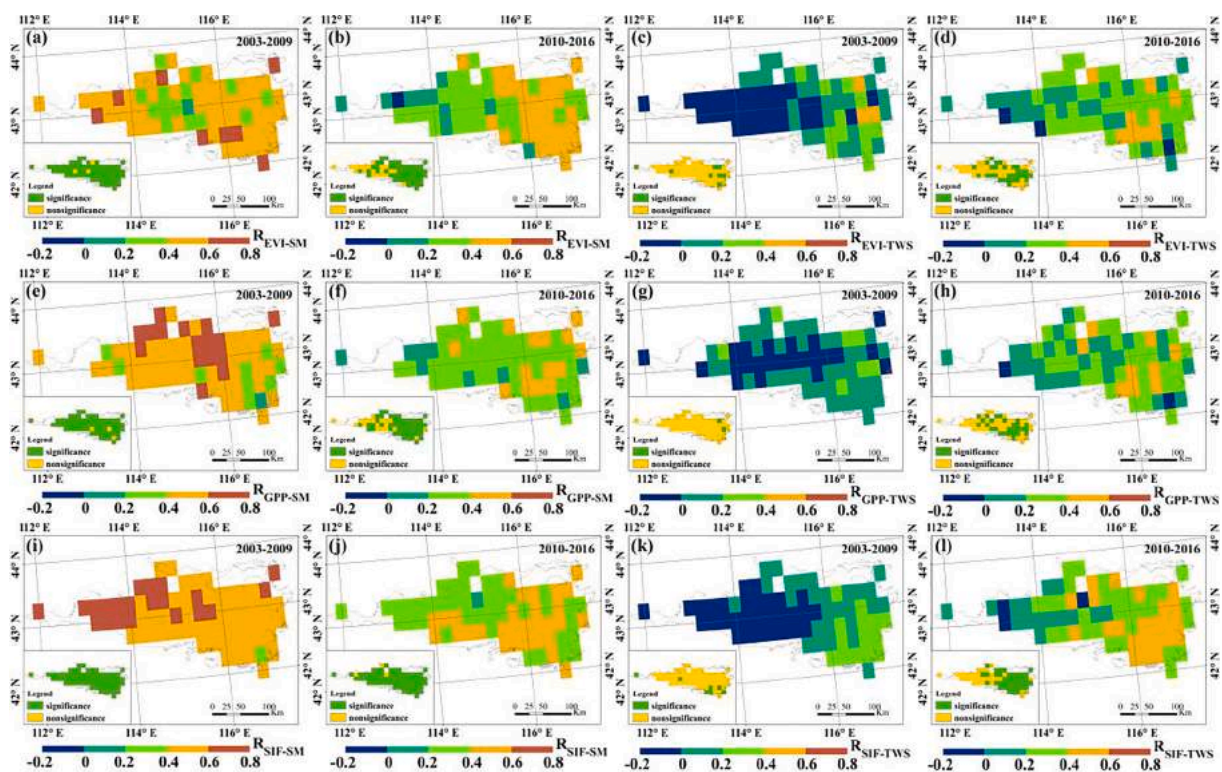

Fig. 6. Partial correlation coefficients for (a) (b) EVI and SM (R_{EVI-SM}), (c) (d) EVI and TWS ($R_{EVI-TWS}$), (e) (f) GPP and SM (R_{GPP-SM}), (g) (h) GPP and TWS ($R_{GPP-TWS}$), (i) (j) SIF and SM (R_{SIF-SM}), (k) (l) SIF and TWS ($R_{SIF-TWS}$) for growing seasons during 2003–2009 and 2010–2016 in the Otindag Sandy Land.

3.4. Vegetation-moisture dynamics during 2003–2016

The results mentioned above indicate that vegetation metrics show

greater sensitivity to SM than TWS. There is a decoupling between surface SM and overall TWS observables before 2010. To further analyze the vegetation-moisture variations in the four sandy lands, we generated
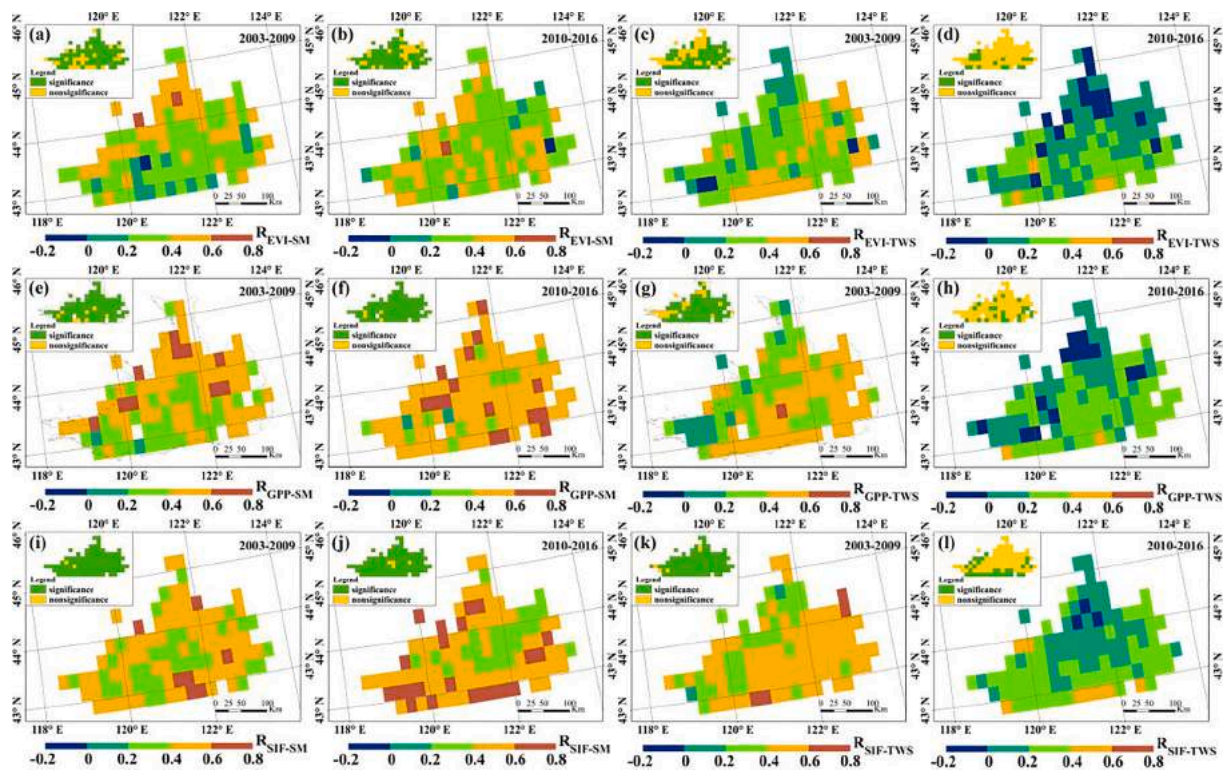
Fig. 7. Partial correlation coefficients for (a) (b) EVI and SM (R_{EVI-SM}), (c) (d) EVI and TWS ($R_{EVI-TWS}$), (e) (f) GPP and SM (R_{GPP-SM}), (g) (h) GPP and TWS ($R_{GPP-TWS}$), (i) (j) SIF and SM (R_{SIF-SM}), (k) (l) SIF and TWS ($R_{SIF-TWS}$) for growing seasons during 2003–2009 and 2010–2016 in the Horqin Sandy Land.
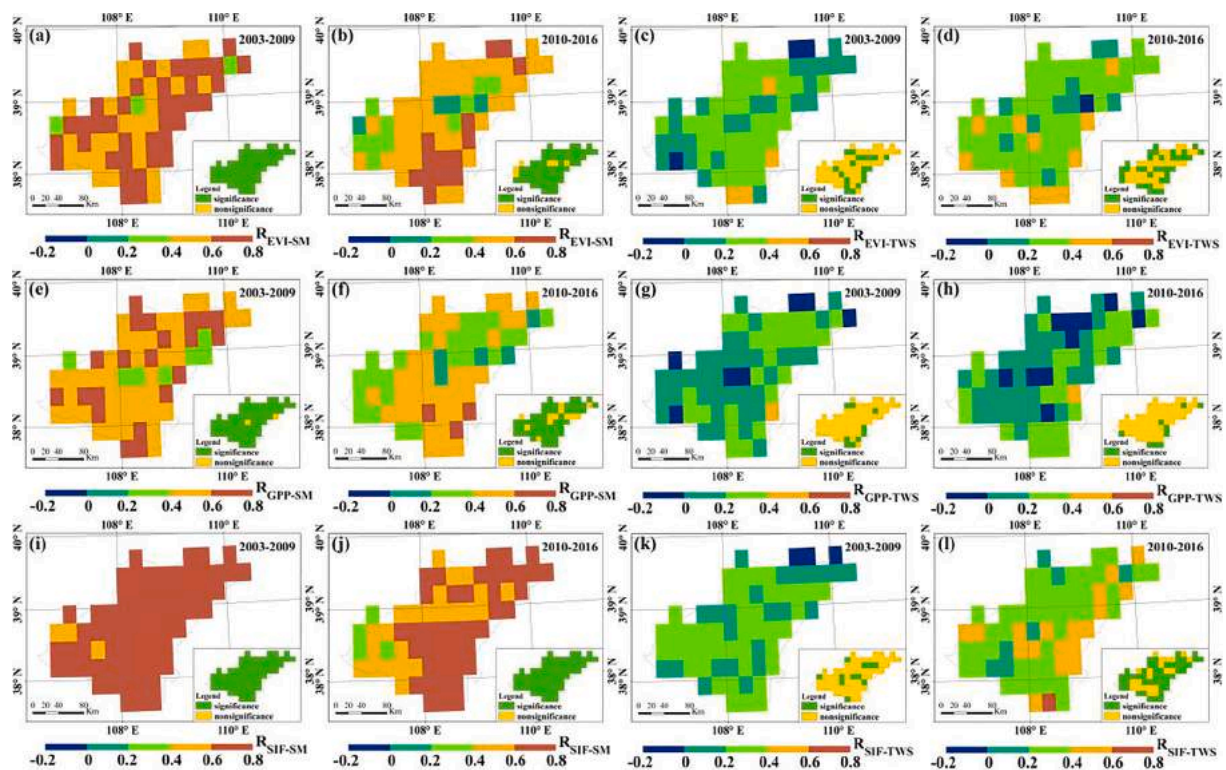

Fig. 8. Partial correlation coefficients for (a) (b) EVI and SM (R_{EVI-SM}), (c) (d) EVI and TWS ($R_{EVI-TWS}$), (e) (f) GPP and SM (R_{GPP-SM}), (g) (h) GPP and TWS ($R_{GPP-TWS}$), (i) (j) SIF and SM (R_{SIF-SM}), (k) (l) SIF and TWS ($R_{SIF-TWS}$), (m) (n) SM and TWS (R_{SM-TWS}) for growing seasons during 2003–2009 and 2010–2016 in the Mu Us Sandy Land.
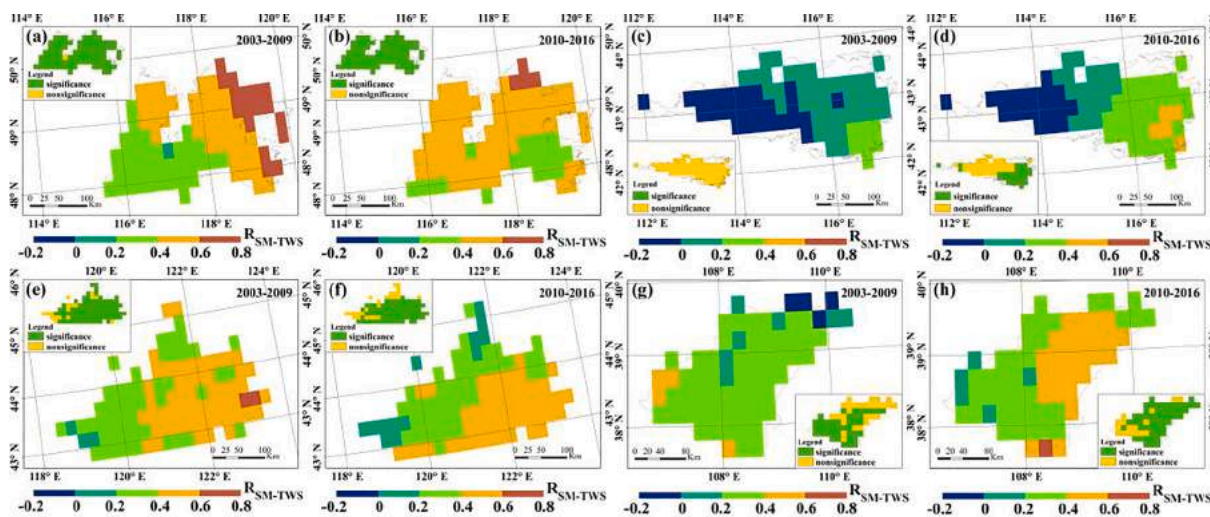
Fig. 9. Partial correlation coefficients for SM and TWS (R$_{SM-TWS}$) for growing seasons during 2003–2009 and 2010–2016 in (a) (b) the Hulunbuir, (c) (d) Otindag, (e) (f) Horqin, and (g) (h) Mu Us Sandy Land.

Fig. 10. Monthly anomalies in the dynamics of EVI (cyan), GPP (blue), SIF (red), SM (purple), TWS (indigo) and precipitation (green) of the (a) (b) Hunlun Buir Sandy Land, (c) (d) Otindag Sandy Land, (e) (f) Horqin Sandy Land, and (g) (h) Mu Us Sandy Land.

the time series of each observable monthly average in the study area (Fig. 10). The long-term dynamics of SIF, GPP and EVI are similar but more congruent 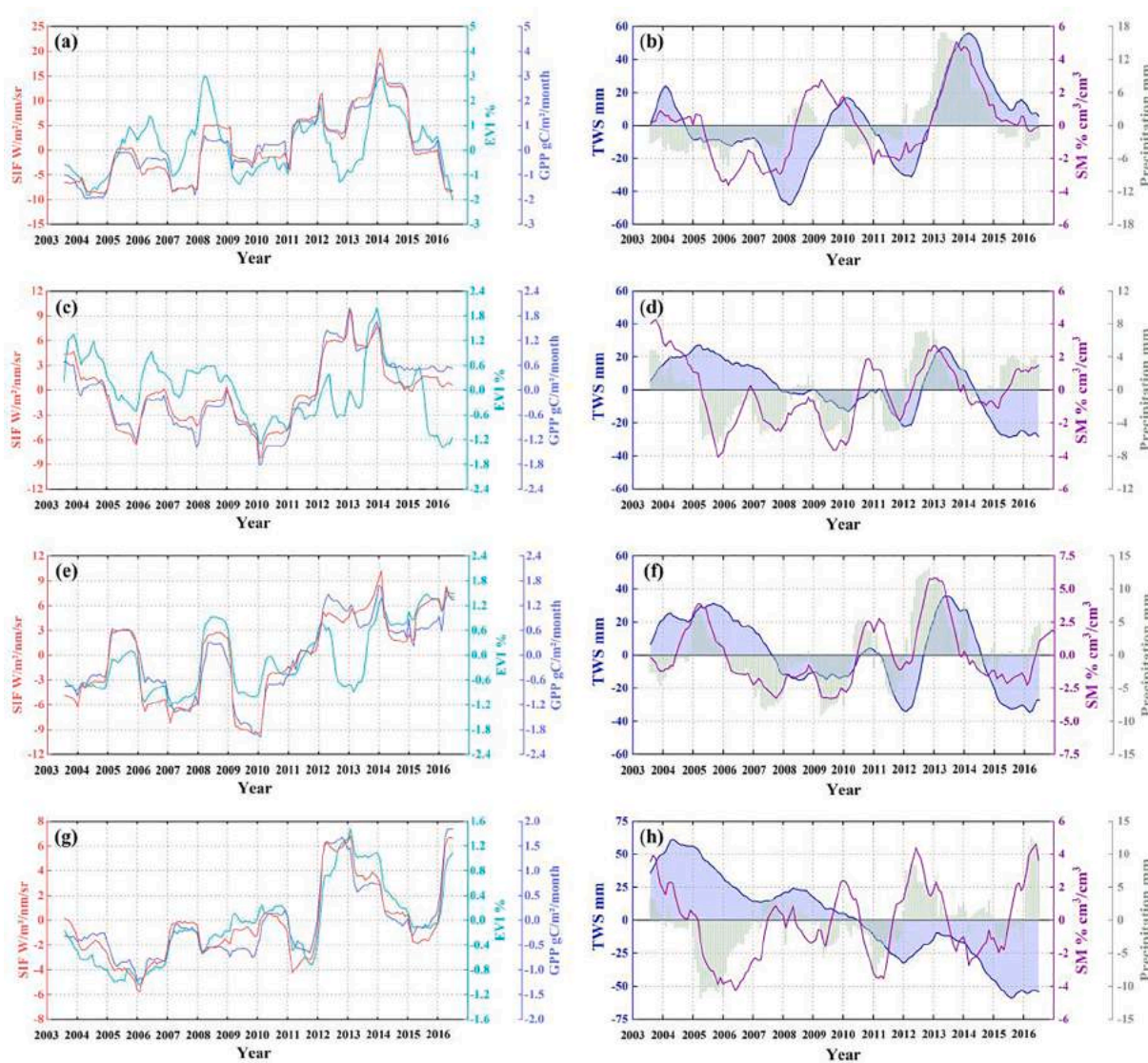changes are apparent between GPP and SIF. In comparison, the dynamics of water storage components present diversity. During 2003–2016, SM shows a similar sensitivity to precipitation, consistent with the dynamic wetting and drying of surface SM. On the contrary, TWS is less sensitive to precipitation during the early period. Compared with GPP, SIF shows higher sensitivity to precipitation gradients (or surface moisture changes) in some details. Therefore, SIF has certain advantages in characterizing the vegetation productivity of the four sandy lands. The four sandy areas also show some differences. Fig. 10(a) shows the continuous improvement of vegetation growth in the Hulunbuir sandy land. Vegetation growth changes have a certain degree of consistency with SM and TWS, but the sensitivity of vegetation indicators to SM is greater than TWS. Prior to 2010, vegetation growth increased aperiodically along with precipitation-driven changes in surface SM. While TWS shows a continuous downward trend from 2004 to 2008, the changes in TWS after 2010 have gradually become consistent with precipitation and SM (Fig. 10(b)). Fig. 10(c) shows that the vegetation growth of the Otindag Sandy Land has been degraded in the early stage and gradually improved in the later stage. The change of vegetation growth has a strong agreement with SM. However, TWS was basically in a continuous downward trend in the early stage and later it gradually improved and converged with precipitation and SM. After 2013, it shows a constant declining trend once again, indicating that TWS is irrelevant to vegetation growth. This result corresponds to the insignificant correlation between vegetation growth and TWS in the partial correlation analysis. Fig. 10(e) shows that the vegetation growth change in the Horqin Sandy Land is more complicated than those of the other three sandy lands. The vegetation fluctuated in the early stage and gradually recovered in the later stage. The change of vegetation growth is not synchronized with the water composition characteristics during 2003–2016. Although there is a certain correlation with SM, there is still an obvious lag time (Fig. 10(f)). Fig. 10(g) shows that vegetation growth in the Mu Us Sandy Land has continued to improve. The vegetation growth is consistent with SM changes, which is slightly lagging compared with SM changes. However, TWS shows a continuous downward trend both before and after 2010, so it is basically unrelated to vegetation growth.

3.5. Memory effect of SM and TWS

From the previous analysis, we found that water compositions (especially precipitation) are decisive for vegetation growth in most sandy lands and have lagging effects on vegetation growth. However, there is a contrasting response of vegetation to SM and TWS over the entire areas which were analyzed. To explore this further, we calculated the autocorrelation functions of SM and TWS during 2003–2009 and 2010–2016 (Fig. 11). Both SM and TWS have similar autocorrelation coefficients in the early and late stages of Hulunbuir Sandy Land. The time scale ratio of SM and TWS down to 0.368 (1/e) in the early stage is 0.72 and 0.78 months, and the later time scales are 0.62 and 0.58 months, respectively. In Otindag Sandy Land, these two satellite time series provide a qualitatively different autocorrelation profile, with a narrower main lobe for SM (0.62 months) and a larger main lobe for TWS (0.76 months) in the early period. In contrast, a wider estimation of the autocorrelation main lobe is obtained for SM (0.72 months) than for TWS (0.54 months) in the later period. Compared with other sandy lands, the situation of Horqin is that TWS generally displays lower persistence than SM through the entire period, leading to slightly lower e-folding times than SM (of 0.7 months vs. 0.84 months before 2010, and of 0.5 months vs. 0.64 months after 2010). The data in Fig. 11 show that SM and TWS obtain opposite autocorrelation curves in the Mu Us Sandy Land before and after 2010. In the early period, the two satellite time series show a similar time scale of 0.94 months. However, the autocorrelation series greatly differ from those obtained during the 2010–2016 period. The SM shows a time scale of 1.1 months, while the TWS shows stronger autocorrelation, especially at the 0.68-month time scale. Although the time scales have fluctuated before and after 2010, there is generally a one-month lag in the persistence or memory effect of both SM and TWS in the four sandy areas.

4. Discussion

4.1. Vegetation-moisture change trend of the four sandy lands

From the perspective of vegetation growth, the four sandy lands show generally increasing trends from 2003 to 2016, consistent with the overall changes in northern China's arid and semi-arid areas (Gang et al., 2019; Ma et al., 2019). Although the vegetation growth in the Otindag and Horqin Sandy Lands decrease before 2010 and increase after 2010, the areas where the vegetation growth improved were larger
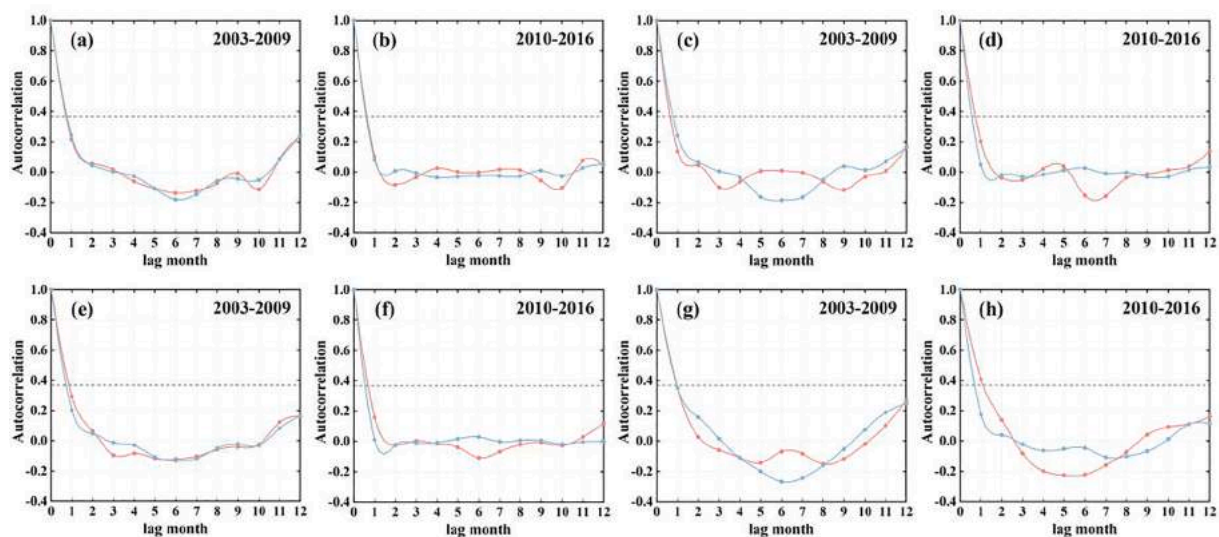

Fig. 11. Autocorrelation functions of TWS (blue) and SM (red) during 2003–2009 and 2010–2016 for the (a) (b) Hunlun Buir Sandy Land, (c) (d) Otindag Sandy Land, (e) (f) Horqin Sandy Land, and (g) (h) Mu Us Sandy Land.

than the degraded areas, showing gradual improvement trends in both cases. This implies that implementing the government's ecological restoration policy has significantly improved the local vegetation conditions, effectively preventing wind and sand fixation and reducing soil erosion (Wang et al., 2020d; Zhang et al., 2012; Zhang et al., 2016b). The ecological environment of the four sandy lands is being restored day by day, and the vegetation damaged in the early stage has largely recovered in the later stage and has especially improved significantly in the Mu Us Sandy Land. Compared with the other three sandy lands, the Mu Us Sandy Land has the smallest proportion of grassland and the largest proportion of sandy vegetation. The vegetation population level is lower, the ecosystem stability is poor, and the vegetation coverage changes greatly under human intervention (Cheng et al., 2012; Cheng et al., 2021; Xiu et al., 2018). In addition, SM also shows a continuous upward trend for the four sandy lands, especially the Horqin Sandy Land which increased significantly (84% anomaly $> 1.4 \times 10^{-2}$ cm^3/cm^3). This implies that soil moisture is largely affected by precipitation, which is specifically manifested in the driving force of rainfall (Wang et al., 2020d; Yang et al., 2017; Yang et al., 2018). Except for the Hulunbuir Sandy Land, which shows an upward trend in the TWS results, the other three sandy lands all present downward trends. The decrease of groundwater level is related to increased large-scale artificial vegetation, including cropland (Fan et al., 2020; Su et al., 2012; Zheng et al., 2012). In particular, the amount of groundwater in the Mu Us Sandy Land has declined the most (97% anomaly < -40 mm), indicating that unreasonable human activities result in the most severe waste of the groundwater resources in the Mu Us sandy land (Cheng et al., 2012; Cheng et al., 2018; Yu et al., 2017). Due to the poorest stability of the Mu Us sandy ecosystem and the profound impact of human activities, the restoration and monitoring of the Mu Us sandy land should be a major focus in the future.

Furthermore, three vegetation metrics all effectively reflect this changing trend of vegetation growth. However, the results show more congruent changes between GPP and SIF, consistent with the findings of previous studies that SIF and GPP have a linear relationship (Kim et al., 2021; Liu et al., 2021; Wagle et al., 2016; Zhang et al., 2016a; Zhang et al., 2016d). This implies that GPP and SIF observations are superior for characterizing vegetation growth. The linear relationship between SIF and GPP also varies among different vegetation types (Frankenberg et al., 2011; Guanter et al., 2012; Kim et al., 2021). Compared with GPP, SIF shows higher sensitivity to precipitation gradients and vegetation type changes inside sandy land. Therefore, SIF has certain advantages for characterizing the productivity of sandy vegetation and capturing the changes in water compositions.

4.2. Vegetation-moisture relationship of the four sandy lands

The Hulunbuir Sandy Land has the highest vegetation productivity among the four sandy lands, followed by the Horqin, and the Mu Us has the lowest vegetation productivity. The spatial distribution of productivity has the characteristic of a decreasing change from the east to the west. In addition, the average annual precipitation also shows an east–west gradient, with drier conditions in the west and wetter in the east. We found that this climate gradient largely determines the regional pattern of the vegetation-moisture relationship (A et al., 2016; Cheng et al., 2018; Fan et al., 2020; Wang et al., 2020b; Zhang et al., 2016c), and this implies that precipitation (or surface moisture) provides favorable natural conditions for vegetation growth and positively correlates with vegetation productivity (Sun et al., 2019; Zheng et al., 2006; Zhou et al., 2015).

The spatial distribution of the vegetation-moisture relationship in Hulunbuir Sandy Land shows a strong zonality law. The correlation of vegetation-moisture in the region from west to east shows a gradual increasing trend, maintaining strong consistency with the rainfall gradient of the entire analyzed area. The high-value area appears in the sandy vegetation area in the northeast, which is the same area where the

correlation between surface water and groundwater is also the highest. According to the vegetation type distribution in Fig. 2, the eastern portion of the sandy land is mainly occupied by sandy vegetation, shrubs, and meadow grasslands, close to the Great Xing'an Mountain forest area. Meanwhile, typical grasslands are widely spread in the middle and western regions. Feng et al. (2017) stated that the sensitivity trend of natural vegetation to water composition is herbaceous vegetation, followed by shrubs and sandy vegetation, and the arbor is the smallest. Therefore, with the enrichment of SM and TWS in the later period, the correlation between vegetation and water composition in the western typical grassland area has increased.

Vegetation growth variation in the Otindag Sandy Land illustrates strong differences between east and west, mainly caused by the uneven distribution of water resources (Jia et al., 2020; Su et al., 2012; Zheng et al., 2006). Water resources in the west are relatively scarce, with annual average precipitation <200 mm. The lack of groundwater makes it difficult to exploit, while the eastern region is rich in water resources, with an average annual precipitation of about 350 mm. Surface water is widely distributed and groundwater is abundant, which provides great development potential (Jia et al., 2020; Su et al., 2012). In addition to sandy vegetation, there are mainly broad-leaved forests, meadow grasslands, croplands and shrubs, with abundant vegetation types in the east of the sandy land. Sandy vegetation and typical grasslands are mainly distributed in the central part, while desert grasslands are in the west. Gang et al. (2019) and Wang et al. (2020c) pointed out that the water use efficiency of different vegetation types in semi-arid areas vary from high to low in the order of cultivated plants > shrubs > meadow grasslands > typical grasslands > desert grasslands. Therefore, when the annual precipitation changes, the vegetation water correlation in the west changes greatly, and in the east it is relatively stable. In addition, due to the vigorous development of irrigation forage lands in the Otindag sandy land after 2000, the amount of groundwater development and utilization has increased significantly, resulting in decreases in the total amount of groundwater and the groundwater level in each year (Su et al., 2012). Therefore, the dependence of vegetation growth on groundwater is reduced, and the precipitation-driven surface soil moisture becomes the main water resource for vegetation growth. This situation also explains why the SM and TWS in the Otindag Sandy Land are not significantly correlated. The vegetation growth conditions in Horqin are more complicated than those in the other three sandy areas, mainly because of the diversity of vegetation types in this area. The southeast region has better vegetation growth conditions, followed by cropland which is widely distributed in the central and south, and the typical grassland vegetation growth in the northwest is poor. Previous studies have shown that cultivated plants have high water use efficiency (Ma et al., 2019; Wang et al., 2020c), which explains the strongest vegetation-moisture correlation in the southern region. Under the combined effect of water-heat conditions and the physiological characteristics of plants, a spatial distribution pattern of vegetation-moisture decline from the southeast to the northwest has been established (Ma et al., 2019; Wang et al., 2020b; Yang et al., 2018). In addition, the average annual total volume of water resources in this area is about 124 $\times 10^8$ m^3, of which groundwater storage accounts for 64 $\times 10^8$ m^3. The water table was probably just below the surface in most areas, making groundwater easier to exploit and it is mostly used for cropland irrigation (Zheng et al., 2012). This implies that in addition to precipitation factors, the dynamic groundwater changes in Horqin Sandy Land are also strongly affected by human activities. After 1970, surface runoff in the area decreased with the increases in temperature and cultivated area. Groundwater has gradually become the main source of the water supply in the study area. The continuous groundwater extraction to irrigate cropland for many years has severely reduced the groundwater storage (He et al., 2018; Zheng et al., 2012). Therefore, the correlation coefficients of groundwater with precipitation and vegetation growth in the study area are low, consistent with the research results of other scholars in the Horqin area (Zheng et al., 2012).

Like the other three sandy lands, precipitation decreases from southeast to northwest due to uneven water and heat conditions in the Mu Us Sandy land. Vegetation growth variation also shows a similar trend, and the regularity of the spatial distribution of vegetation-moisture is more significant. There are meadow grasslands and desert grasslands on the western edge of the sandy land, and the southeastern edge is rich in groundwater resources. In addition to reasons similar to those in the Otindag and Horqin, coal mining in this area discharges groundwater, reducing groundwater and water flow. The water environment has also been destroyed (Cheng et al., 2012; Zou et al., 2014). Therefore, the relationship between vegetation and water in sandy land is largely affected by human activities.

4.3. Vegetation sensitivities to surface SM and overall TWS

From the above discussion, the regional pattern of the vegetation-moisture relationship is mainly affected by the precipitation-driven surface soil moisture. It is also dependent on the types of underlying vegetation functions, consistent with previous studies based on multiple driving factors for vegetation growth in semi-arid areas. As Rodriguez-Iturbe et al. (1999) pointed out, soil moisture is an important factor of the ecological environment and the source of life for plants on the earth's surface. Yang et al. (2017) also stated an important relationship between the distribution patterns of sandy pioneer plants and soil water content. In addition, this relationship may be affected by different vegetation communities (Yang et al., 2018). In particular, the relationship between sandy vegetation and groundwater level differs depending on the vegetation populations: vegetation growth depends on groundwater, and groundwater level is the controlling factor for vegetation coverage. In contrast, vegetation that does not rely on groundwater has a different coverage (Cheng et al., 2012). The predominant xerophyte vegetation in the four sandy lands has the widest distribution range. The water requirement for the growth of these types of vegetation mainly relies on surface soil moisture, which implies that groundwater is not the main factor controlling vegetation growth in sandy areas (Cheng et al., 2012; Zou et al., 2014). Therefore, vegetation growth changes have a certain degree of consistency with SM and TWS, but the sensitivity of vegetation productivity to SM is greater than it is to TWS.

The influence of soil moisture and total water storage on vegetation growth has a lag effect. In addition to the influence of water storage components in the same period on vegetation changes, the previous period water conditions also have a certain impact on vegetation growth (Zhang and Xiao 2005). The time scale estimate obtained from the autocorrelation can characterize the inertia of the time series, or how long the anomaly can persist (A et al., 2016; Piles et al., 2021). Our results show that SM and TWS basically have a one-month lag in persistence, consistent with previous studies about the lag effect in vegetation responses to water compositions in semi-arid areas (Hua et al., 2019; Piles et al., 2021). Importantly, abnormal climate changes could adjust this inertia to some extent. The time scale in the early period is generally larger than that in the late period, which indicates that the sandy vegetation requires larger or more constant water replenishment to change the shortage of water supply in the early period. As Inner Mongolia transitions from the dry period to the wet period, the recovery time of water components is becoming relatively shortened, and the constraints on vegetation growth will also be weakened. Therefore, the vegetation growth in the four sandy lands has recovered significantly in the later stage.

5. Conclusion

This paper combines multi-source satellite observation records to characterize the vegetation growth and water supply patterns in the four sandy lands of China. The sensitivity of vegetation to changes in surface soil moisture and deeper groundwater resources is explored as well. These analyses have led to four main conclusions. (1) The vegetation growth of the four sandy lands shows a generally increasing trend from 2003 to 2016. Although the vegetation growth in the Otindag and Horqin sandy lands decreased before 2010, it increased after 2010. The improved area of vegetation growth is more than the degraded area, showing a trend of gradual improvement. SM also shows a continuous upward trend for the four sandy lands, especially the Horqin Sandy Land which increased significantly (84% of the area anomaly $> 1.4 \times 10^{-2}$ cm^3/cm^3). Except for the Hulunbuir Sandy Land which shows an upward trend in TWS results, the other three sandy lands all present a downward trend. In particular, the amount of groundwater in the Mu Us Sandy Land has declined the most (97% of the area anomaly < -40 mm). (2) The results also show that compared with EVI and GPP, SIF is more sensitive to the changes in precipitation gradients and vegetation types in sandy lands. Therefore, SIF has certain advantages for characterizing sandy vegetation's productivity and capturing changes in moisture. (3) The spatial pattern of the vegetation-moisture relationship follows the gradient of annual average precipitation, which indicates that precipitation (or surface SM) provides favorable natural conditions for vegetation growth and is positively correlated with vegetation productivity. Meanwhile, due to the continuous decline of groundwater, the dependence of vegetation on groundwater was gradually reduced. Therefore, vegetation growth changes have a certain degree of consistency with SM and TWS, but the sensitivity of vegetation growth to surface SM changes is stronger than that of the overall TWS ($P < 0.05$, $R_{SM} > R_{TWS}$). (4) In addition, the persistence or memory effect of the four sandy lands for SM and TWS generally have an approximately one-month lag, especially the Mu Us Sandy Land which has the longest persistence (0.94 months and 1.1 months, respectively). The time scale in the early period is generally larger than that in the later period, which indicates that sandy vegetation needs greater or more permanent water replenishment to compensate for the early water supply shortage. As Inner Mongolia transitions from the dry season to the rainy season, the recovery time of water components is relatively shortened, and the constraints on vegetation growth will also be weakened. Therefore, the vegetation growth of the four sandy lands in the later period has recovered significantly.

This paper aims to provide scientific evidence for guiding the development of effective measures to prevent the expansion of sandy land, protect groundwater, and improve water resource utilization efficiency in the future. However, this paper has certain limitations because of the coarse resolution and relatively short-term time series provided by GRACE TWS. Therefore, future studies should use groundwater observation data with better data quality whenever possible to more accurately characterize the interactions between water composition factors and ecosystems.

CRediT authorship contribution statement

Xinyi Liu: Conceptualization, Formal analysis, Methodology, Software, Validation, Writing – original draft. **Quan Lai:** Data curation, Methodology, Resources, Software, Writing – review & editing. **Shan Yin:** Conceptualization, Investigation, Validation, Writing – review & editing. **Yuhai Bao:** Funding acquisition, Project administration, Investigation, Supervision. **Song Qing:** Investigation, Software, Validation. **Li Mei:** Data curation, Investigation, Software. **Lingxin Bu:** Data curation, Writing – review & editing.

Declaration of Competing Interest

The authors declare that they have no known competing financial interests or personal relationships that could have appeared to influence the work reported in this paper.

Acknowledgments

Appendix A. Supplementary data

Supplementary data to this article can be found online at https://doi.org/10.1016/j.ecolind.2022.108711.

References:

A, G., Velicogna, I., Kimball, J.S., Du, J., Kim, Y., Colliander, A., Njoku, E., 2016. Satellite-observed changes in vegetation sensitivities to surface soil moisture and total water storage variations since the 2011 Texas drought. Environ. Res. Lett. 12 (5), 054006. https://doi.org/10.1088/1748-9326/aa6965.

Bacour, C., Maignan, F., MacBean, N., Porcar-Castell, A., Flexas, J., Frankenberg, C., Peylin, P., Chevallier, F., Vuichard, N., Bastrikov, V., 2019. Improving estimates of gross primary productivity by assimilating solar-induced fluorescence satellite retrievals in a terrestrial biosphere model using a process-based SIF model. J. Geophys. Res. Biogeosci. 124 (11), 3281–3306.

Bandopadhyay, S., Rastogi, A., Rascher, U., Rademske, P., Schickling, A., Cogliati, S., Julitta, T., Mac Arthur, A., Hueni, A., Tomelleri, E., Celesti, M., Burkart, A., Stróżecki, M., Sakowska, K., Gąbka, M., Rosadziński, S., Sojka, M., Iordache, M.-D., Reusen, I., Van Der Tol, C., Damm, A., Schuettemeyer, D., Juszczak, R., 2019. Hyplant-derived sun-induced fluorescence—A new opportunity to disentangle complex vegetation signals from diverse vegetation types. Remote Sens. 11 (14), 1691. https://doi.org/10.3390/rs11141691.

Bao, G., Qin, Z., Bao, Y., Zhou, Y., Li, W., Sanjjav, A., 2014. NDVI-based long-term vegetation dynamics and its response to climatic change in the Mongolian Plateau. Remote Sens. 6 (9), 8337–8358.

Cao, R., Chen, J., Shen, M., Tang, Y., 2015. An improved logistic method for detecting spring vegetation phenology in grasslands from MODIS EVI time-series data. Agric. For. Meteorol. 200, 9–20.

Cheng, D., Wang, W., Hou, G., Yang, H., Li, Y., Zhang, E., 2012. Relationship between vegetation and groundwater in Mu Us desert. J. Jilin Univ. (Earth Science Edition) 42, 184–189.

Cheng, M., Zhong, L., Ma, Y., Zou, M., Ge, N., Wang, X., Hu, Y., 2019. A study on the assessment of multi-source satellite soil moisture products and reanalysis data for the Tibetan Plateau. Remote Sens. 11 (10), 1196. https://doi.org/10.3390/rs11101196.

Cheng, Y., Li, X., Wang, Y., Zhan, H., Yang, W., Jiang, Q., 2020. New measures of deep soil water recharge during the vegetation restoration process in semi-arid regions of northern China. Hydrol. Earth Syst. Sci. 24 (12), 5875–5890.

Cheng, Y.-B., Middleton, E., Zhang, Q., Huemmrich, K., Campbell, P., Corp, L., Cook, B., Kustas, W., Daughtry, C., 2013. Integrating solar induced fluorescence and the photochemical reflectance index for estimating gross primary production in a cornfield. Remote Sens. 5 (12), 6857–6879.

Cheng, Y., Yang, W., Zhan, H., Jiang, Q., Shi, M., Wang, Y., Li, X., Xin, Z., 2021. On Change of soil moisture distribution with vegetation reconstruction in Mu Us sandy land of China, with newly designed lysimeter. Front. Plant Sci. 12, 182.

Cheng, Y.-B., Zhan, H.-B., Yang, W.-B., Bao, F., 2018. Deep soil water recharge response to precipitation in Mu Us Sandy Land of China. Water Sci. Eng. 11 (2), 139–146.

Dai, Y., Dong, Z., Li, H., He, Y., Li, J., Guo, J., 2019. Effects of checkerboard barriers on the distribution of aeolian sandy soil particles and soil organic carbon. Geomorphology 338, 79–87.

Damm, A., Guanter, L., Paul-Limoges, E., van der Tol, C., Hueni, A., Buchmann, N., Eugster, W., Ammann, C., Schaepman, M.E., 2015. Far-red sun-induced chlorophyll fluorescence shows ecosystem-specific relationships to gross primary production: an assessment based on observational and modeling approaches. Remote Sens. Environ. 166, 91–105.

Duveiller, G., Cescatti, A., 2016. Spatially downscaling sun-induced chlorophyll fluorescence leads to an improved temporal correlation with gross primary productivity. Remote Sens. Environ. 182, 72–89.

Fahad, S., Sonmez, O., Saud, S., Wang, D., Wu, C., Adnan, M., Turan, V., 2021a. Plant Growth Regulators for Climate-Smart Agriculture. CRC Press.

Fahad, S., Sonmez, O., Saud, S., Wang, D., Wu, C., Adnan, M., Turan, V., 2021b. Developing Climate-Resilient Crops: Improving Global Food Security and Safety. CRC Press.

Fahad, S., Sonmez, O., Saud, S., Wang, D., Wu, C., Adnan, M., Turan, V., 2021c. Sustainable Soil and Land Management and Climate Change. CRC Press.

Fahad, S., Sonmez, O., Saud, S., Wang, D., Wu, C., Adnan, M., Turan, V., 2021d. Climate Change and Plants: Biodiversity, Growth and Interactions. CRC Press.

Fahad, S., Ullah, A., Ali, U., Ali, E., Saud, S., Hakeem, K.R., Alharby, H., Sabagh, A.E., Barutcular, C., Kamran, M. (2019). Drought tolerance in plantsrole of phytohormones and scavenging system of ROS., *Plant Tolerance to Environmental Stress* (pp. 103-114): CRC Press.

Fan, J., Wang, L., Qin, J., Zhang, F., Xu, Y., 2020. Evaluating cultivated land stability during the growing season based on precipitation in the Horqin Sandy Land, China. *J. Environ. Manage.* 276, 111269. https://doi.org/10.1016/j.jenvman.2020.111269.

Feng, Q., Zhao, W., Fu, B., Ding, J., Wang, S., 2017. Ecosystem service trade-offs and their influencing factors: a case study in the Loess Plateau of China. Sci. Total Environ. 607-608, 1250–1263.

Frankenberg, C., Fisher, J.B., Worden, J., Badgley, G., Saatchi, S.S., Lee, J.-E., Toon, G.C., Butz, A., Jung, M., Kuze, A., Yokota, T., 2011. New global observations of the terrestrial carbon cycle from GOSAT: patterns of plant fluorescence with gross primary productivity. Geophys. Res. Lett. 38 (17), n/a–n/a.

Frankenberg, C., O'Dell, C., Berry, J., Guanter, L., Joiner, J., Köhler, P., Pollock, R., Taylor, T.E., 2014. Prospects for chlorophyll fluorescence remote sensing from the Orbiting Carbon Observatory-2. Remote Sens. Environ. 147, 1–12.

Gang, C., Zhang, Y., Guo, L., Gao, X., Peng, S., Chen, M., Wen, Z., 2019. Drought-induced carbon and water use efficiency responses in dryland vegetation of northern China. Front. Plant Sci. 10, 224.

Guanter, L., Aben, I., Tol, P., Krijger, J.M., Hollstein, A., Köhler, P., Damm, A., Joiner, J., Frankenberg, C., Landgraf, J., 2014. Potential of the TROPOspheric Monitoring Instrument (TROPOMI) onboard the Sentinel-5 Precursor for the monitoring of terrestrial chlorophyll fluorescence. Atmos. Meas. Tech. Discuss. 7, 12545–12588.

Guanter, L., Frankenberg, C., Dudhia, A., Lewis, P.E., Gómez-Dans, J., Kuze, A., Suto, H., Grainger, R.G., 2012. Retrieval and global assessment of terrestrial chlorophyll fluorescence from GOSAT space measurements. Remote Sens. Environ. 121, 236–251.

Hasanuzzaman, M., Fujita, M., Oku, H., Islam, M.T., 2019. Plant Tolerance to Environmental Stress: Role of Phytoprotectants. CRC Press.

Hashimoto, H., Wang, W., Milesi, C., White, M.A., Ganguly, S., Gamo, M., Hirata, R., Myneni, R.B., Nemani, R.R., 2012. Exploring simple algorithms for estimating gross primary production in forested areas from satellite data. Remote Sens. 4 (1), 303–326.

He, Z., Zhang, T., Liu, X., Shang, X., 2018. Water-yield relationship responses of maize to ridge-furrow planting systems coupled with multiple irrigation levels in China's horqin sandy land. Agronomy 8 (10), 221. https://doi.org/10.3390/agronomy8100221.

Hu, S., Mo, X., 2020. Detecting regional GPP variations with statistically downscaled solar-induced chlorophyll fluorescence (SIF) based on GOME-2 and MODIS data. Int. J. Remote Sens. 41 (23), 9206–9228.

Hua, L.i., Wang, H., Sui, H., Wardlow, B., Hayes, M.J., Wang, J., 2019. Mapping the spatial-temporal dynamics of vegetation response lag to drought in a semi-arid region. Remote Sens. 11 (16), 1873. https://doi.org/10.3390/rs11161873.

Jeong, S.-J., Schimel, D., Frankenberg, C., Drewry, D.T., Fisher, J.B., Verma, M., Berry, J. A., Lee, J.-E., Joiner, J., 2017. Application of satellite solar-induced chlorophyll fluorescence to understanding large-scale variations in vegetation phenology and function over northern high latitude forests. Remote Sens. Environ. 190, 178–187.

Ji, L., Peters, A.J., 2003. Assessing vegetation response to drought in the northern Great Plains using vegetation and drought indices. Remote Sens. Environ. 87 (1), 85–98.

Ji, X., Kang, E., Chen, R., Zhao, W., Zhang, Z., Jin, B., 2006. The impact of the development of water resources on environment in arid inland river basins of Hexi region, Northwestern China. Environ. Geol. 50 (6), 793–801.

Jia, D., Li, X., Zhang, Y., Feng, Y., Liu, D. (2020). Analysis on Water Use Strategies of Natural Poplar in Hunshandake Sandy Land, China. *Environmental Progress & Sustainable Energy*, e13579.

Joiner, J., Guanter, L., Lindstrot, R., Voigt, M., Vasilkov, A.P., Middleton, E.M., Huemmrich, K.F., Yoshida, Y., Frankenberg, C., 2013. Global monitoring of terrestrial chlorophyll fluorescence from moderate-spectral-resolution near-infrared satellite measurements: methodology, simulations, and application to GOME-2. Atmos. Meas. Tech. 6 (10), 2803–2823.

Kairis, O., Karavitis, C., Kounalaki, A., Salvati, L., Kosmas, C., 2013. The effect of land management practices on soil erosion and land desertification in an olive grove. Soil Use Manage. 29 (4), 597–606.

Kim, J., Ryu, Y., Dechant, B., Lee, H., Kim, H.S., Kornfeld, A., Berry, J.A., 2021. Solar-induced chlorophyll fluorescence is non-linearly related to canopy photosynthesis in a temperate evergreen needleleaf forest during the fall transition. Remote Sens. Environ. 258, 112362. https://doi.org/10.1016/j.rse.2021.112362.

Köhler, P., Frankenberg, C., Magney, T.S., Guanter, L., Joiner, J., Landgraf, J., 2018. Global Retrievals of Solar-Induced Chlorophyll Fluorescence With TROPOMI: first results and intersensor comparison to OCO-2. Geophys. Res. Lett. 45 (19), 10,456–10,463.

Kong, D., Zhang, Y., Gu, X., Wang, D., 2019. A robust method for reconstructing global MODIS EVI time series on the Google Earth Engine. ISPRS J. Photogr. Remote Sens. 155, 13–24.

Li, S., Ren, H.D., Xue, L., Chang, J., Yao, X.H., 2014. Influence of bare rocks on surrounding soil moisture in the karst rocky desertification regions under drought conditions. CATENA 116, 157–162.

Liao, C., Liu, B., Xu, Y., Li, Y., Li, H., 2019. Effect of topography and protecting barriers on revegetation of sandy land, Southern Tibetan Plateau. Sci. Rep. 9, 1–10.

Liu, X., Liu, Z., Liu, L., Lu, X., Chen, J., Du, S., Zou, C., 2021. Modelling the influence of incident radiation on the SIF-based GPP estimation for maize. Agric. For. Meteorol. 307, 108522. https://doi.org/10.1016/j.agrformet.2021.108522.

Ma, X., Zhao, C., Yan, W., Zhao, X., 2019. Influences of 1.5° C and 2.0° C global warming scenarios on water use efficiency dynamics in the sandy areas of northern China. Sci. Total Environ. 664, 161–174.

Mohammed, G.H., Colombo, R., Middleton, E.M., Rascher, U., van der Tol, C., Nedbal, L., Goulas, Y., Pérez-Priego, O., Damm, A., Meroni, M., 2019. Remote sensing of solar-induced chlorophyll fluorescence (SIF) in vegetation: 50 years of progress. Remote Sens. Environ. 231, 111177.

Musa, A., Zhang, Y., Cao, J., Wang, Y., Liu, Y., 2019. Relationship between root distribution characteristics of Mongolian pine and the soil water content and groundwater table in Horqin Sandy Land, China. Trees 33 (4), 1203–1211.

Piles, M., Munoz-Mari, J., Guerrero-Curieses, A., Camps-Valls, G., Rojo-Alvarez, J.L., 2021. Autocorrelation metrics to estimate soil moisture persistence from satellite time series: application to semiarid regions. IEEE Trans. Geosci. Remote Sens. 1–17.

Qiu, B., Chen, J.M., Ju, W., Zhang, Q., Zhang, Y., 2019. Simulating emission and scattering of solar-induced chlorophyll fluorescence at far-red band in global vegetation with different canopy structures. Remote Sens. Environ. 233, 111373. https://doi.org/10.1016/j.rse.2019.111373.

Rodriguez-Iturbe, I., D'Odorico, P., Porporato, A., Ridolfi, L., 1999. On the spatial and temporal links between vegetation, climate, and soil moisture. Water Resour. Res. 35 (12), 3709–3722.

Sims, D.A., Rahman, A.F., Cordova, V.D., El-Masri, B.Z., Baldocchi, D.D., Flanagan, L.B., Goldstein, A.H., Hollinger, D.Y., Misson, L., Monson, R.K., Oechel, W.C., Schmid, H. P., Wofsy, S.C., Xu, L., 2006. On the use of MODIS EVI to assess gross primary productivity of North American ecosystems. J. Geophys. Res. Biogeosci. 111 (G4) https://doi.org/10.1029/2006JG000162.

Song, L., Zhu, J., Yan, Q., Li, M., Yu, G., 2015. Comparison of intrinsic water use efficiency between different aged Pinus sylvestris var. mongolica wide windbreaks in semiarid sandy land of northern China. Agrofor. Syst. 89, 477–489.

Su, H., Li, Y., Liu, W., Xu, H., Sun, O.J., 2014. Changes in water use with growth in Ulmus pumila in semiarid sandy land of northern China. Trees 28, 41–52.

Su, H., Li, Y., Su, B., Sun, J., 2012. Effects of groundwater decline on photosynthetic characteristics and stress tolerance of Ulmus pumila in Hunshandake Sandy Land, China. *Chin. J. Plant Ecol.gy* 36, 177.

Su, K., Zheng, W., Yin, W., Hu, L., Shen, Y., 2022. Improving the accuracy of groundwater storage estimates based on groundwater weighted fusion model. Remote Sens. 14 (1), 202. https://doi.org/10.3390/rs14010202.

Sun, B., Li, Z., Gao, W., Zhang, Y., Gao, Z., Song, Z., Qin, P., Tian, X., 2019. Identification and assessment of the factors driving vegetation degradation/regeneration in drylands using synthetic high spatiotemporal remote sensing Data—A case study in Zhenglanqi, Inner Mongolia, China. *Ecol. Ind.* 107, 105614. https://doi.org/10.1016/j.ecolind.2019.105614.

Vicente-Serrano, S.M., Gouveia, C., Camarero, J.J., Begueria, S., Trigo, R., Lopez-Moreno, J.I., Azorin-Molina, C., Pasho, E., Lorenzo-Lacruz, J., Revuelto, J., Moran-Tejeda, E., Sanchez-Lorenzo, A., 2013. Response of vegetation to drought time-scales across global land biomes. Proc. Natl. Acad. Sci. 110 (1), 52–57.

Wagle, P., Zhang, Y., Jin, C., Xiao, X., 2016. Comparison of solar-induced chlorophyll fluorescence, light-use efficiency, and process-based GPP models in maize. Ecol. Appl. 26, 1211–1222.

Wang, C., Graham, R.M., Wang, K., Gerland, S., Granskog, M.A., 2019. Comparison of ERA5 and ERA-Interim near-surface air temperature, snowfall and precipitation over Arctic sea ice: effects on sea ice thermodynamics and evolution. Cryosphere 13 (6), 1661–1679.

Wang, F., Pan, X., Gerlein Safdi, C., Cao, X., Wang, S., Gu, L., Wang, D., Lu, Q., 2020b. Vegetation restoration in N orthern China: a contrasted picture. Land Degrad. Dev. 31, 669–676.

Wang, J., Qin, S., Zhang, Y., 2020c. Spatial-temporal patterns of vegetation water use efficiency in the Mu Us Desert. J. Desert Res. 40, 120.

Wang, L., Ma, A., Zhang, H., Zhang, J., Dong, Q., Fu, G., 2020d. Effects of long-term vegetation restoration on distribution of deep soil moisture in semi-arid Northwest of China. J. Soil Sci. Plant Nutr. 20 (4), 2123–2132.

Wang, Y., Zhang, J., Ma, Q., Zhu, M., 2016. Response of aeolian desertification to regional climate change in Horqin sandy land at beginning of 21st century. Trans. Chin. Soc. Agric. Eng. 32, 177–185.

Wu, J., Chen, X., Xu, L., Qian, J., Liu, Z., 2021. The spatial pattern of the belowground bud bank and its responses to soil water status in the interdune lowlands of active sand dunes of Inner Mongolia, China. *Restoration Ecol.* 29 (2) https://doi.org/10.1111/rec.v29.210.1111/rec.13223.

Xie, S., Mo, X., Hu, S., Liu, S., 2020. Contributions of climate change, elevated atmospheric CO2 and human activities to ET and GPP trends in the Three-North Region of China. Agric. For. Meteorol. 295, 108183. https://doi.org/10.1016/j.agrformet.2020.108183.

Xiu, L., Yan, C., Li, X., Qian, D., Feng, K., 2018. Monitoring the response of vegetation dynamics to ecological engineering in the Mu Us Sandy Land of China from 1982 to 2014. Environ. Monitor. Assess. 190, 1–18.

Yang, T., Ala, M., Zhang, Y., Wu, J., Wang, A., Guan, D., Minasny, B., 2018. Characteristics of soil moisture under different vegetation coverage in Horqin Sandy Land, northern China. PLoS One 13 (6), e0198805. https://doi.org/10.1371/journal.pone.0198805.

Yang, T., Cao, J., Wang, Y., Liu, Y., 2017. Soil moisture influences vegetation distribution patterns in sand dunes of the Horqin Sandy Land, Northeast China. Ecol. Eng. 105, 95–101.

Yu, X., Huang, Y., Li, E., Li, X., Guo, W., 2017. Effects of vegetation types on soil water dynamics during vegetation restoration in the Mu Us Sandy Land, northwestern China. J. Arid Land 9 (2), 188–199.

Yu, X., Huang, Y., Li, E., Li, X., Guo, W., 2018. Effects of rainfall and vegetation to soil water input and output processes in the Mu Us Sandy Land, northwest China. Catena 161, 96–103.

Zhang, G., Dong, J., Xiao, X., Hu, Z., Sheldon, S., 2012. Effectiveness of ecological restoration projects in Horqin Sandy Land, China based on SPOT-VGT NDVI data. Ecol. Eng. 38 (1), 20–29.

Zhang, Q., Fan, K., Singh, V.P., Sun, P., Shi, P., 2018b. Evaluation of remotely sensed and reanalysis soil moisture against in situ observations on the Himalayan-Tibetan Plateau. J. Geophys. Res. Atmos. 123 (14), 7132–7148.

Zhang, Q., Xiao, F., 2005. Analysis of vegetation index sensitivity to soil moisture in Northern China. Chin. J. Ecol.

Zhang, Y., Guanter, L., Berry, J.A., van der Tol, C., Yang, X.i., Tang, J., Zhang, F., 2016a. Model-based analysis of the relationship between sun-induced chlorophyll fluorescence and gross primary production for remote sensing applications. Remote Sens. Environ. 187, 145–155.

Zhang, Y., Peng, C., Li, W., Tian, L., Zhu, Q., Chen, H., Fang, X., Zhang, G., Liu, G., Mu, X., Li, Z., Li, S., Yang, Y., Wang, J., Xiao, X., 2016b. Multiple afforestation programs accelerate the greenness in the 'Three North' region of China from 1982 to 2013. Ecol. Ind. 61, 404–412.

Zhang, Y., Xiao, X., Guanter, L., Zhou, S., Ciais, P., Joiner, J., Sitch, S., Wu, X., Nabel, J., Dong, J., Kato, E., Jain, A.K., Wiltshire, A., Stocker, B.D., 2016c. Precipitation and carbon-water coupling jointly control the interannual variability of global land gross primary production. Sci. Rep. 6 (1) https://doi.org/10.1038/srep39748.

Zhang, Y., Xiao, X., Jin, C., Dong, J., Zhou, S., Wagle, P., Joiner, J., Guanter, L., Zhang, Y., Zhang, G., Qin, Y., Wang, J., Moore, B., 2016d. Consistency between sun-induced chlorophyll fluorescence and gross primary production of vegetation in North America. Remote Sens. Environ. 183, 154–169.

Zheng, X., Zhu, J.J., Yan, Q.L., Song, L.N., 2012. Effects of land use changes on the groundwater table and the decline of Pinus sylvestris var. mongolica plantations in southern Horqin Sandy Land, Northeast China. *Agric. Water Manage.* 109, 94–106.

Zheng, Y.R., Xie, Z.X., Robert, C., Jiang, L.H., Shimizu, H., 2006. Did climate drive ecosystem change and induce desertification in Otindag sandy land, China over the past 40 years? J. Arid Environ. 64 (3), 523–541.

Zhou, D., Zhao, X., Hu, H., Shen, H., Fang, J., 2015. Long-term vegetation changes in the four mega-sandy lands in Inner Mongolia, China. Landscape Ecol. 30 (9), 1613–1626.

Zou, H., Bi, Y., Zhu, C., Du, T., Han, B., 2014. Effect of mining subsidence on soil moisture dynamic changes of sandy land. J. China Univ. Min. Technol. 3.

Further reading

Wang, C., Guan, K., Peng, B., Chen, M., Jiang, C., Zeng, Y., Wu, G., Wang, S., Wu, J., Yang, X., Frankenberg, C., Köhler, P., Berry, J., Bernacchi, C., Zhu, K., Alden, C., Miao, G., 2020a. Satellite footprint data from OCO-2 and TROPOMI reveal significant spatio-temporal and inter-vegetation type variabilities of solar-induced fluorescence yield in the US Midwest. Remote Sens. Environ. 241, 111728. https://doi.org/10.1016/j.rse.2020.111728.

Zhang, J., Zhang, Y., Qin, S., Wu, B., Wu, X., Zhu, Y., Shao, Y., Gao, Y., Jin, Q., Lai, Z., 2018a. Effects of seasonal variability of climatic factors on vegetation coverage across drylands in northern China. Land Degrad. Dev. 29 (6), 1782–1791.

Original Articles

Exploring grassland ecosystem water use efficiency using indicators of precipitation and soil moisture across the Mongolian Plateau

Xinyi Liu [a], Quan Lai [a,b,*], Shan Yin [a,b], Yuhai Bao [a,b], Song Qing [a,b], Sainbuyan Bayarsaikhan [c], Lingxin Bu [a], Li Mei [a], Zhiru Li [a], Jialong Niu [a], Yumeng Yang [a]

[a] College of Geographical Science, Inner Mongolia Normal University, Hohhot 010022, China
[b] Inner Mongolia Key Laboratory of Remote Sensing and Geographic Information Systems, Inner Mongolia, Normal University, Hohhot 010022, China
[c] Department of Geography, School of Arts and Sciences, National University of Mongolia, Ulaanbaatar 14201, Mongolia

ARTICLE INFO

Keywords:
Precipitation use efficiency
Soil water use efficiency
Precipitation
Soil moisture
Mongolian Plateau's grasslands

ABSTRACT

Grassland ecosystem dominates in the Mongolian Plateau, mostly located in its arid and semi-arid regions. Although the ecosystem is an important source for agriculture, it is also a fragile system ecologically. This system is one of the most sensitive areas to global climate change. Precipitation (PPT) and soil moisture (SM) are important water sources in the grassland ecosystem, and their changes would greatly affect vegetation growth. This paper generates the precipitation use efficiency (PUE) and soil water use efficiency (SWUE) of Mongolian Plateau grassland based on multi-source remote sensing data to investigate the spatio-temporal distribution pattern and identify the driving factors. Results showed four main findings. Firstly, two water use efficiency (WUE) indicators show a generally increasing trend from 2000 to 2018, with average PUE and SWUE 1.07 gC·m^{-2}·mm^{-1} and 1.03 gC/kg·H$_2$O, respectively. They have similar spatial distribution patterns, consistent with the available water resources, decreasing from northeast to southwest. However, grassland vegetation growth is more sensitive to soil moisture than precipitation, and the dynamic change of SWUE is smoother and more significant than PUE. Secondly, due to the higher species richness, better vegetation biological characteristics and less severe growth environment, meadow grassland has the highest PUE and SWUE, followed by typical grassland and desert steppe. Thirdly, PUE and SWUE are relatively low in extremely arid and humid regions. In areas with relatively moderate water conditions (PPT in 148–360 mm, SM in 0.14–0.35 cm^3/cm^3), two indicators increase with the abundance of moisture conditions and reach the maximum. Fourthly, there is a positive linear relationship between PUE (SWUE) with precipitation and a unimodal correlation between PUE (SWUE) with temperature across the entire grassland. However, a varying correlation exists in different grassland ecosystems, especially meadow grassland. Together with analyzing past and future trends, this study provides strong evidence to reflect the impact of global climate change and the management and protection of the grassland ecosystems in arid and semi-arid regions.

1. Introduction

Water use efficiency (WUE) in terrestrial ecosystems is a significant indicator of carbon and water cycle coupling (Gentine et al., 2019; Jones, 2004). WUE is defined as the ratio of ecosystem gross primary productivity (GPP) to evapotranspiration (ET), which reflects the interactions between ecosystem productivity and water availability (Gentine et al., 2019; Kato et al., 2004; Le Houérou et al., 1988). Climate change will cause more variable precipitation, as will soil moisture directly affected by precipitation infiltration. Precipitation and soil moisture are important water sources for ecosystem evapotranspiration, and their changes will greatly affect the vegetation growth and water-carbon cycle, which in turn lead to changes in WUE of different vegetation types (Breshears and Barnes, 1999; Chen et al., 2004; Daly and Porporato, 2005; Wei and Dirmeyer, 2012). Therefore, it is feasible to employ precipitation and soil moisture as alternatives to investigate ecosystem WUE. Monitoring and evaluating variations in ecosystem WUE under different hydrological and climatic conditions has become an important mission. Understanding how ecosystem functions respond to climate change is essential (Roderick et al., 2014; Trenberth and

Asrar, 2012; Xu et al., 2020). Previous studies on ecosystems in different world regions have shown that GPP positively correlates with water supply conditions (Bai et al., 2008; Huxman et al., 2004; Paruelo et al., 1999; Sala et al., 1988; Sun and Du, 2017). In addition, water availability is a significant controlling factor for vegetation growth and community composition in terrestrial ecosystems, especially grassland ecosystems (Huxman et al., 2004; Liu et al., 2017; Mu et al., 2017; Vermeire et al., 2009). Water scarcity is a severe problem affecting socio-economic development in arid and semi-arid regions (Xia et al., 2017; Sharafatmandrad and Khosravi Mashizi, 2021; Priyan, 2021). Effective use of limited available water resources requires a sustainable balance between water demands and water resources, which becomes a key issue for the future management of grassland ecosystems (Deng et al., 2006; Kuslu et al., 2010; Roby et al., 2020; Sharafatmandrad and Khosravi Mashizi, 2021; Priyan, 2021). Therefore, this paper intends to study further the water use efficiency of grassland ecosystems, including precipitation and soil moisture, to understand the influence of climate change on the grassland ecosystems.

Precipitation Use Efficiency (PUE) is defined as the ratio of GPP to precipitation (PPT), reflecting the relationship between the assimilation process of ecosystem vegetation photosynthesis and water consumption characteristics (Bai et al., 2008; Huxman et al., 2004; Lauenroth et al., 2000; Paruelo et al., 1999). At present, many studies on PUE changes with precipitation gradients have been conducted on a variety of spatial and temporal scales, including temperate grasslands (Gilgen and Buchmann, 2009), alpine grasslands (Yang et al., 2010), Loess Plateau (Jia et al., 2015), Inner Mongolia Plateau (Mu et al., 2014), Tibetan Plateau (Zhou et al., 2020), Northwest China grasslands (Ren et al., 2010), global grasslands (Paruelo et al., 1999) and terrestrial ecosystems (Huxman et al., 2004). The general result is that PUE initially increases and subsequently decreases with precipitation (Hooper et al., 2005; Hu et al., 2010; Mu et al., 2017; Yang et al., 2010; Zhou et al., 2020). PUE is low in arid and humid regions and peaks in areas with relatively moderate precipitation (Bai et al., 2008; Sun and Du, 2017). In addition, soil moisture is the main water source for ecosystem evapotranspiration. Compared with precipitation, it has a closer relationship with vegetation growth and ecosystems (Chen et al., 2014; He et al., 2017). Many previous studies have clarified that soil moisture deficit would lead to a decline in photosynthesis and net primary productivity (Carter and Sheaffer, 1983; Meir et al., 2015), indicating that using soil moisture to explore ecosystem WUE is more direct and effective. Soil water use efficiency (SWUE) is defined as the ratio of GPP to soil moisture (SM) (He et al., 2017). There are relatively few studies on SWUE, mainly on the global scale. The general conclusion is that SWUE is relatively high in humid ecosystems near the equator, while relatively low in arid and high-latitude ecosystems (He et al., 2017).

Grassland is the most widely distributed terrestrial ecosystem in the Mongolian Plateau, accounting for about 60 % of the area. It is an important source for agriculture, mostly located in its arid and semi-arid regions, with a fragile ecological environment and one of the most sensitive areas to global climate change (Joyce et al., 2016; Mu et al., 2014; White et al., 2012; Winslow et al., 2003). As the most important limiting factor for grassland ecosystem function, precipitation determines the ecosystem function and its variability to a large extent (Bai et al., 2008; Mu et al., 2017; Sun and Du, 2017). Although the studies on PUE are relatively mature, soil moisture use efficiency in grassland ecosystems has not been evaluated yet, and the relationship and difference between PUE and SWUE are rarely studied. Therefore, this study aims to define two water use efficiency indicators, assess the sensitivity of Mongolian Plateau grassland GPP to PPT and SM, and explore the spatio-temporal patterns and changing trends of PUE and SWUE in Mongolian Plateau grassland from 2000 to 2018. We also investigate the relationship between the spatial distribution of PUE, SWUE and water conditions, compare the differences between the two indicators in different grassland types, and explore the control mechanism under different climatic factors on two water use efficiency indicators.

Determine the optimal range of using precipitation and soil moisture to improve the water use efficiency, promote vegetation growth, and avoid water waste for grassland ecosystem. Combined with the analysis of past and future trends, identify key areas of concern for effectively protecting grassland ecosystems. We expect this study's results to offer a deep understanding of the vegetation productivity process in arid and semi-arid regions and provide a basis for assessing the impact of global climate change on grassland ecosystem carbon and water cycles.

2. Data and methods

2.1. Study area

The main part of the Mongolian Plateau, including Mongolia and the Inner Mongolia Autonomous Region of China was selected as the study area (Fig. 1). This study area is a 1.59×10^6 km^2 grassland across the Mongolia Plateau, which covers 59 % of the land area of the Mongolia Plateau. It is landlocked in the inland Plateau of northeastern Asia (87°40′E ~ 122°15′E, 53°08′N ~ 37°46′N). It is located in the transition zone from the Gobi Desert in Central Asia to the forests of Siberia, involving arid, semi-arid and semi-humid regions (Fig. 2(a)). The main grassland types include typical grassland (TYG), meadow grassland (MEG) and desert grassland (DRS). Its topography is mainly mountainous and Plateau (Fig. 2(b)). The terrain presents a pattern of high west and low east (3899 m-92 m). According to meteorological data (2000–2018), the precipitation in the growing season for the study period ranges from 44.8 to 460.2 mm (Fig. 2(c)), and the growing season temperature ranges from 27.1 °C to 29.4 °C (Fig. 2(d)).

2.2. Data sources

2.2.1. The land cover types data

The distribution areas of the three types of grassland across the Mongolia Plateau are delineated based on the Global Land Cover 2000 Project (GLC2000) product (https://forobs.jrc.ec.europa.eu/products/glc2000/data_access.php) and the MODIS land cover dataset (MOD12Q1) from (https://lpdaacsvc.cr.usgs.gov/appeears/task/area).

2.2.2. GPP data

Several recent studies state that solar-induced chlorophyll fluorescence (SIF) can effectively characterize vegetation gross primary productivity (GPP) (Bacour et al., 2019; Duveiller and Cescatti, 2016). Compared with the coarse resolution SIF retrieved directly from the satellites, GOSIF has a better spatial resolution (0.05°×0.05°), continuous global coverage and longer records (2000–2018) (Li and Xiao, 2019). We chose the GPP product derived from GOSIF (https://globalecology.unh.edu//data.html).

2.2.3. The meteorological data

Considering the influence of snow cover in winter on the Mongolian Plateau, the growing season meteorological data from April to October is used to evaluate the dynamic changes in vegetation growth (Bao et al., 2014). We analyze the 2 m air temperature, total precipitation, and potential evapotranspiration (PET) data of the fifth-generation ECMWF reanalysis (ERA-5) (Wang et al., 2019). The monthly 0.1°×0.1° meteorological data is obtained from (https://cds.climate.copernicus.eu/cdsapp#!/dataset/reanalysis-era5-land-monthly-means?tab=form). They are processed into continuous annual growing season meteorological datasets.

Aridity Index (AI) indicates the degree of climate aridity, defined as the ratio of precipitation to potential evapotranspiration. We calculate the AI as follows:
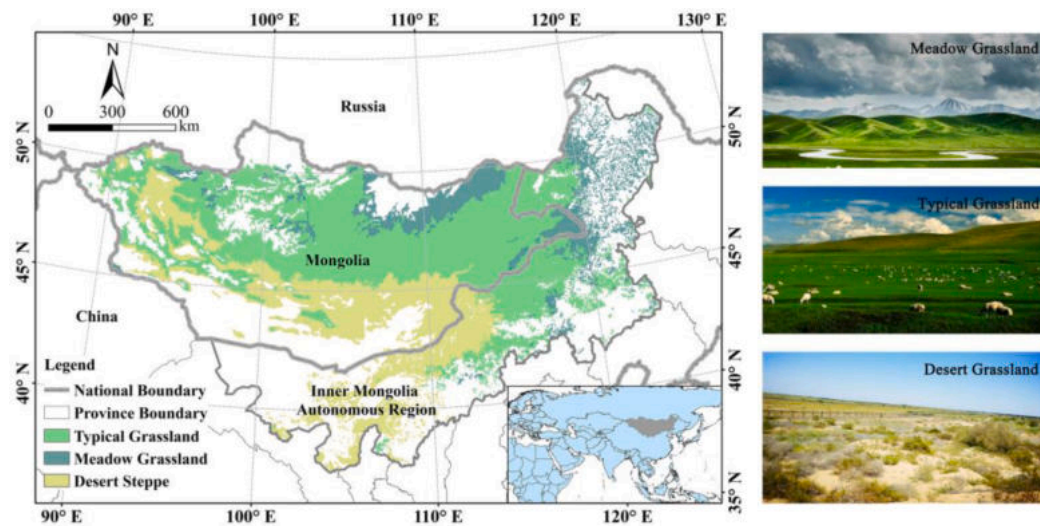
$$AI = \frac{PPT}{PET} \tag{1}$$

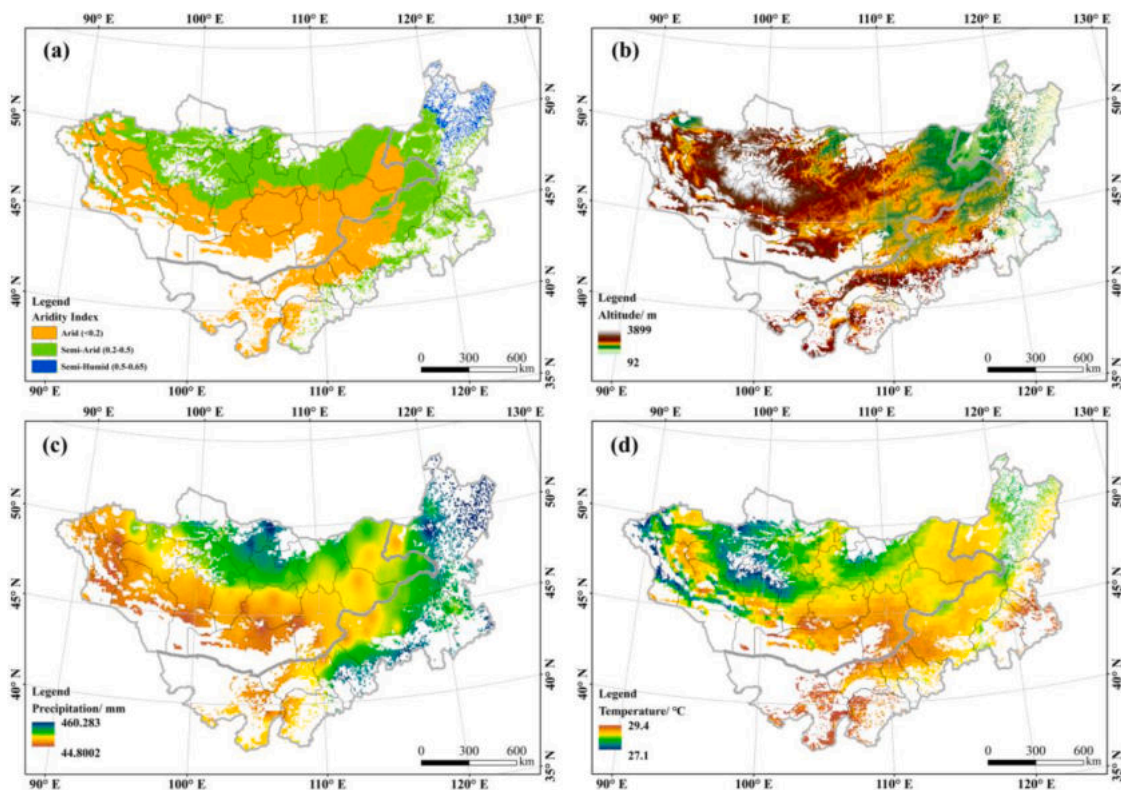**Fig. 1.** Location and grasslands distribution of the Mongolian Plateau.

Fig. 2. Spatial patterns of (a) aridity index, (b) altitude, (c) growing season precipitation and (d) growing season mean temperature of the Mongolian Plateau.

where PPT is the average growing season precipitation (mm), PET is the average growing season potential evapotranspiration (mm). According to the standard established by the United Nations Environment Program (1992), the Mongolian Plateau is divided into the "arid region" as $0 < AI < 0.2$, "semi-arid region" is $0.2 < AI < 0.5$, and "semi-humid region" is $0.5 < AI < 0.65$ (Fig. 2(c)).

2.2.4. Soil moisture data

The ERA-5 SM product provides a monthly $0.1° \times 0.1°$ resolution with precise accuracy and performance (See Fig. S1 for comparing soil moisture products) (Cheng et al., 2019; Zhang et al., 2018). We choose the 0–7 cm volumetric soil moisture to characterize the surface water

content changes in the study areas (Zhang et al., 2018), which is available at https://cds.climate.copernicus.eu/cdsapp/dataset/.

2.2.5. Elevation data

The Digital Elevation Model data (GDEMV2) are about 30 m resolution, obtained from the Geospatial Data Cloud (http://www.gscloud.cn/#page1/1). For consistency, all datasets finally generated the long-term series (2000–2018) with a yearly $0.1°$ to match the ERA-5 data.

2.3. Methods

2.3.1. Calculation of PUE and SWUE

PUE and SWUE are defined as the ratio of GPP to precipitation and soil moisture, respectively.

$$PUE = \frac{GPP}{PPT} \tag{2}$$

$$SWUE = \frac{GPP}{SM} \tag{3}$$

where GPP is the total growing season grasslands productivity ($gC \cdot m^{-2} \cdot mm^{-1}$). PPT is the growing season total precipitation (mm). SM is the average growing season soil moisture (cm^3/cm^3). We calculate the PUE and SWUE in each grid cell from 2000 to 2018 using the raster calculation function in ArcGIS.

2.3.2. Statistical analysis

Pearson's correlation coefficient is applied to examine the spatial correlation between the GPP and moisture conditions. Significance of correlation is assessed at $P < 0.05$. Statistical analysis of the variations of PUE and SWUE with longitude and latitude scales. Analyzing the spatial relationship between PUE and precipitation, SWUE and soil moisture. This study calculates the growing season average PUE (SWUE) from a range with a set step size of 0.01 mm precipitation ((cm^3/cm^3) soil moisture). In addition, differences in average PUE and SWUE among different grassland ecosystems are evaluated, respectively.

2.3.3. Sen's slope

The Sen's slope trend analysis mainly describes the rising or falling trend characteristics in the time series of the PUE (SWUE) data. It can effectively reduce noise interference (Gocic and Trajkovic, 2013; Sen, 1968). The formula is as follows:

$$\beta = Median\left(\frac{x_j - x_i}{j - i}\right), \forall_j > i \tag{4}$$

where $1 < j < i < n$, n is the length of the study period, x_i and x_j are the values of growing season PUE (SWUE) in year i and j respectively, *Median* is the median function, and β is the Sen's slope degree. When $\beta > 0$, PUE (SWUE) presents an upward trend. The larger the value of β, the more obvious the upward trend, and vice versa.

2.3.4. Mann-Kendall test

The Mann-Kendall (MK) test is applied to assess the significance level of Sen's slope trend. This method reveals the trend change characteristics of time series well. And it is recommended for trend analysis and research of meteorological and hydrological variables (Gocic and Trajkovic, 2013; Kendall, 1948). The formula is as follows:

$$S = \sum_{i=1}^{n-1} \sum_{j=i+1}^{n} sgn(x_j - x_i) \tag{5}$$

$$sgn(x_j - x_i) = \begin{cases} 1, & x_j - x_i > 0 \\ 0, & x_j - x_i = 0 \\ -1, & x_j - x_i < 0 \end{cases} \tag{6}$$

When $n \geq 10$, the standard normal test statistic Z of S can be calculated as follows:

$$Z = \begin{cases} \dfrac{S-1}{\sqrt{VAR(S)}}, & S > 0 \\ 0, & S = 0 \\ \dfrac{S+1}{\sqrt{VAR(S)}}, & S < 0 \end{cases} \tag{7}$$

$$VAR(S) = \frac{n(n-1)(2n+5) - \sum_{i=1}^{m} t_i(t_i-1)(2t_i+5)}{18} \tag{8}$$

where n is the number of data points in the series, m is the number of repeated datasets in the series, and t_i is the number of repeated data values in the i th group. At a given significance level, p = 0.05, the normal distribution threshold is $Z_{1-p/2}$. When $|Z| \leq Z_{1-p/2}$, accept the null hypothesis (the trend is insignificant), if $|Z| > Z1-p/2$, reject the null hypothesis (the trend is significant), indicating that PUE (SWUE) has a significant increase ($Z > 0$) or decrease ($Z < 0$) trend. According to Sen's slope and MK test results, four types of PUE (SWUE) changes are obtained, including significant increase, insignificant increase, significant decrease, and insignificant decrease.

2.3.5. Hurst exponent and rescaled range analysis

The Hurst exponent is widely utilized to analyze the correlation of long-term series data to obtain the long-term persistence characteristics (Flynn and Pereira, 2013). We use Rescaled range (R/S) analysis (Hurst exponent) to calculate whether the long-term PUE (SWUE) series (2000–2018) for a continued trend in the future. The formulas of R/S analysis are as follows (Parry et al., 2007; Tong et al., 2018a; Tong et al., 2018b):

Given a time series of $x(t)$ as:

$$\langle x \rangle_t = \frac{1}{\tau} \sum_{t=1}^{\tau} x(t) \quad t = 1, 2, 3 \dots \tag{9}$$

where t is the number of data points in the series, x is the data value in the series, τ is the total number of data points in the series, $\langle x \rangle_t$ is the mean value in the series.

$$x(t, \tau) = \sum_{u=1}^{\tau} \left(x(u) - \langle x \rangle_t \right) \quad 1 \leqslant t \leqslant \tau \tag{10}$$

Where $x(t,\tau)$ is the cumulative deviation, and u is the number of repeated datasets in the series.

$$R(\tau) = \max_{1 \leqslant t \leqslant \tau} X(t, \tau) - \min_{1 \leqslant t \leqslant \tau} X(t, \tau) \tau = 1, 2, 3 \dots \tag{11}$$

where $R(\tau)$ is the extreme deviation.

$$S(\tau) = \left[\frac{1}{\tau} \sum_{t=1}^{\tau} \left(x(t) - \langle x \rangle \tau \right)^2 \right]^{\frac{1}{2}} \quad \tau = 1, 2, 3 \dots \tag{12}$$

where $S(\tau)$ is the standard deviation sequence.

$$R/S = R(\tau)/S(\tau) \tag{13}$$

where R/S is the rescaled range.

$$R/S \propto \left(\frac{\tau}{2} \right)^H \tag{14}$$

where H is the Hurst exponent. It shows that the Hurst phenomenon exists in the time series. When H = 0.5, there are no changes. When $0.5 < H < 1$, it indicates that the process will continue, and the future trend has a consistency with the past. When $0 < H < 0.5$, it implies that the future trend is the opposite of the past.

2.3.6. Partial correlation analysis

Finally, we use GPP as the control variable to calculate the partial correlation coefficient to explore the response of the Mongolian Plateau grassland PUE and SWUE to changes in climatic factors (precipitation and temperature). This method can effectively remove the influence of the control variables and measure the degree of correlation between two random variables (Akritas and Siebert, 1996).

3. Results

3.1. Responses of GPP to PPT and SM across the Mongolian Plateau's grasslands

Fig. 3 shows the spatial correlation and significance of GPP to precipitation and soil moisture of the Mongolian Plateau's grasslands during 2000–2018. A significant positive correlation was observed between GPP and PPT in Inner Mongolia and Eastern Mongolia, while the insignificant negative correction between them was found in the Khangai-Khentei Mountains Region in Western Mongolia and the Greater Xing'an Mountains in Northeast Inner Mongolia (Fig. 3(a)). The response of GPP to SM shows that grassland vegetation growth is largely limited by soil moisture. More than 71.7 % of the study area exhibits a significant positive correlation, of which 43.4 % has a strong correlation (R_{GPP-SM} greater than 0.8), indicating that as compared to PPT, SM greatly influences GPP (Fig. 3(b)). Therefore, we further analyze the strong correlation between soil moisture and grassland vegetation growth by comparing PUE and SWUE.

3.2. Spatial patterns of PUE and SWUE across the Mongolian Plateau's grasslands

3.2.1. Spatial distribution of PUE and SWUE

The spatial distribution of average PUE and SWUE from 2000 to 2018 is shown in Fig. 4. There is a solid spatial agreement among PUE and SWUE across the Mongolian Plateau's grasslands, with a step-wise gradient from southwest to northeast. Their distributions show similar patterns, with relatively low values in arid areas and higher values in semi-humid areas. The PUE value ranges from<0.7 gC·m^{-2}·mm^{-1} to >3.5 gC·m^{-2}·mm^{-1}. The PUE of the semi-humid and high-altitude ecosystems near the Greater Xing'an Mountains and the Khangai-Khentei Mountains Region is relatively high, whereas lower values are found in the arid ecosystems at the edge of the Altai Gaadach Gov. There is a huge difference in PUE between biomes (Fig. 4(a)). Meadow grassland has the highest PUE, followed by typical grassland, and desert steppe has a lower PUE. This spatial distribution pattern also applies to the SWUE. Compared with the spatial distribution of PUE, SWUE shows notable speckling with values ranging from<0.6 gC/kg·H$_2$O to greater than 3.0 gC/kg·H$_2$O. However, there is no longer higher SWUE near the Khangai-Khentei Mountains Region, and the transition to the surrounding grassland is relatively smooth.

3.2.2. Variations in PUE and SWUE with longitude and latitude

Fig. 5 displays the results of variation in PUE and SWUE with latitude and longitude. From the longitudinal changes (Fig. 5(a), (c)), the two indicators across the Mongolian Plateau's grasslands show a similar "increase-decrease-increase" trend from west to east. However, differences in the spatial distribution of PUE and SWUE are evident. The PUE value fluctuates greatly with longitude. It increases sharply to the peak value of 3.32 gC·m^{-2}·mm^{-1} at 103°E, then drops dramatically at a rate of 0.34 gC·m^{-2}·mm^{-1} per degree, and increases sharply again after 108°E. Compared with PUE, the dynamic change of SWUE is smoother. There is a mild increase and decrease west of 103°E and between 103 and 108°E for SWUE. SWUE increases sharply east of 108°E to the maximum value of 2.90 gC/kg·H$_2$O. While both PUE and SWUE rebound slightly east of 120°E. From the latitudinal changes (Fig. 5(b), (d)), the two indicators show a similar "slight fluctuation-increase-decline" trend from south to north. The PUE and SWUE values fluctuate slightly in the region below 46°N, rapidly increasing to the maximum in the 46-51°N area, followed by a downward trend above 51°N. The maximum values of the two indicators are 2.80 gC·m^{-2}·mm^{-1} and 2.80 gC/kg·H$_2$O, respectively.

3.2.3. The relationship between the spatial distribution of PUE, SWUE and the water composition factors

As shown in Fig. 6(a), the PUE of the Mongolian Plateau grasslands shows a "rapid increase-sharp decrease-steady increase-slight decrease" trend throughout the precipitation range. In areas where the growing season precipitation is <147 mm, PUE increases to the first peak at 106 mm and then decreases with the increase in precipitation. This area corresponds spatially to the arid desert steppe region of the southwestern Mongolian Plateau (Fig. 6(b)). The areas with PUE > 1.5 are mainly distributed in the Khangai-Khentei Mountains Region. The grassland area with growing season precipitation of 148–359 mm accounts for 61.03 % of the total grassland area, and the typical grassland and meadow grassland are alternately distributed. PUE increases steadily with the increase in precipitation ($R^2 = 0.56$, P < 0.05), the rate of change is about 0.63 gC·m^{-2}·mm^{-1} per 100 mm, and reaches the second peak at 359 mm. This growing season precipitation range corresponds to the north and southeast areas of the Mongolian Plateau, spanning from arid, semi-arid to sub-humid regions. Areas with growing season precipitation greater than 360 mm are mainly located in northeastern Inner Mongolia's semi-humid meadow grassland regions. Overall, the spatial distribution of grassland PUE increases in precipitation.

SWUE shows a similar trend to PUE, with a "modest increase-slight decrease-rapid increase-sharp decrease" trend in the entire soil moisture range (Fig. 7(a)). In arid desert steppe regions with SM <0.141 cm^3/cm^3, SWUE increases and then decreases with the increase of SM. In areas of SM = 0.068 cm^3/cm^3, the first smaller peak appears in SWUE. In the range of 0.141–0.345 cm^3/cm^3, SWUE increases rapidly with the rise of SM ($R^2 = 0.65$, P < 0.05), the changing rate is about 8.3 gC/kg·H$_2$O per cm^3/cm^3, and reaches the maximum at 0.345 cm^3/cm^3. The
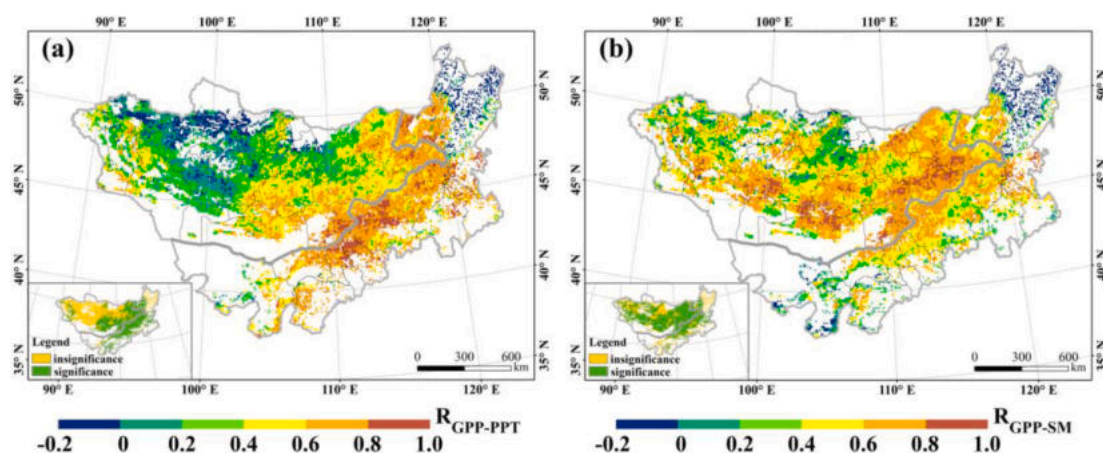

Fig. 3. The response of (a) GPP to PPT and (b) SM of the Mongolian Plateau grassland ecosystems from 2000 to 2018.
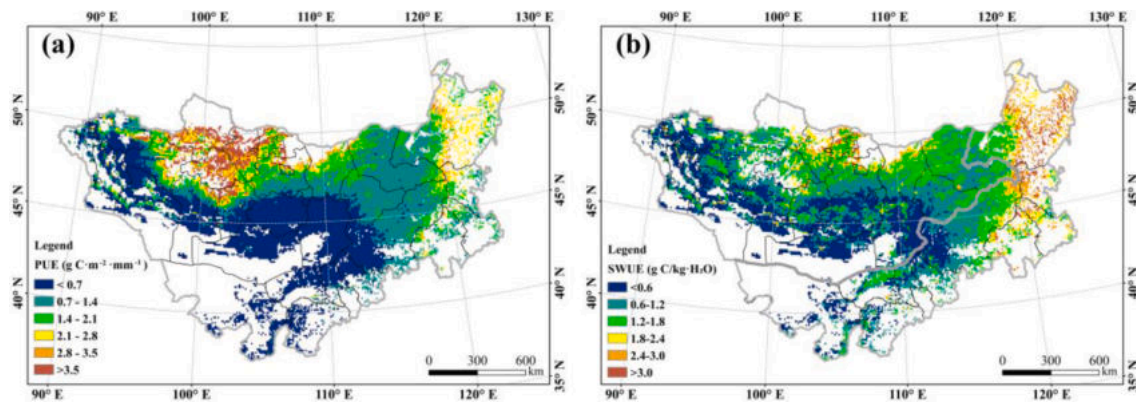
Fig. 4. Spatial distribution and dynamics of (a) PUE and (b) SWUE across the Mongolian Plateau's grasslands from 2000 to 2018.
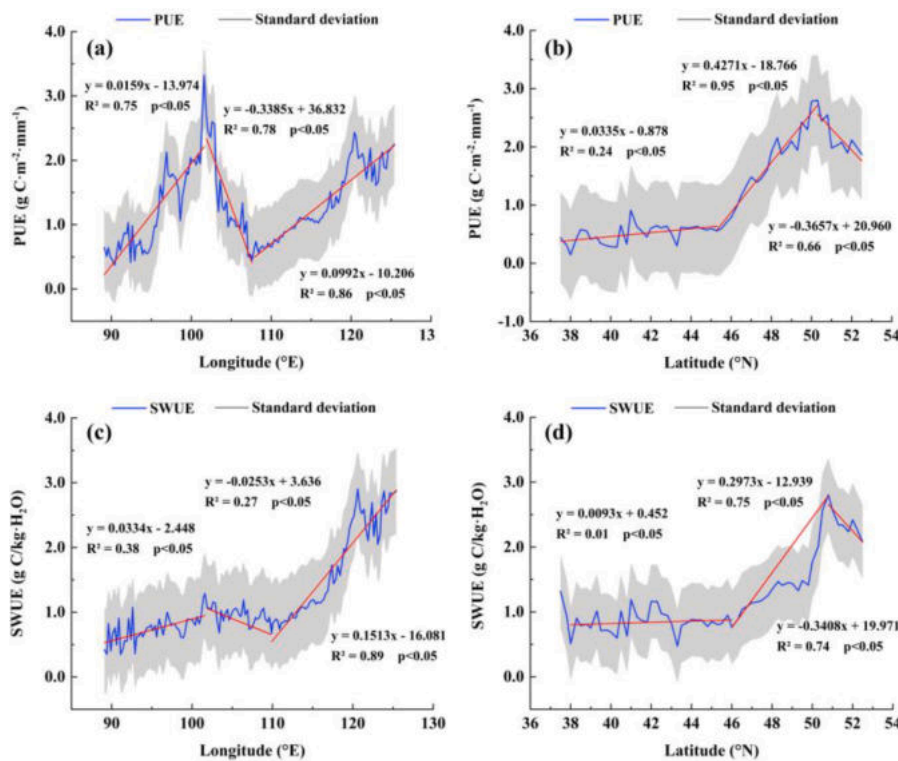

Fig. 5. Variations in (a) (b) PUE and (c) (d) SWUE with longitude and latitude across the Mongolian Plateau's grasslands from 2000 to 2018.

grassland area in this range accounts for 72.16 % of the total grassland area, almost occupying all typical grasslands and meadows grassland in semi-arid and semi-humid regions (Fig. 7(b)). Areas with soil moisture greater than 0.345 cm^3/cm^3 are scattered in northeastern Inner Mongolia, Dornod and Suekhbaatar Aymags of Mongolia. However, SWUE rebounds slightly after the SM reaches 0.391 cm^3/cm^3.

3.3. PUE and SWUE for different grassland types during 2000–2018

Fig. 8 summarizes the average PUE and SWUE of the growing season across the Mongolian Plateau grassland biome from 2000 to 2018, which are 1.07 $gC·m^{-2}·mm^{-1}$ and 1.03 $gC/kg·H_2O$, respectively. There are significant differences in various grassland types. Meadow grassland has the highest PUE and SWUE, followed by typical grassland, and desert steppe has the lowest values. It is obvious that typical grassland dominates the grassland types (57.04 %) of the Mongolian Plateau, so that the two WUEs metrics of typical grassland are closer to the average values of entire grasslands. Generally, relatively humid ecosystems have

higher PUE and SWUE, whereas arid ecosystems exhibit opposite patterns (He et al., 2017).

As shown in Fig. 9, the two WUEs indicators of the Mongolian Plateau grasslands show an overall upward trend from 2000 to 2018, whereas SWUE increased more significantly. The inter-annual variation of PUE fluctuates greatly, while SWUE is relatively stable. Among the three grassland types, the PUE values of meadow grassland and typical grassland have larger fluctuation ranges, which are 1.04–1.54 $gC·m^{-2}·mm^{-1}$ and 0.82–1.47 $gC·m^{-2}·mm^{-1}$, respectively. The desert steppe has a relatively small range, ranging from 0.48—0.74 $gC·m^{-2}·mm^{-1}$. The larger PUE of various grassland types mainly appeared in 2005, 2009 and 2011, and the lower values appeared in 2003, 2008 and 2012, with high and low values alternately appearing. However, SWUE values change in a small range, showing a gradually increasing trend year by year, with maximum values in 2012 and minimum values in 2007.
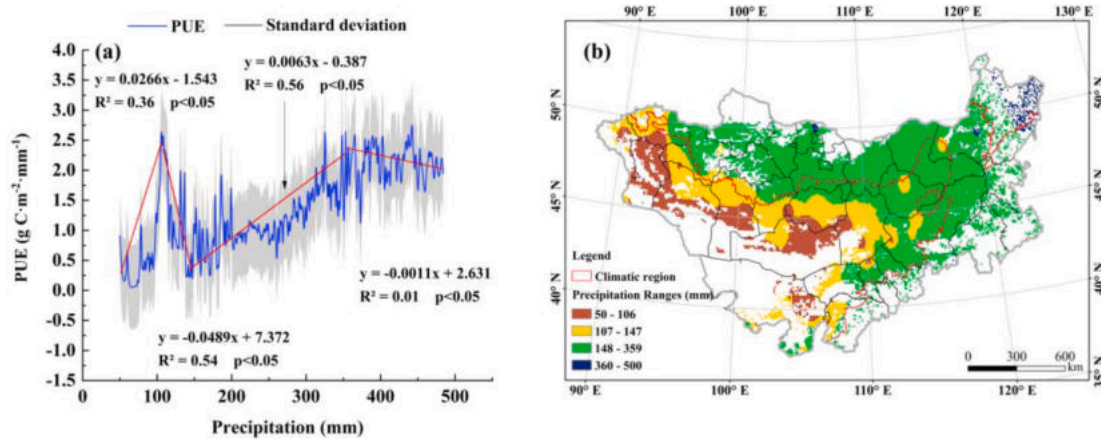
Fig. 6. Pattern of changes in PUE with precipitation (a) and the spatial distribution of areas with different precipitation ranges (b) in the Mongolian Plateau's grasslands.
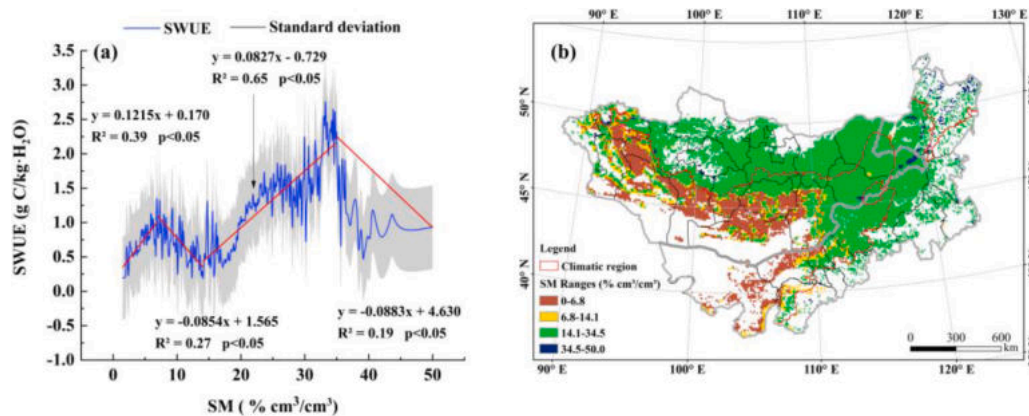

Fig. 7. Pattern of changes in SWUE with soil moisture (a) and the spatial distribution of areas with different soil moisture ranges (b) in the Mongolian Plateau's grasslands.
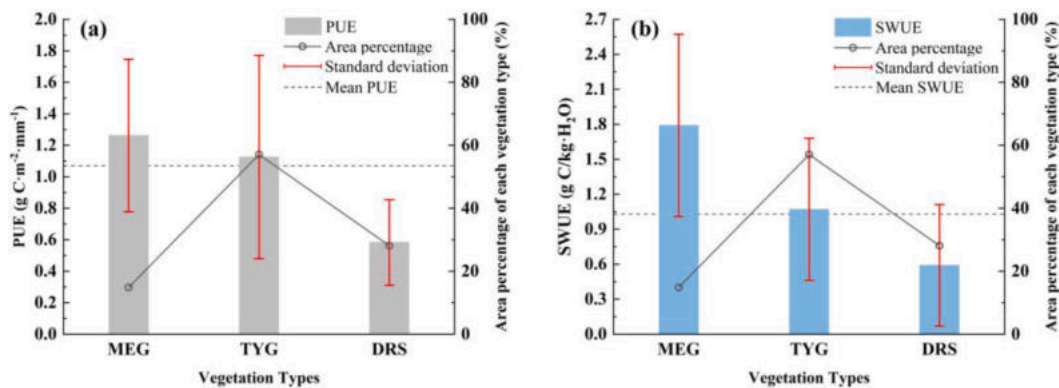

Fig. 8. Characteristics of (a) PUE and (b) SWUE in different grassland ecosystems from 2000 to 2018.

3.4. Variation trends of PUE and SWUE across the Mongolian Plateau's grasslands

In addition to the inter-annual variation trend of PUE and SWUE, further studies about the spatial variation trends of two indicators in the Mongolian Plateau grassland have also been detected. We use Sen's slope trend analysis to calculate the linear trend of PUE (Fig. 10(a)). There are 61.39 % of the grasslands have a positive slope, indicating that the PUE increased in most areas from 2000 to 2018. Especially in the

hinterland of the Mongolian Plateau, the positive trend is more concentrated. While the areas where PUE decreased are mainly located in the central and eastern portion of Inner Mongolia and scattered in the Great Lakes Region of northwestern Mongolia. Fig. 10(b) shows the significance of the linear regression trend using the MK test (P = 0.05). Approximately 96.70 % of the grassland has not passed the MK test, indicating no changing trend within those regions. In contrast, the areas with significantly reduced PUE are 5.23×10^4 km^2, accounting for only 3.30 % of the grassland area. In eastern Inner Mongolia, these areas
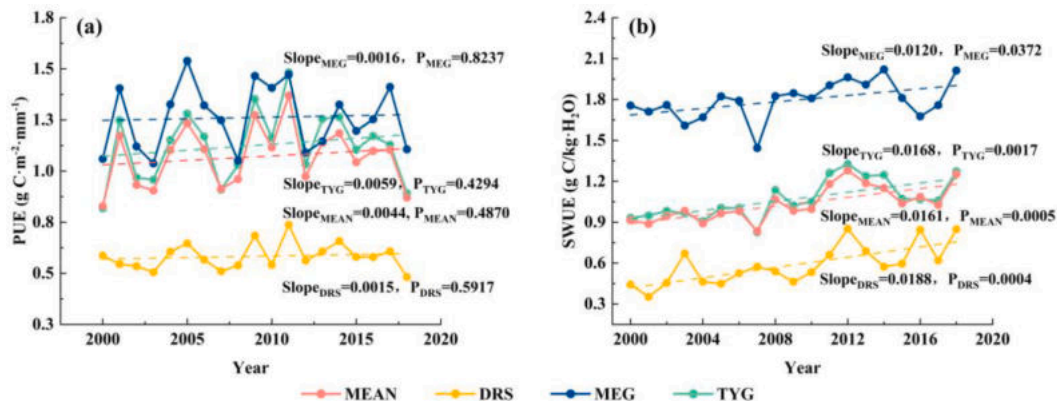
Fig. 9. Inter-annual variations of (a) PUE and mean precipitation, (b) SWUE and mean soil moisture of grasslands in the Mongolian Plateau from 2000 to 2018.
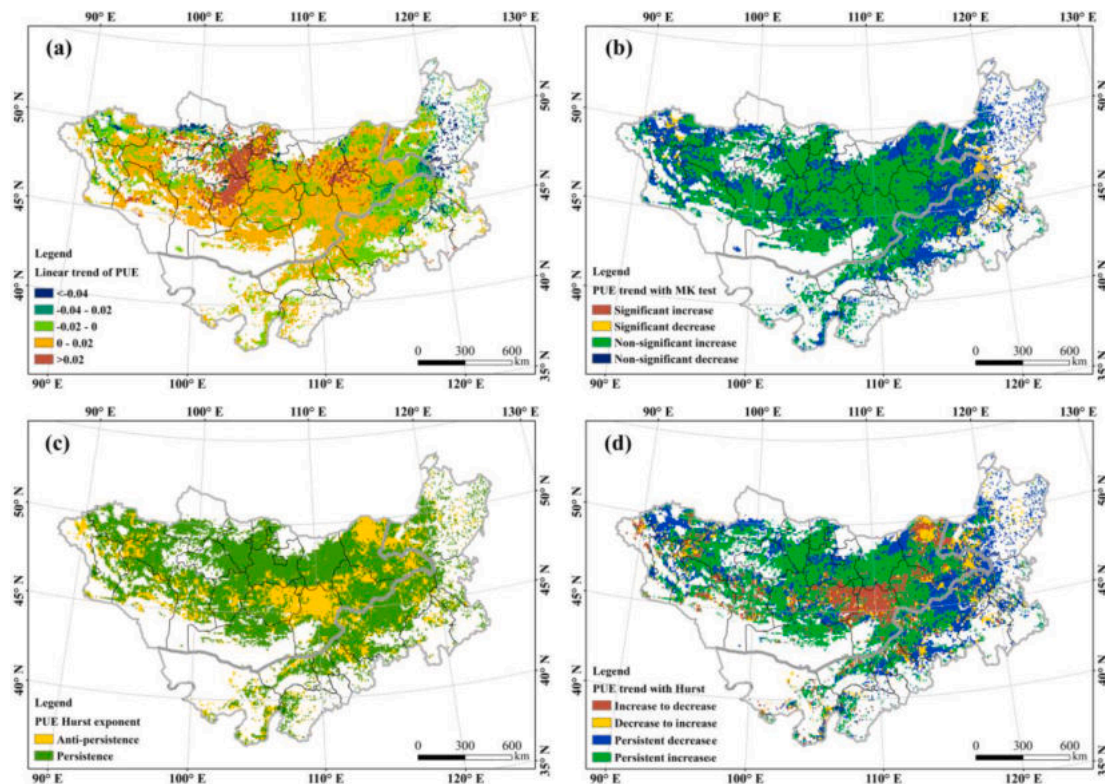

Fig. 10. (a) Linear trend, (b) significance test, (c) Hurst exponent and (d) sustainability of PUE in the Mongolian Plateau's grasslands from 2000 to 2018.

scatter in Hulunbuir, Hinggan League, Xilin Gol, Tongliao, and Chifeng City. In addition, these areas are also distributed in Dornod Aymag in the east of Mongolia, Ubsa Aymag and Hovd Aymag in the west. According to the variation trend of PUE, we use Hurst exponent analysis to explore its long-term persistence characteristics. Fig. 10(c) exhibits that 76.81 % of the grassland has long-term persistence characteristics and will continue to maintain the original change trend, whereas 23.19 % of the regions have anti-persistence characteristics and will reverse the previous change trend. Combining the previous linear change trend, we obtain the future change trend of PUE (Fig. 10(d)). PUE of 29.08 % of the grassland will continue to decline in the future. These areas are mainly distributed in Hulunbuir, Hinggan League, Xilin Gol League, Tongliao City in eastern Inner Mongolia and high-latitude regions of Mongolia. In addition, PUE will decrease persistently in some areas scattered in central Mongolia. However, PUE in 47.35 % of the grassland will continue to improve in the future, where is concentrated in the hinterland of Mongolia Plateau except for the Central Gobi. It indicates that

the relatively severe grassland growth environment in the central Gobi area leads to its more complicated future variation trend than in other regions.

Linear trend analysis shows that SWUE in 57.99 % of the grasslands with a positive slope (Fig. 11(a)), indicating that SWUE has also improved in most areas. Compared with PUE, the regions of SWUE changes are relatively scattered. Similarly, the changing trend of SWUE in 98.03 % of the grasslands is non-significant (Fig. 11(b)). SWUE significantly reduced areas scattered in the Greater Xing'an Mountains and the Great Lakes Region. As shown in Fig. 11(c), 64.32 % of the grassland area will continue to maintain the original change trend, while 35.68 % will change to the opposite trend. Notably, the area of SWUE with a reversal trend is also concentrated in the central Gobi areas, similar to that of PUE, whereas SWUE shows more speckling. The areas where SWUE will continue to decrease in the future scatter in various regions of the Mongolian Plateau, but still with 29.08 % of the grassland. In addition, 44.69 % of the grassland will improve in the future, mainly
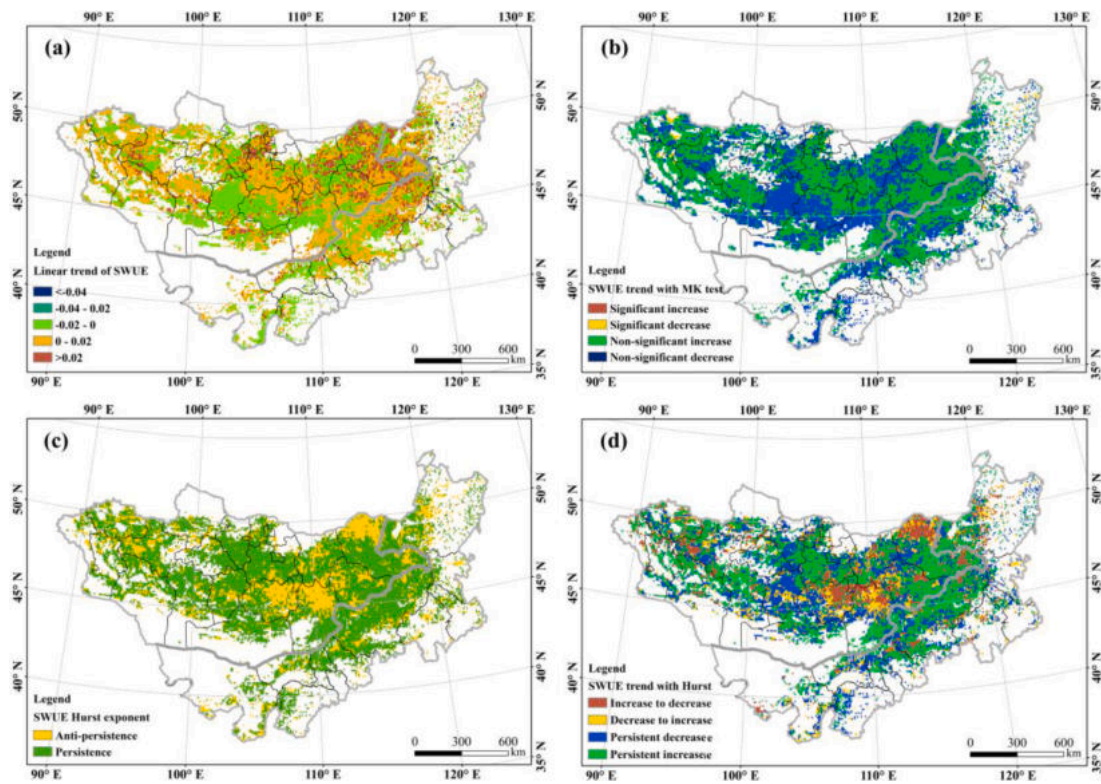
Fig. 11. (a) Linear trend, (b) significance test, (c) Hurst exponent and (d) sustainability of SWUE in the Mongolian Plateau's grasslands from 2000 to 2018.
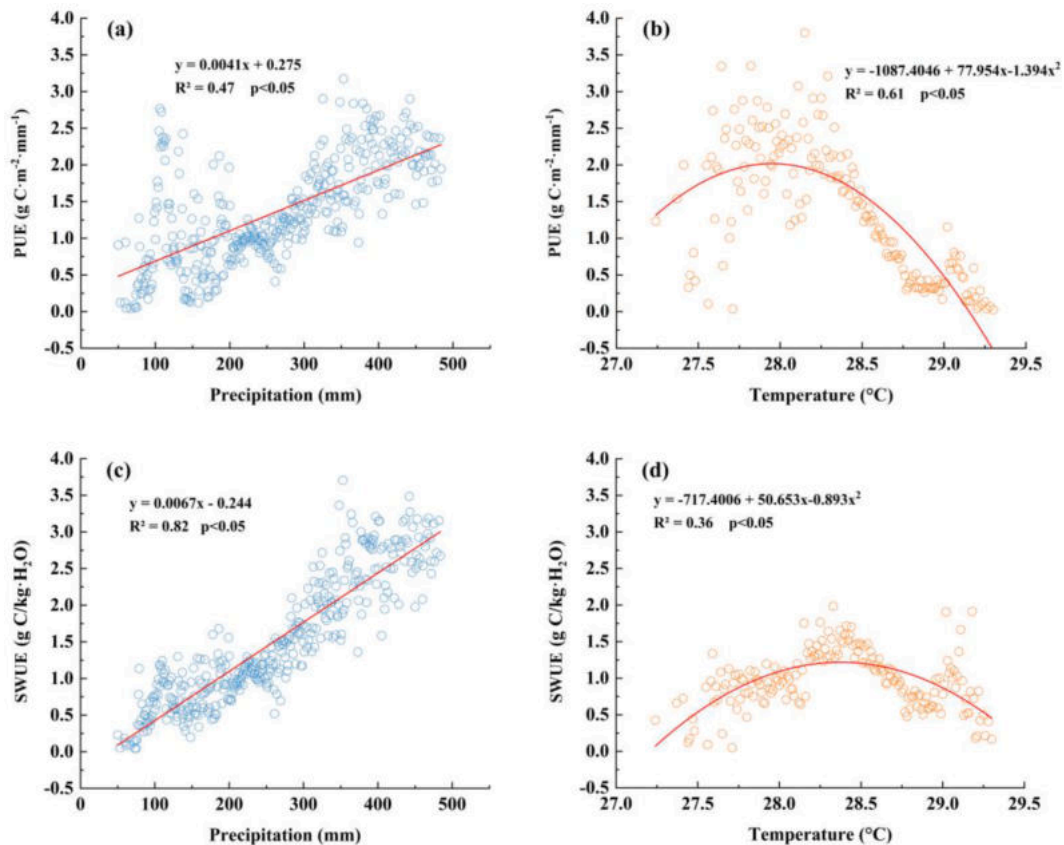

Fig. 12. Relationships of (a) (b) PUE, (c) (d) SWUE with precipitation and temperature from 2000 to 2018.

distributed in semi-arid typical grassland regions (Fig. 11(d)). It implies that the soil moisture conditions in the semi-arid region are more suitable for the growth of typical grasslands.

3.5. Driving factors of PUE and SWUE in various ecosystems

Precipitation and temperature are the most important driving factors affecting vegetation growth in arid and semi-arid regions. We calculated the partial correlation under the controlled variable of GPP to explore the responses of PUE and SWUE to climatic factors in the Mongolian Plateau grassland. Generally, there is a positive linear correlation between PUE and precipitation ($R^2 = 0.47$, P < 0.05), but a larger peak appears where the precipitation is near 100 mm (Fig. 12(a)). A unimodal correlation exists between PUE and temperature ($R^2 = 0.61$, P < 0.05) (Fig. 12(b)) and peaks at 28.2℃. Similarly, there is a positive linear correlation between SWUE and precipitation ($R^2 = 0.82$, P < 0.05), and the correlation is stronger than that between PUE and precipitation. SWUE has a peak where the precipitation is close to 100 mm, but the peak is much smaller than PUE (Fig. 12(c)). The relationship between SWUE and temperature is similar to that between PUE and temperature, with a peak at 28.3 °C. SWUE is less sensitive to temperature than PUE ($R^2 = 0.36$, P < 0.05) (Fig. 12(d)).

As mentioned above, we applied a similar analysis to different grassland ecosystems. Fig. 13(a)-(c) shows that the precipitation has a diverse correlation with PUE in different grassland ecosystems. The meadow grassland PUE negatively correlates with precipitation (R = −0.09, P < 0.05), indicating PUE_{MEG} would decline with increased precipitation under the controlled GPP. While PUE of typical grassland and desert steppe positively correlates with precipitation. These two grasslands account for 85.16 % of the whole grassland area, representing the overall trend of the Mongolian Plateau grassland. In contrast, the temperature has the same negative correlation with PUE for all grassland types with high correlation coefficients ranging from −0.51 to −0.72 (P < 0.05) (Fig. 13(d)-(f)). From the perspective of SWUE, the three grassland types all have a strong positive correlation with precipitation and are significantly higher than that of PUE (Fig. 13(g)-(i)). However, there is a positive correlation between the temperature and

SWUE for all grassland types (Fig. 13(j)-(l)), and the correlation coefficient is much lower than that of PUE. Except for typical grasslands (R = 0.49, P < 0.05), temperature insignificantly correlated with SWUE in other types of grasslands. This temperature-SWUE relationship implies that the ability of grassland ecosystem vegetation to absorb soil moisture is less affected by temperature.

4. Discussion

4.1. Spatial distribution and changes in PUE and SWUE

From the spatial patterns of PUE and SWUE, it can be seen that the two indicators have similar spatial patterns. Their spatial distributions are consistent with the available water resources, decreasing from northeast to southwest, which is similar to the latest studies on water use efficiency (Dong et al., 2021; Sun et al., 2022; Zhu et al., 2020). Due to the different species richness of the three grassland types, meadow grasslands have the highest PUE and SWUE, followed by typical grasslands and desert steppes. Previous studies have illustrated a positive correlation between species richness and GPP, especially on a larger scale (Hobi et al., 2017; Phillips et al., 2008; Power and Cardinale, 2009; Tilman et al., 2001). Due to the complementary niches, more species may imply more efficient use of precipitation and soil moisture (Bai et al., 2004; Yang et al., 2010). Higher species richness may also mean that ecosystems contain more functional groups that respond to higher moisture (Hobi et al., 2017; Phillips et al., 2008; Power and Cardinale, 2009; Ren et al., 2010). In addition, human activities and ecosystem degradation leading to land cover change greatly affect the PUE and SWUE of desert steppe (Tesfaye et al., 2021; Oliveira et al., 2021; Akiyama and Kawamura, 2007). The two indicators in relatively humid ecosystems are generally higher than arid ecosystems, especially in the Greater Xing'an Mountains in the northeast. This could be explained by the fact that wet ecosystems have a higher leaf area than grasslands in arid ecosystems, preventing soil evaporation from soil water loss (Hungate et al., 2002). In addition, humid ecosystems receive nutrient enrichment or have high nutrient turnover. More favorable water, sunlight, and temperature conditions, consistent with the presence of
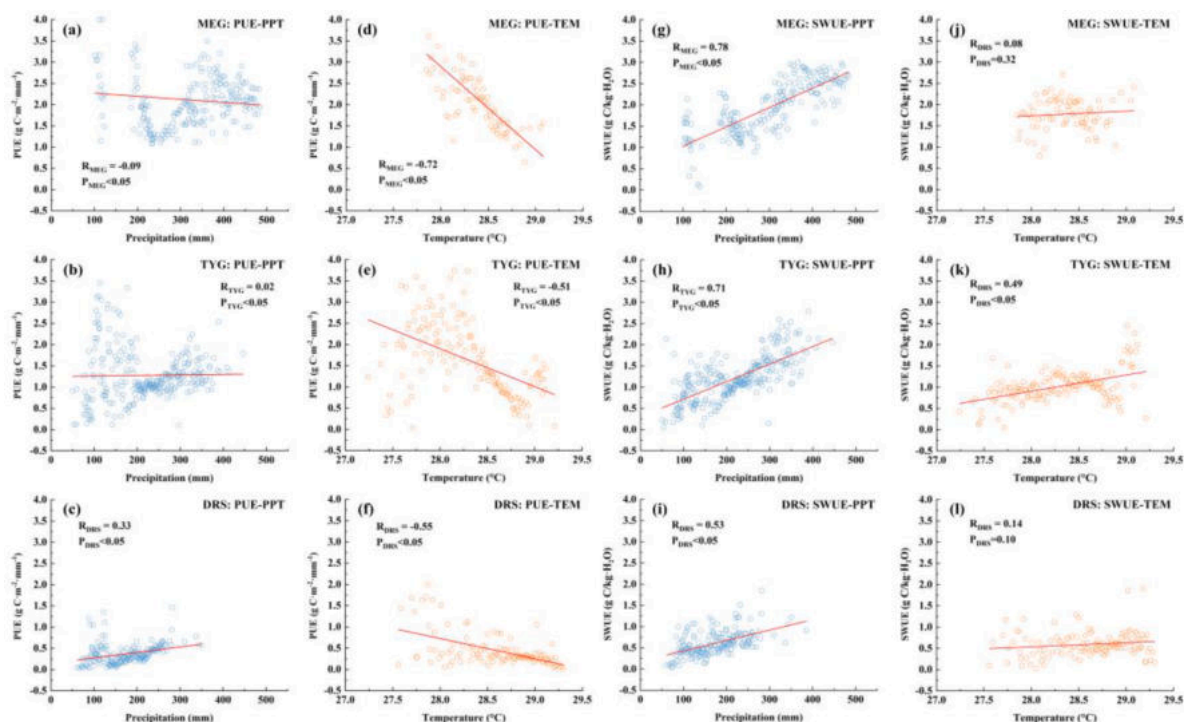

Fig. 13. Relationships of PUE, SWUE with climatic factors in various grassland ecosystems from 2000 to 2018.

dense vegetation, resulted in the higher GPP and PUE (SWUE) (He et al., 2017; A et al., 2015; NOE and Childers, 2007). Other factors, including soil texture and vegetation types, may also affect the differences in PUE and SWUE between arid and wet ecosystems (Breshears and Barnes, 1999; He et al., 2017; Vereecken et al., 1989).

There are also differences in the spatial distribution of PUE and SWUE. The PUE of the Khangai-Khentei Mountains Region is significantly higher than that of the surrounding areas, which is the same area where the insignificant negative correlations between GPP and PUE. This indicates that precipitation is not the most important factor, while temperature and leaf area greatly affect GPP and PUE in high-altitude areas (Hu et al., 2010; Hirota et al., 2006; Gilgen and Buchmann, 2009; Kuslu et al., 2010; Sun and Du, 2017). At the same time, the spatial changes of SWUE in this area are relatively smooth. The higher PUE may be due to the influence of the topography. The amount of precipitation received and runoff occurring everywhere on the surface are unequal, leading to a decrease in the available precipitation and supplementation of soil moisture. Despite of that precipitation variability increases greatly with altitude, soils can temporarily store rainfall and gradually leach it which results in slow changes in soil moisture (Cheng et al., 2020; Ohnuki et al., 2008). Therefore, the PUE value in this area is relatively high, while the SWUE is relatively stable.

Furthermore, the two indicators have highly consistent spatial distribution patterns in the longitude and latitude scales. However, the range of variation of PUE with longitude is significantly larger than that of SWUE. The maximum PUE and relatively small peaks of SWUE exist at around 103°E, which spatially corresponds to the Khangai-Khentei Mountains Region, consistent with our previous results on spatial distribution. The arid area with PPT < 100 mm is located in the area west of 103°E. Precipitation is the main limiting factor for vegetation growth in the arid region (Huxman et al., 2004; Mu et al., 2017; Mu et al., 2014). The average precipitation from 2000 to 2018 increased, which improved the water supply capacity of the soil, strengthened the efficiency of photosynthesis and increased GPP (Huxman et al., 2004; Jia et al., 2015; Mu et al., 2014; Sun and Du, 2017). PUE and SWUE increase accordingly as well. The decreasing trend of two indicators in 103-108°E may be that the longitudinal increase rate of GPP is less than that of moisture conditions. The same is true for rebounds after 120°E. The regional of 108-120°E has obvious longitudinal zonality. With longitude increases, moisture conditions, vegetation productivity and two WUEs indicators increase rapidly (Bai et al., 2008; Mu et al., 2017; Mu et al., 2014; Sun et al., 2018). The two indicators of the regions below 46°N degrees fluctuate smoothly. The reason may be that the GPP increases linearly with the abundance of water availabilities, resulting in a relatively stable water use efficiency (Bai et al., 2004). The regional zonality within the range of 46-51°N is evident, and two indicators increase rapidly with latitude. The low temperature in areas higher than 51°N inhibits vegetation growth and GPP, which leads to a decrease in PUE and SWUE (Hu et al., 2010; Soolanayakanahally et al., 2009; Sun and Du, 2017).

4.2. Variation regularity of water use efficiency with the gradient of water composition factors

There is a peak in PUE and SWUE in the extremely arid area of Mongolian Plateau grassland, consistent with the results of previous studies (Hu et al., 2010; Mu et al., 2017; Mu et al., 2014; Sun and Du, 2017). In addition, Wu et al. (2009) stated that on the arid side of precipitation (PPT < 150 mm), the spatial distribution of PUE increases and then decreases with the rise of precipitation. The reasons why grassland PUE (SWUE) is abnormal in extremely arid regions include: firstly, the redistribution of precipitation caused by topographical factors may be one of the reasons for the high PUE of the grassland in this area. The grassland grows better under limited precipitation because the regional runoff and soil moisture are recharged by the ice and snow meltwater from the high mountains (Lowry et al., 2011; Mu et al., 2017; Yang et al.,

2010). Secondly, plants with strong rooting systems in arid areas can utilize the soil moisture in the deep layer. At the same time, they have lower canopy conductance and higher production per unit of water consumption (Jobbágy and Sala, 2000; Mu et al., 2017). Thirdly, the proportion of sandy soil in the surface layer of the desert steppe is relatively high, and the infiltration rate of precipitation tends to increase. The available precipitation for vegetation growth decreases, which greatly increases the PUE. It also explains why PUE has a larger peak than SWUE (Le Houérou et al., 1988; Mu et al., 2017). Fourth, some C4 extreme xerophytes are mostly constructive or dominant species of vegetation in extremely arid areas, including *Haloxylon ammodendron*, *Calligortum mongolicum*, *Salsola passerine*, *S. laricifolia*. Compared with C3 plants, C4 plants have a lower transpiration rate and higher photosynthesis rate in an arid environment, so PUE and SWUE may also be higher (Roby et al., 2020; Winslow et al., 2003).

Furthermore, soil moisture is saturated for a long time in humid areas with high annual precipitation. Vegetation roots and soil microorganisms are restricted by oxygen supply and greatly reduce biological activity (Austin and Vitousek, 1998; Perez-Priego et al., 2015). Meantime, the supersaturated rainfall forms surface runoff, which causes the loss of key nutrients (N, P) that are susceptible to leaching from the ecosystem, and indirectly stresses vegetation growth (Austin and Vitousek, 1998). Coupled with the high maintenance respiration and growth respiration caused by high production potential, the two indicators of vegetation decrease with water conditions (Liu et al., 2017; Mu et al., 2017).

Our findings illustrate that in areas with a precipitation range between 148 and 360 mm or soil moisture within 0.14–0.35 cm^3/cm^3, PUE (SWUE) is more sensitive to the changes in water compositions. Sala et al. (1988) believed that the grassland PUE changes with the precipitation gradient in a parabolic pattern. PUE increases with the annual precipitation in 150–500 mm and peaks in 400–600 mm (Hu et al., 2010). The results of this study are slightly different, mainly because we utilize the precipitation in the growing season instead of the annual precipitation, which results in a slightly lower PUE. The increased precipitation in the Mongolian Plateau has improved the soil water supply, and increased vegetation's photosynthesis efficiency and GPP (Mu et al., 2017; Mu et al., 2014; Sun and Du, 2017). Therefore, two WUEs indicators gradually increase within relatively moderate moisture conditions.

4.3. Differences between PUE and SWUE of different grassland types

From the results mentioned above, the increasing trend of two indicators in Mongolian Plateau grasslands from 2000 to 2018 may be related to global warming, especially in the middle and high latitudes (Parry et al., 2007; Tong et al., 2018a; Tong et al., 2018b). The Mongolian Plateau has less heat due to high latitudes and high altitudes. The raised temperatures may cause prolonged vegetation growing season, accelerated growth rate, and enhanced photosynthesis, thereby promoting vegetation growth and improving PUE and SWUE (Huang et al., 2016; Tong et al., 2018a). In addition, the inter-annual variation of PUE fluctuates greatly, indicating that precipitation is more susceptible to the external environment and climate change. However, the soil can temporarily store rainfall and gradually drain it (Cheng et al., 2020; Ohnuki et al., 2008). Therefore, SWUE is relatively more stable than PUE. The average PUE of grasslands on the Mongolian Plateau is 1.07 $gC·m^{-2}·mm^{-1}$, which is within the range of the global arid region grassland PUE (0.05–1.81 $gC·m^{-2}·mm^{-1}$) proposed by Le Houérou et al. (1988). There are significant differences (P < 0.05) in grassland biomes, the PUE from high to low is meadow grassland (1.26 $gC·m^{-2}·mm^{-1}$)-typical grassland (1.13 $gC·m^{-2}·mm^{-1}$)-desert grassland (0.58 $gC·m^{-2}·mm^{-1}$). This result is similar to the PUE result obtained by Mu et al. (2017) in Northwest China grassland. The average SWUE is 1.03 $gC/kg·H_2O$, which is lower than the global grassland SWUE of 2.10$gC/kg·H_2O$ reported by He et al. (2017). It may be because the temperate

savanna was excluded from the grassland group in their study, leading to a higher SWUE of grassland. However, He et al. (2017) also proposed that a relatively high SWUE was observed in humid ecosystems, while lower values were found in arid and high-latitude ecosystems, same as our study results.

From the discussion mentioned above, it is clear that species richness determines the PUE and SWUE of different grassland types. However, they are also restricted by the biological characteristics of individual vegetation and the growth environment (Keddy, 1992; Mu et al., 2017; Tilman, 2020). The desert steppe has the lowest PUE and SWUE. On the one hand, the growing season rainfall in this area is only about 300 mm, and a large amount of evaporation makes the soil water deficit for a long time, which greatly restricts the growth of plants and the maintenance of ecosystem functions (Bogeat-Triboulot et al., 2007; Shao et al., 2009). On the other hand, the desert steppe plants usually have a higher root-to-shoot ratio, smaller leaf area, lower stomatal conductance and other characteristics, resulting in a lower relative growth rate and the lowest PUE and SWUE (Keddy, 1992; Tilman, 2020). The higher PUE and SWUE of meadow grassland also benefit from the abundant precipitation. In addition, the meadow grassland plants have a higher meristem density, resulting in a higher relative growth rate and production potential (Knapp and Smith, 2013; Mu et al., 2017). The typical grassland is widely distributed in various precipitation ranges, and the moderate PUE and SWUE are attributed to the trade-off of multiple factors.

4.4. Driving factors of PUE and SWUE

Further analysis of different climatic factors reveals that the Mongolian Plateau grassland's PUE and SWUE show different response patterns to precipitation and temperature in different grassland ecosystems. Due to the limited precipitation range in the Mongolian Plateau (50–500 mm), the relationship between PUE and precipitation tends to have a positive linear correlation in our study area, and those patterns have all been discussed in the previous analysis (Hu et al., 2010; Mu et al., 2017; Sun and Du, 2017; Zhou et al., 2020). However, it also reflects a negative relationship between PUE and precipitation in semi-humid regions' meadow grassland. On the one hand, in the relatively humid area (PPT > 400 mm), the vegetation growth is limited due to supersaturated precipitation, and PUE decreases with water conditions (Mu et al., 2017; Wu et al., 2009). On the other hand, the high-altitude Khangai-Khentei Mountains Region (PPT < 200 mm) contains some alpine meadows, which will also impact PUE. Therefore, the PUE of the meadow steppe exhibited different responses to precipitation than other grassland types.

Moreover, the interaction effect of temperature and precipitation may also be one of the reasons why the correlation between two indicators and moisture conditions initially increases and subsequently decreases with the moisture gradient (Mu et al., 2017; Mu et al., 2014; Sun and Du, 2017; Yang et al., 2010; Zhou et al., 2020). Temperature and PUE (SWUE) show an obvious unimodal correlation in the entire grassland ecosystem. The increased temperature can extend the growing season of grassland and increase dry-matter accumulation (Sun and Du, 2017; Zhou et al., 2020), resulting in the PUE (SWUE) increase with temperature. In addition, temperature significantly impacts water use efficiency by affecting the evapotranspiration rates. When the temperature reaches the threshold, the evapotranspiration rate increases with temperature and causes the water use efficiency to decrease (Sun and Du, 2017; Vereecken et al., 1989; Yang et al., 2010). However, there are opposite correlations between temperature-PUE and temperature-SWUE in various grassland ecosystems. This temperature-SWUE relationship means that the ability of the grassland ecosystem to absorb soil moisture may be affected by air temperature and soil temperature (Onwuka and Mang, 2018).

5. Conclusion

This paper calculates the PUE and SWUE of Mongolian Plateau grassland from 2000 to 2018 based on multi-source remote sensing data, including observed precipitation and soil moisture data. We explore the spatial and temporal distribution pattern and driving factors of this region's two water use efficiency indicators. These analyses have led to the following main conclusions. (1) The two indicators of the Mongolian Plateau grassland show an overall upward trend from 2000 to 2018, and the average PUE and SWUE are 1.07 $gC \cdot m^{-2} \cdot mm^{-1}$ and 1.03 $gC/kg \cdot H_2O$, respectively. There is a solid spatial agreement between PUE and SWUE, with a step-wise gradient from northeast to southwest, consistent with the available water sources. However, the Khangai-Khentei Mountainous Region has a significantly higher PUE than that in the surrounding area because of the influence of the terrain. (2) The two metrics of Mongolian Plateau grassland are relatively low in extremely arid and humid regions. In areas with relatively moderate water conditions, water use efficiency increases with the abundance of moisture conditions and reaches its maximum value. (3) Within the different moisture conditions ranges, the spatial distribution of PUE and SWUE differs greatly from the moisture factors. In the 148–359 mm precipitation range, PUE increases significantly with the precipitation ($R^2 = 0.56$, P < 0.05) and peaks at 359 mm. In the 0.141–0.345 cm^3/cm^3 soil moisture range, SWUE increased rapidly with SM ($R^2 = 0.65$, P < 0.05). SWUE reaches a peak in the area of SM = 0.068 cm^3/cm^3. (4) There are significant differences among grassland biomes. Meadow grassland has the highest PUE and SWUE, followed by typical grassland and desert steppe. It is mainly due to the different species richness, vegetation's biological characteristics, and the growth environment of the three grassland types. (5) Generally, there is a positive linear correlation between PUE (SWUE) and precipitation, with two peaks at 100 mm and 460 mm. And there is an unimodal correlation between PUE (SWUE) and temperature, with the peak value at about 28.3 °C. However, there are some differences in different grassland ecosystems, especially the meadow grassland. This phenomenon may be due to plants losing water in a humid environment to absorb more soil nutrients. The results of our analysis will help to improve strategies for regulating precipitation and soil water use in the Mongolian Plateau, in order to maintain healthy grassland ecosystems.

Continuing declining water use efficiency in the central Gobi areas of Mongolia deserves major attention. This paper provided a basis for guiding the formulation of effective measures for grassland ecosystem management and protection, improving water resources utilization efficiency, and coping with the impact of global climate change on the carbon–water cycle of grassland ecosystems.

CRediT authorship contribution statement

Xinyi Liu: Conceptualization, Methodology, Software, Validation, Formal analysis, Writing – original draft. **Quan Lai:** Resources, Data curation, Methodology, Software, Writing – review & editing. **Shan Yin:** Conceptualization, Investigation, Validation, Writing – review & editing. **Yuhai Bao:** Supervision, Investigation, Project administration, Funding acquisition. **Song Qing:** Investigation, Validation, Software. **Sainbuyan Bayarsaikhan:** Conceptualization, Investigation, Validation. **Lingxin Bu:** Data curation, Writing – review & editing. **Li Mei:** Data curation, Software, Investigation. **Zhiru Li:** Visualization, Validation. **Jialong Niu:** Software, Investigation. **Yumeng Yang:** Data curation, Investigation.

Declaration of Competing Interest

Data availability

Data will be made available on request.

Appendix A. Supplementary data

Supplementary data to this article can be found online at https://doi.org/10.1016/j.ecolind.2022.109207.

References

A, A., Malenovsky, Z., Ková, J.O., Gallé, A., Rascher, U., Mohammed, G., 2015. Meta-analysis assessing potential of steady-state chlorophyll fluorescence for remote sensing detection of plant water, temperature and nitrogen stress. Remote Sens. Environ. 168, 420–436.

Akiyama, T., Kawamura, K., 2007. Grassland degradation in China: methods of monitoring, management and restoration. Grassland Sci. 53, 1–17.

Akritas, M.G., Siebert, J., 1996. A test for partial correlation with censored astronomical data. MNRAS 278, 919–924.

Austin, A.T., Vitousek, P.M., 1998. Nutrient dynamics on a precipitation gradient in Hawai'i. Oecologia 113, 519–529.

Bacour, C., Maignan, F., MacBean, N., Porcar Castell, A., Flexas, J., Frankenberg, C., Peylin, P., Chevallier, F., Vuichard, N., Bastrikov, V., 2019. Improving Estimates of Gross Primary Productivity by Assimilating Solar-Induced Fluorescence Satellite Retrievals in a Terrestrial Biosphere Model Using a Process-Based SIF Model. J. Geophys. Res. Biogeosci. 124, 3281–3306.

Bai, Y., Han, X., Wu, J., Chen, Z., Li, L., 2004. Ecosystem stability and compensatory effects in the Inner Mongolia grassland. Nature 431, 181–184.

Bai, Y., Wu, J., Xing, Q., Pan, Q., Huang, J., Yang, D., Han, X., 2008. Primary production and rain use efficiency across a precipitation gradient on the Mongolia plateau. Ecology 89, 2140–2153.

Bao, G., Qin, Z., Bao, Y., Zhou, Y., Li, W., Sanjjav, A., 2014. NDVI-based long-term vegetation dynamics and its response to climatic change in the Mongolian Plateau. Remote Sensing 6, 8337–8358.

Bogeat-Triboulot, M., Brosché, M., Renaut, J., Jouve, L., Le Thiec, D., Fayyaz, P., Vinocur, B., Witters, E., Laukens, K., Teichmann, T., 2007. Gradual soil water depletion results in reversible changes of gene expression, protein profiles, ecophysiology, and growth performance in Populus euphratica, a poplar growing in arid regions. Plant Physiol. 143, 876–892.

Breshears, D.D., Barnes, F.J., 1999. Interrelationships between plant functional types and soil moisture heterogeneity for semiarid landscapes within the grassland/forest continuum: a unified conceptual model. Landscape Ecol. 14, 465–478.

Carter, P.R., Sheaffer, C.C., 1983. Alfalfa Response to Soil Water Deficits. I. Growth, Forage Quality, Yield, Water Use, and Water-Use Efficiency 1. Crop Sci. 23, 669–675.

Chen, T., De Jeu, R., Liu, Y.Y., Van der Werf, G.R., Dolman, A.J., 2014. Using satellite based soil moisture to quantify the water driven variability in NDVI: A case study over mainland Australia. Remote Sens. Environ. 140, 330–338.

Chen, Z., Grasby, S.E., Osadetz, K.G., 2004. Relation between climate variability and groundwater levels in the upper carbonate aquifer, southern Manitoba, Canada. J. Hydrol. 290, 43–62.

Cheng, Y., Li, X., Wang, Y., Zhan, H., Yang, W., Jiang, Q., 2020. New measures of deep soil water recharge during the vegetation restoration process in semi-arid regions of northern China. Hydrol. Earth Syst. Sci. 24, 5875–5890.

Cheng, M., Zhong, L., Ma, Y., Zou, M., Ge, N., Wang, X., Hu, Y., 2019. A Study on the Assessment of Multi-Source Satellite Soil Moisture Products and Reanalysis Data for the Tibetan Plateau. Remote Sens. 11, 1196.

Daly, E., Porporato, A., 2005. A review of soil moisture dynamics: from rainfall infiltration to ecosystem response. Environ. Eng. Sci. 22, 9–24.

Deng, X., Shan, L., Zhang, H., Turner, N.C., 2006. Improving agricultural water use efficiency in arid and semiarid areas of China. Agric. Water Manag. 80, 23–40.

Dong, G., Zhao, F., Chen, J., Qu, L., Jiang, S., Chen, J., Shao, C., 2021. Divergent forcing of water use efficiency from aridity in two meadows of the Mongolian Plateau. J. Hydrol. 593, 125799.

Duveiller, G., Cescatti, A., 2016. Spatially downscaling sun-induced chlorophyll fluorescence leads to an improved temporal correlation with gross primary productivity. Remote Sens. Environ. 182, 72–89.

Flynn, M.N., Pereira, W., 2013. Ecological diagnosis from biotic data by Hurst exponent and the R/S analysis adaptation to short time series. Biomatematica 23, 1–14.

Gentine, P., Green, J.K., Guérin, M., Humphrey, V., Seneviratne, S.I., Zhang, Y., Zhou, S., 2019. Coupling between the terrestrial carbon and water cycles—a review. Environ. Res. Lett. 14, 83003.

Gilgen, A.K., Buchmann, N., 2009. Response of temperate grasslands at different altitudes to simulated summer drought differed but scaled with annual precipitation. Biogeosciences 6, 2525–2539.

Gocic, M., Trajkovic, S., 2013. Analysis of changes in meteorological variables using Mann-Kendall and Sen's slope estimator statistical tests in Serbia. Glob. Planet. Change 100, 172–182.

He, B., Wang, H., Huang, L., Liu, J., Chen, Z., 2017. A new indicator of ecosystem water use efficiency based on surface soil moisture retrieved from remote sensing. Ecol. Ind. 75, 10–16.

Hirota, M., Tang, Y., Hu, Q., Hirata, S., Kato, T., Mo, W., Cao, G., Mariko, S., 2006. Carbon dioxide dynamics and controls in a deep-water wetland on the Qinghai-Tibetan Plateau. Ecosystems 9, 673–688.

Hobi, M.L., Dubinin, M., Graham, C.H., Coops, N.C., Clayton, M.K., Pidgeon, A.M., Radeloff, V.C., 2017. A comparison of Dynamic Habitat Indices derived from different MODIS products as predictors of avian species richness. Remote Sens. Environ. 195, 142–152.

Hooper, D.U., Chapin Iii, F.S., Ewel, J.J., Hector, A., Inchausti, P., Lavorel, S., Lawton, J.H., Lodge, D.M., Loreau, M., Naeem, S., 2005. Effects of biodiversity on ecosystem functioning: a consensus of current knowledge. Ecol. Monogr. 75, 3–35.

Hu, Z., Yu, G., Fan, J., Zhong, H., Wang, S., Li, S., 2010. Precipitation-use efficiency along a 4500-km grassland transect. Glob. Ecol. Biogeogr. 19, 842–851.

Huang, M., Piao, S., Zeng, Z., Peng, S., Ciais, P., Cheng, L., Mao, J., Poulter, B., Shi, X., Yao, Y., 2016. Seasonal responses of terrestrial ecosystem water-use efficiency to climate change. Glob. Change Biol. 22, 2165–2177.

Hungate, B.A., Reichstein, M., Dijkstra, P., Johnson, D., Hymus, G., Tenhunen, J.D., Hinkle, C.R., Drake, B.G., 2002. Evapotranspiration and soil water content in a scrub-oak woodland under carbon dioxide enrichment. Glob. Change Biol. 8, 289–298.

Huxman, T.E., Smith, M.D., Fay, P.A., Knapp, A.K., Shaw, M.R., Loik, M.E., Smith, S.D., Tissue, D.T., Zak, J.C., Weltzin, J.F., 2004. Convergence across biomes to a common rain-use efficiency. Nature 429, 651–654.

Jia, X., Xie, B., Shao, M.A., Zhao, C., 2015. Primary productivity and precipitation-use efficiency in temperate grassland in the Loess Plateau of China. PLoS ONE 10, e135490.

Jobbágy, E.G., Sala, O.E., 2000. Controls of grass and shrub aboveground production in the Patagonian steppe. Ecol. Appl. 10, 541–549.

Jones, H., 2004. What is water use efficiency. Water use efficiency in plant biology 27–41.

Joyce, C.B., Simpson, M., Casanova, M., 2016. Future wet grasslands: ecological implications of climate change. Ecosyst. Health Sustainability 2, e1240.

Kato, T., Kimura, R., Kamichika, M., 2004. Estimation of evapotranspiration, transpiration ratio and water-use efficiency from a sparse canopy using a compartment model. Agric. Water Manag. 65, 173–191.

Keddy, P.A., 1992. A pragmatic approach to functional ecology. Funct. Ecol. 6, 621–626.

Kendall, M.G., 1948. Rank correlation methods.

Knapp, K.A., Smith, M.D., 2013. Variation among biomes in temporal dynamics of aboveground primary production, from 1975 to 1998, LTER.

Kuslu, Y., Sahin, U., Tunc, T., Kiziloglu, F.M., 2010. Determining water-yield relationship, water use efficiency, seasonal crop and pan coefficients for alfalfa in a semiarid region with high altitude. Bulgarian J. Agric. Sci. 16, 482–492.

Lauenroth, W.K., Burke, I.C., Paruelo, J.M., 2000. Patterns of production and precipitation-use efficiency of winter wheat and native grasslands in the central Great Plains of the United States. Ecosystems 3, 344–351.

Le Houérou, H.N., Bingham, R.L., Skerbek, W., 1988. Relationship between the variability of primary production and the variability of annual precipitation in world arid lands. J. Arid Environ. 15, 1–18.

Li, X., Xiao, J., 2019. A Global, 0.05-Degree Product of Solar-Induced Chlorophyll Fluorescence Derived from OCO-2, MODIS, and Reanalysis Data. Remote Sens. 11, 517.

Liu, B., Guan, H., Zhao, W., Yang, Y., Li, S., 2017. Groundwater facilitated water-use efficiency along a gradient of groundwater depth in arid northwestern China. Agric. For. Meteorol. 233, 235–241.

Lowry, C.S., Loheide, S.P., Moore, C.E., Lundquist, J.D., 2011. Groundwater controls on vegetation composition and patterning in mountain meadows. Water Resour. Res. 47.

Meir, P., Wood, T.E., Galbraith, D.R., Brando, P.M., Da Costa, A.C., Rowland, L., Ferreira, L.V., 2015. Threshold responses to soil moisture deficit by trees and soil in tropical rain forests: insights from field experiments. Bioscience 65, 882–892.

Mu, S., Zhou, K., Qi, Y., Chen, Y., Fang, Y., Zhu, C., 2014. Spatio-temporal patterns of precipitation-use efficiency of vegetation and their controlling factors in Inner Mongolia. Chin. J. Plant Ecol. 38, 1.

Mu, S., You, Y., Zhu, C., Zhou, K., 2017. Spatio-temporal patterns of precipitation-use efficiency of grassland in Northwestern China. Acta Ecol. Sin. 37, 1458–1471.

NJ, T.D.M. (1992). World atlas of desertification. In: United Nations Environment Programme, Edward Arnold, London, 69pp.

Noe, G.B., Childers, D.L., 2007. Phosphorus budgets in Everglades wetland ecosystems: the effects of hydrology and nutrient enrichment. Wetlands Ecol. Manag. 15, 189–205.

Ohnuki, Y., Kimhean, C., Shinomiya, Y., Toriyama, J., 2008. Distribution and characteristics of soil thickness and effects upon water storage in forested areas of Cambodia. Hydrol. Process. Int. J. 22, 1272–1280.

Oliveira, M., Santos, C., Oliveira, G.D., Perez-Marin, A.M., Santos, C., 2021. Effects of human-induced land degradation on water and carbon fluxes in two different Brazilian dryland soil covers. Sci. Total Environ. 792, 148458.

Onwuka, B., Mang, B., 2018. Effects of soil temperature on some soil properties and plant growth. Adv. Plants Agric. Res 8, 34.

Parry, M.L., Canziani, O., Palutikof, J., Van der Linden, P., Hanson, C., 2007. Climate change 2007-impacts, adaptation and vulnerability: Working group II contribution to the fourth assessment report of the IPCC. Cambridge University Press.

Paruelo, J.M., Lauenroth, W.K., Burke, I.C., Sala, O.E., 1999. Grassland precipitation-use efficiency varies across a resource gradient. Ecosystems 2, 64–68.

Perez-Priego, O., Guan, J., Rossini, M., Fava, F., Wutzler, T., Moreno, G., Carvalhais, N., Carrara, A., Kolle, O., Julitta, T., Schrumpf, M., Reichstein, M., Migliavacca, M., 2015. Sun-induced chlorophyll fluorescence and photochemical reflectance index improve remote-sensing gross primary production estimates under varying nutrient availability in a typical Mediterranean savanna ecosystem. Biogeosciences 12, 6351–6367.

Phillips, L.B., Hansen, A.J., Flather, C.H., 2008. Evaluating the species energy relationship with the newest measures of ecosystem energy: NDVI versus MODIS primary production. Remote Sens. Environ. 112, 4381–4392.

Power, L.D., Cardinale, B.J., 2009. Species richness enhances both algal biomass and rates of oxygen production in aquatic microcosms. Oikos 118, 1703–1711.

Priyan, K., 2021. Issues and challenges of groundwater and surface water management in semi-arid regions. Groundwater Resources Development and Planning in the Semi-Arid Region. Springer, pp. 1–17.

Ren, Z., Li, Q., Chu, C., Zhao, L., Zhang, J., Ai, D., Yang, Y., Wang, G., 2010. Effects of resource additions on species richness and ANPP in an alpine meadow community. J. Plant Ecol. 3, 25–31.

Roby, M.C., Scott, R.L., Moore, D.J., 2020. High Vapor Pressure Deficit Decreases the Productivity and Water Use Efficiency of Rain-Induced Pulses in Semiarid Ecosystems. J. Geophys. Res. Biogeosci. 125, e2020J–e5665.

Roderick, M.L., Sun, F., Lim, W.H., Farquhar, G.D., 2014. A general framework for understanding the response of the water cycle to global warming over land and ocean. Hydrol. Earth Syst. Sci. 18, 1575–1589.

Sala, O.E., Parton, W.J., Joyce, L.A., Lauenroth, W.K., 1988. Primary production of the central grassland region of the United States. Ecology 69, 40–45.

Sen, P.K., 1968. Estimates of the regression coefficient based on Kendall's tau. J. Am. Stat. Assoc. 63, 1379–1389.

Shao, H., Chu, L., Jaleel, C.A., Manivannan, P., Panneerselvam, R., Shao, M., 2009. Understanding water deficit stress-induced changes in the basic metabolism of higher plants–biotechnologically and sustainably improving agriculture and the ecoenvironment in arid regions of the globe. Crit. Rev. Biotechnol. 29, 131–151.

Sharafatmandrad, M., Khosravi Mashizi, A., 2021. Temporal and spatial assessment of supply and demand of the water-yield ecosystem service for water scarcity management in arid to semi-arid ecosystems. Water Resour. Manage. 35, 63–82.

Soolanayakanahally, R.Y., Guy, R.D., Silim, S.N., Drewes, E.C., Schroeder, W.R., 2009. Enhanced assimilation rate and water use efficiency with latitude through increased photosynthetic capacity and internal conductance in balsam poplar (Populus balsamifera L.). Plant, Cell Environ. 32, 1821–1832.

Sun, J., Du, W., 2017. Effects of precipitation and temperature on net primary productivity and precipitation use efficiency across China's grasslands. GIScience Rem. Sens. 54, 881–897.

Sun, M., Ren, A., Gao, Z., Wang, P., Mo, F., Xue, L., Lei, M., 2018. Long-term evaluation of tillage methods in fallow season for soil water storage, wheat yield and water use efficiency in semiarid southeast of the Loess Plateau. Field Crops Res. 218, 24–32.

Sun, M., Gao, X., Zhang, Y., Song, X., Zhao, X., 2022. A new solution of high-efficiency rainwater irrigation mode for water management in apple plantation: Design and application. Agric. Water Manag. 259, 107243.

Tesfaye, S., Taye, G., Birhane, E., van der Zee, S.E., 2021. Spatiotemporal variability of ecosystem water use efficiency in northern Ethiopia during 1982–2014. J. Hydrol. 603, 126863.

Tilman, D., 2020. Plant Strategies and the Dynamics and Structure of Plant Communities (MPB-26), 26. Princeton University Press.

Tilman, D., Reich, P.B., Knops, J., Wedin, D., Mielke, T., Lehman, C., 2001. Diversity and productivity in a long-term grassland experiment. Science 294, 843–845.

Tong, S., Lai, Q., Zhang, J., Bao, Y., Lusi, A., Ma, Q., Li, X., Zhang, F., 2018a. Spatiotemporal drought variability on the Mongolian Plateau from 1980–2014 based on the SPEI-PM, intensity analysis and Hurst exponent. Sci. Total Environ. 615, 1557–1565.

Tong, S., Zhang, J., Bao, Y., Lai, Q., Lian, X., Li, N., Bao, Y., 2018b. Analyzing vegetation dynamic trend on the Mongolian Plateau based on the Hurst exponent and influencing factors from 1982–2013. J. Geog. Sci. 28, 595–610.

Trenberth, K.E., Asrar, G.R., 2012. Challenges and opportunities in water cycle research: WCRP contributions. The Earth's Hydrological Cycle 515–532.

Vereecken, H., Maes, J., Feyen, J., Darius, P., 1989. Estimating the soil moisture retention characteristic from texture, bulk density, and carbon content. Soil Sci. 148, 389–403.

Vermeire, L.T., Heitschmidt, R.K., Rinella, M.J., 2009. Primary productivity and precipitation-use efficiency in mixed-grass prairie: a comparison of northern and southern US sites. Rangeland Ecol. Manage. 62, 230–239.

Wang, C., Graham, R.M., Wang, K., Gerland, S., Granskog, M.A., 2019. Comparison of ERA5 and ERA-Interim near-surface air temperature, snowfall and precipitation over Arctic sea ice: effects on sea ice thermodynamics and evolution. Cryosphere 13, 1661–1679.

Wei, J., Dirmeyer, P.A., 2012. Dissecting soil moisture-precipitation coupling. Geophys. Res. Lett. 39.

White, S.R., Carlyle, C.N., Fraser, L.H., Cahill Jr, J.F., 2012. Climate change experiments in temperate grasslands: synthesis and future directions. In: The Royal Society.

Winslow, J.C., Hunt Jr, E.R., Piper, S.C., 2003. The influence of seasonal water availability on global C3 versus C4 grassland biomass and its implications for climate change research. Ecol. Model. 163, 153–173.

Wu, X., Liu, H., Ren, J., He, S., Zhang, Y., 2009. Water-dominated vegetation activity across biomes in mid-latitudinal eastern China. Geophys. Res. Lett. 36.

Xia, J., Ning, L., Wang, Q., Chen, J., Wan, L., Hong, S., 2017. Vulnerability of and risk to water resources in arid and semi-arid regions of West China under a scenario of climate change. Clim. Change 144, 549–563.

Xu, Z., Cheng, L., Luo, P., Liu, P., Zhang, L., Li, F., Liu, L., Wang, J., 2020. A Climatic Perspective on the Impacts of Global Warming on Water Cycle of Cold Mountainous Catchments in the Tibetan Plateau: A Case Study in Yarlung Zangbo River Basin. Water 12, 2338.

Yang, Y., Fang, J., Fay, P.A., Bell, J.E., Ji, C., 2010. Rain use efficiency across a precipitation gradient on the Tibetan Plateau. Geophys. Res. Lett. 37, n/a-n/a.

Zhang, Q., Fan, K., Singh, V.P., Sun, P., Shi, P., 2018. Evaluation of Remotely Sensed and Reanalysis Soil Moisture Against In Situ Observations on the Himalayan-Tibetan Plateau. J. Geophys. Res. Atmos. 123, 7132–7148.

Zhou, T., Liu, M., Sun, J., Li, Y., Shi, P., Tsunekawa, A., Zhou, H., Yi, S., Xue, X., 2020. The patterns and mechanisms of precipitation use efficiency in alpine grasslands on the Tibetan Plateau. Agric. Ecosyst. Environ. 292, 106833.

Zhu, Y., Wang, G., Xin, Z., 2020. Water use strategy of Ammopiptanthus mongolicus community in a drought year on the Mongolian Plateau. J. Plant Ecol. 13, 793–800.

Spatio-temporal patterns and control mechanism of the ecosystem carbon use efficiency across the Mongolian Plateau

Xinyi Liu [a], Quan Lai [a,b,*], Shan Yin [a,b], Yuhai Bao [a,b], Siqin Tong [a,b], Zolzaya Adiya [c], Amarjargal Sanjjav [c], Rihe Gao [d]

[a] *College of Geographical Science, Inner Mongolia Normal University, Hohhot 010022, China*
[b] *Inner Mongolia Key Laboratory of Remote Sensing and Geographic Information Systems, Inner Mongolia, Normal University, Hohhot 010022, China*
[c] *Institute of Geography and Geoecology, Mongolian Academy of Sciences, Ulaanbaatar 14201, Mongolia*
[d] *College of Geography and Environmental Sciences, Tianjin Normal University, Tianjin 300382, China*

HIGHLIGHTS

- CUE is relatively higher in dry, cool climates and lower in humid, warm conditions.
- Climatic factors impact CUE more than soil variables but meadow grassland is opposite.
- Climate factors of precipitation and water availability index had the greatest influence on CUE.
- Soil factors of pH and organic content had the greatest influence on CUE.
- Synergy of water availability index and precipitation contributes most to CUE.

GRAPHICAL ABSTRACT
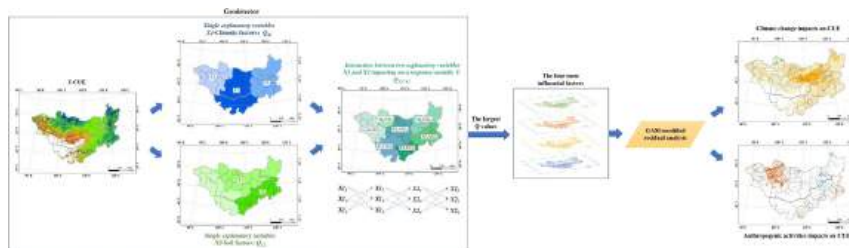
ARTICLE INFO

ABSTRACT

Carbon use efficiency (CUE) is a crucial parameter that reflects the carbon storage within ecosystems, providing insight into the potential for carbon sequestration at the ecosystem scale and its feedback on climate change. The Mongolian Plateau exemplifies an arid and semi-arid region with a delicate ecological environment that displays heightened sensitivity to global climate change. Understanding the variation and control of CUE is critical for assessing regional carbon. However, few studies have focused on the interaction of factors influencing CUE; furthermore, how CUE responds to climate change and anthropogenic activities remains unclear. Here, we aimed to investigate spatiotemporal patterns and their control mechanisms by generating CUE data based on multi-source remote sensing data. CUE demonstrated a slow downward trend from 2000 to 2018, with higher values in relatively dry–cool regions and lower values in relatively humid–warm regions. Furthermore, CUE values were ranked by biome as follows: grassland > sandy vegetation > cropland > shrubs > forest, driven by climate characteristics, vegetation coverage, water stress, stand age, and management practices. Additionally, climatic factors affected CUE more than the soil variables, except for alpine meadows. The climate factors of precipitation (PPT), index of water availability (IWA) ($Q_{PPT} = 0.487$, $Q_{IWA} = 0.444$), and soil factors, e.g., pH and soil organic content (SOC) ($Q_{PH} = 0.397$, $Q_{SOC} = 0.372$), had the greatest influence on CUE. Finally, most two explanatory factors interacted to effectively enhance the explanation of CUE; the synergy of the IWA and PPT contributed the most to CUE ($Q_{IWA \cap PPT} = 0.604$). Moreover, the joint effect of climate change and anthropogenic activities was identified as the major contributor (68 %) to the decline in CUE within this region. This study

---

presents compelling evidence highlighting the importance of considering climate change and anthropogenic disturbances in ecosystem management and conservation efforts in arid and semi-arid regions.

1. Introduction

The terrestrial carbon cycle is a key process in biogeochemical cycles (Cox et al., 2000; Falkowski et al., 2000). Ecosystem carbon use efficiency (CUE) is the ratio of the net primary productivity (NPP) to the gross primary productivity (GPP). This metric quantifies the effectiveness of vegetation in sequestering carbon by converting atmospheric CO_2 into vegetation biomass (Dillaway and Kruger, 2014; Manzoni et al., 2012; Tucker et al., 2013). It also determines how respiration affects vegetation productivity (Albrizio and Steduto, 2003; Delucia et al., 2007).

CUE facilitates comparisons of carbon cycles in different ecosystems, plant organs, individuals, communities, and timescales (Albrizio and Steduto, 2003; Allison et al., 2010; Bradford and Crowther, 2013). A high CUE indicates that vegetation releases less carbon into the atmosphere, promoting carbon stability and long-term sequestration (Li et al., 2019; Manzoni et al., 2012). The Ecosystem CUE has attracted attention from researchers globally because it can help to determine whether terrestrial ecosystems are carbon sources or sinks, as well as understand and predict ecosystem responses and functional changes caused by climate change and anthropogenic disturbance (Chen and Yu, 2019; Ise et al., 2010).

Previous studies have shown that CUE is approximately 0.5, which indicates relative stability across ecosystems and climatic conditions (Albrizio and Steduto, 2003; Waring et al., 1998; Zhang et al., 2009). However, other studies have found that CUE exhibits significant spatial variation in different ecosystems, geographical locations, and climates (Zhang et al., 2009; Chen and Yu, 2019; Khalifa et al., 2018; Li et al., 2019). Several studies have investigated CUE at various spatiotemporal scales, including global, regional, and ecosystem (Zhang et al., 2009; Tucker et al., 2013; Zhang et al., 2014). CUE varies widely globally (0.20–0.80), with an average value of 0.52 (Tang et al., 2019; Delucia et al., 2007). CUE increases with latitude (Feng et al., 2021; Tang et al., 2019), where differences are primarily determined by climatic characteristics (Manzoni et al., 2012; Ganjurjav et al., 2022; Reichstein et al., 2007). CUE increases with altitude at a regional scale, from 0.30 at sea level to 0.60 at 1000 m, implying a direct or indirect correlation between CUE and temperature (TA) (Ganjurjav et al., 2022; Feng et al., 2021).

Additionally, CUE varies according to the ecosystem type (He et al., 2018; Tang et al., 2019; Bradford and Crowther, 2013). Choudhury (2000) pointed out that the CUE of ecosystems with dense vegetation is lower than that of sparse vegetation; the CUE of forests and shrubs is nearly 30 % lower than that of farmland and grassland. According to Li et al. (2019), the annual CUE of different ecosystems is as follows: grassland (0.567), wetland (0.542), mixed forest (0.480), and broadleaf forest (0.479). Albrizio and Steduto (2003) indicated that artificially planted crops generally have a higher CUE than natural vegetation. Such studies have illustrated that CUE has a variable value rather than a constant one of 0.5. The primary cause of this discrepancy is a result of neglecting the impact of environmental factors (Kwon and Larsen, 2013; Delucia et al., 2007).

The variation in the CUE is highly influenced by climatic factors. The impact of TA and PPT on CUE has been extensively examined and analyzed (Chen and Yu, 2019; Adingo et al., 2021; Dillaway and Kruger, 2014; Tucker et al., 2013). However, studies have rarely examined the combined effects of other climate and soil factors on CUE. Moreover, anthropogenic activities, including deforestation, grazing, fertilization, and land use changes, also greatly affect the CUE of terrestrial ecosystems (Adingo et al., 2021; Dong et al., 2020). However, few studies have independently separated the relative effects of climate change and anthropogenic activities on CUE changes. Therefore, quantitative analysis of the spatiotemporal variation in CUE and its determinants would provide researchers with a deeper understanding of how climate change and anthropogenic activities affect carbon processes across diverse ecosystems (Bradford and Crowther, 2013; Choudhury, 2000; Tang et al., 2019).

The Mongolian Plateau is a representative arid and semi-arid region, marked by its dry climate, low precipitation, intense evaporation rates, and complex ecological environment. It has diverse vegetation ecosystems, where the interaction with surrounding environmental factors constitutes a multifaceted ecological phenomenon that profoundly influences the carbon cycle within East Asia. This region is susceptible to the impacts of climate change and anthropogenic disturbances due to its distinctive geographic location and climatic characteristics (Dong et al., 2020; Long et al., 2010).

CUE is a vital indicator of the adaptability of vegetation to constantly changing environmental conditions (Chen and Yu, 2019; Saurer et al., 2004); understanding its variation and control is crucial for regional carbon assessments. Although Dong et al. (2020) investigated the influencing factors of CUE across the Mongolian Plateau, their study focused on quantitative aspects between CUE and individual factors (TA and PPT); they did not evaluate the influence of other environmental factors. How CUE responds to climate change and anthropogenic activities remains unclear. Additionally, few studies have investigated the interaction of factors influencing CUE. Traditional analytical approaches are often criticized for assuming a linear relationship between climate and vegetation, as linear models cannot adequately capture the nonlinear and complex responses of ecosystems to external disturbances (Benedetti and Abrahamowicz, 2004; Souza et al., 2018). This is not conducive to understanding the carbon cycle process and its mechanism across the Mongolian Plateau.

We hypothesized that the CUE of the Mongolian Plateau is influenced by a sophisticated interplay of environmental factors, encompassing air temperature (TA), precipitation (PPT), index of water availability (IWA), vapor pressure deficit (VPD), solar radiation (RAD), sunshine duration (SSD), atmospheric CO_2 concentration (CO_2), fraction of sand and clay, soil pH, soil organic content (SOC), and cationic exchange capacity (CEC). We further hypothesized that the CUE responses to these factors are nonlinear and vary across different ecosystems in the region. Additionally, we anticipate that both climate change and anthropogenic activities will significantly affect CUE. Therefore, the objectives of this study are to evaluate the contributions of individual factors, interactions between two explanatory factors, as well as the impacts of climate change and anthropogenic activities on CUE. We aim to achieve this through the use of geodetectors and a generalized additive model-modified residual analysis. The specific responses to climatic and soil factors in different ecosystems were explored. The findings of this study will enhance our comprehension of the carbon exchange dynamics between the biosphere and atmosphere in arid and semi-arid regions, advance our ability to predict future ecosystem carbon cycle scenarios and establish a theoretical foundation for regional economic development and environmental conservation efforts.

2. Data and methods

2.1. Study area

The Mongolian Plateau is located in the inland area of East Asia, with an approximate area of 2.7×10^6 km², of which grasslands account for the largest proportion (62.20 %). The main vegetation types, from largest to smallest, are typical grassland (TYG), desert steppe (DRS),

meadow grassland (MEG), needleleaf forest (ENF), cropland (CRO), sandy vegetation (SVG), alpine meadow (ALM), broadleaf forest (DBF), and shrubs (SHR) (Fig. 1).

Fig. 2a illustrates the aridity index (AI) of the study area, covering the arid, semi-arid, and semi-humid regions from southwest to northeast. The terrain is dominated by mountains and plateaus (Fig. 2b), with an 82–4165 m altitude. Meteorological data from 2000 to 2018 show that the growing season PPT varied from 23.5 to 480.2 mm (Fig. 2c), and the average temperature was −2.6 to 21.9 °C (Fig. 2d).

2.2. Data

The GPP data was derived from the Global OCO-2-based Solar-Induced Fluorescence (GOSIF) dataset (https://globalecology.unh.edu//data.html), with superior spatial and temporal resolution (0.05°, 8-day) (Li and Xiao, 2019).

The distribution of nine vegetation types across the Mongolian Plateau was obtained by combining the Global Land Cover 2000 Project (GLC2000) dataset (https://forobs.jrc.ec.europa.eu/glc2000/data) and the Moderate Resolution Imaging Spectroradiometer (MODIS) land cover dataset (MOD12Q1, https://lpdaac.usgs.gov/products/mcd12q1v006/).

Given the impact of winter snow cover on vegetation growth, this study focused on analyzing meteorological data during the growing season (April–October) (Liu et al., 2022a, 2022b; Bao et al., 2014). Monthly 2 m TA and PPT data (0.1°) were acquired from the Fifth Generation European Centre for Medium-Range Weather Forecasts (ECMWF) Reanalysis (ERA-5) (https://www.ecmwf.int/en/forecasts/dataset/ecmwf-reanalysis-v5). Additionally, we analyzed monthly SSD data (0.25°) from the ECMWF Reanalysis of the 20th century (ERA-20C) (https://rda.ucar.edu/datasets/ds626.0/dataaccess/). Moreover,

monthly data on the vapor pressure deficit (VPD) at a grid resolution of 0.5° × 0.5° were acquired from the University of East Anglia's Climatic Research Unit (https://crudata.uea.ac.uk/cru/data/hrg/).

The IWA was determined as the ratio of the actual evapotranspiration (AET) to the potential evapotranspiration (PET) (Chen and Yu, 2019). MODIS 8-day AET and PET data (MOD16A2) at a resolution of 500 m were required from the Numerical Terra dynamic Simulation Group at the University of Montana (http://www.ntsg.umt.edu/). Furthermore, the Aridity Index (AI = PPT/PET) was employed to measure climate aridity. According to the standard established by the United Nations Environment Program (NJ, 1992), the Mongolian Plateau was categorized into arid (0 < AI < 0.2), semi-arid (0.2 < AI < 0.5), and semi-humid regions (0.5 < AI < 0.65) as shown in Fig. 2a.

The high-resolution (3 h, 10 km) global surface RAD dataset (1983–2018) was obtained from the National Tibetan Plateau/Third Pole Environment Data Center (https://data.tpdc.ac.cn/zh-hans/data/be562de3-6367-402f-956d-59f7c21ad294).

The re-gridded Harmonized World Soil Database (v1.2) released by the Oak Ridge National Laboratory Distributed Active Archive Center (https://daac.ornl.gov/cgi-bin/dsviewer.pl?ds_id=1247) provides soil parameters for the topsoil (0–30 cm) at a spatial resolution of 0.05° for 2000, including the fraction of sand and clay, soil pH, SOC, and CEC.

The Geospatial Data Cloud provides approximately 30 m of Digital Elevation Model (DEM) data (https://gisgeography.com/free-global-dem-data-sources/). We obtained the MODIS Normalized Difference Vegetation Index (NDVI) dataset (MOD15A2H, 16-day, 500 m) from https://appeears.earthdatacloud.nasa.gov/task/area. Additionally, the atmospheric carbon dioxide dataset was obtained from the 2008–2020 Global 100 km and 2015–2020 Global 50 km GOSAT and OCO-2 Atmospheric CO_2 Column Concentration datasets from the Institute of Aerospace Information Innovation, Chinese Academy of Sciences (htt
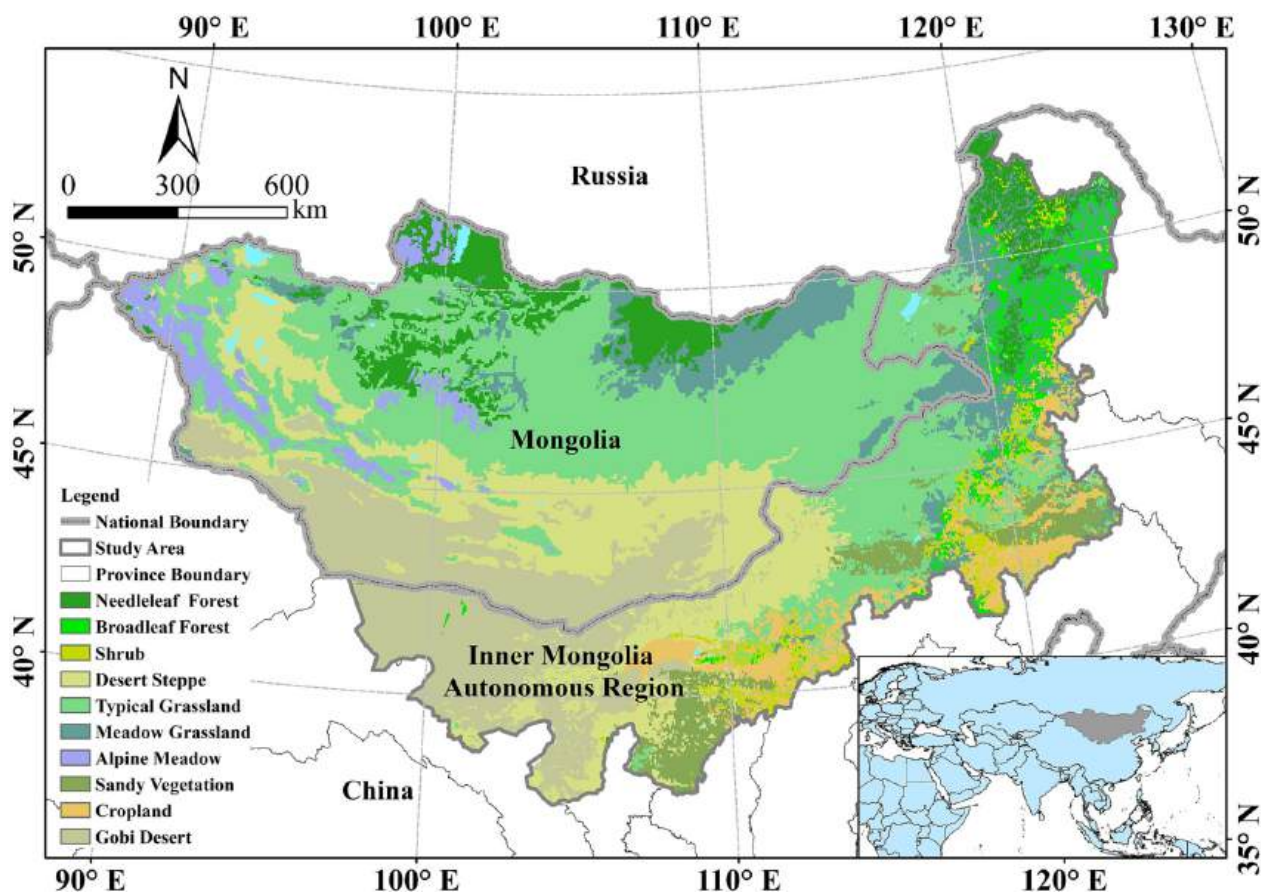

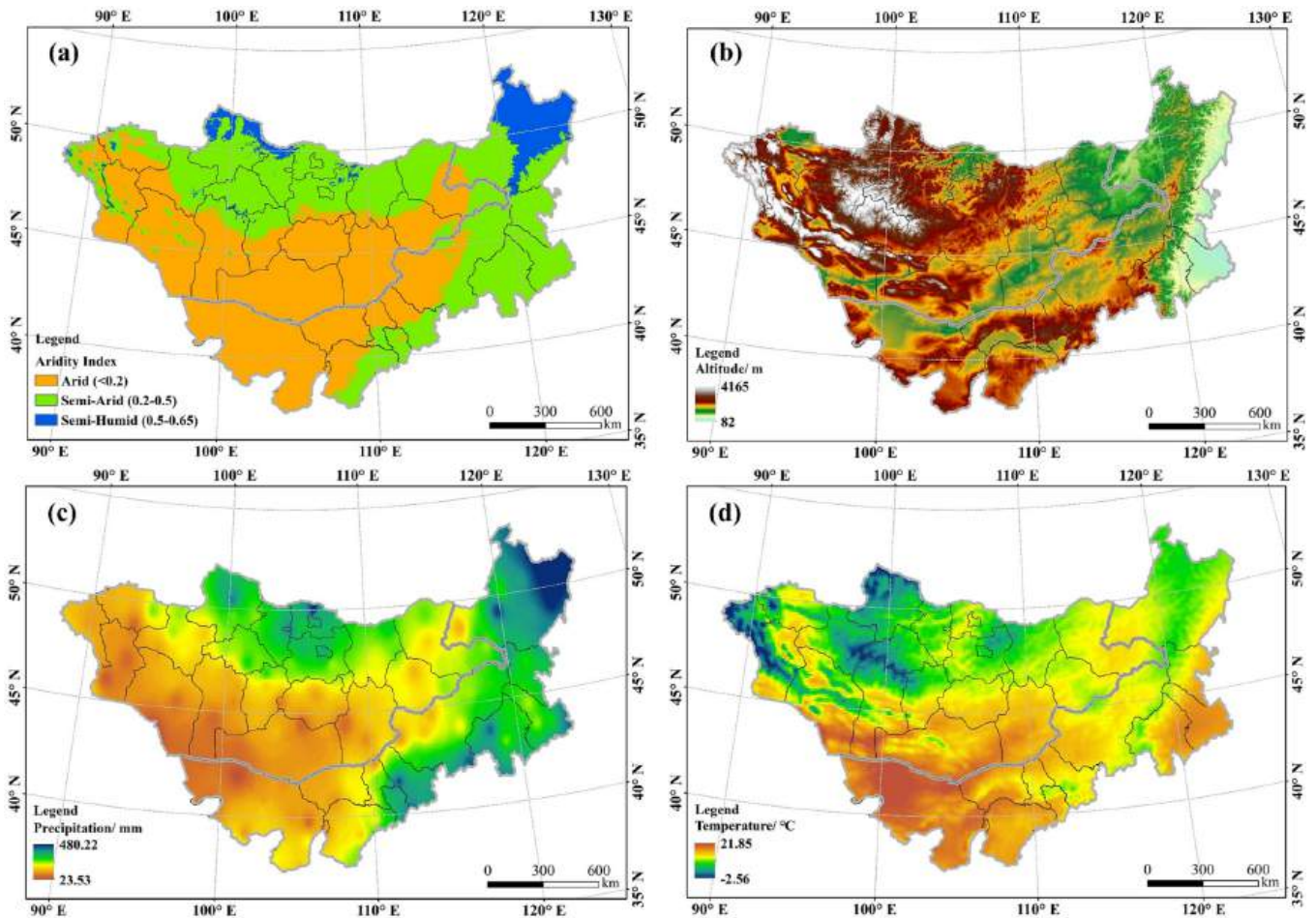**Fig. 1.** Location and vegetation distribution of the Mongolian Plateau.

Fig. 2. Spatial distributions of the (a) climatic regions, (b) altitude, (c) precipitation during the growing season, and (d) average temperature during the growing season across the Mongolian Plateau.

ps://data.casearth.cn/sdo/detail/6253cddc819aec49731a4bc3). For consistency in the analysis, all datasets were ultimately processed into a continuous time-series covering the period from 2000 to 2018, with the exception of the CO$_2$ dataset. The spatial resolution of the datasets was generated to match the RAD data, resulting in a yearly resolution of 0.1°.

2.3. Methods

2.3.1. CUE calculation

CUE is defined as the ratio of the NPP to the GPP:

$$CUE = \frac{NPP}{GPP}, \tag{1}$$

where the NPP is the annual growing season NPP (gC·m^{-2}·mm^{-1}) and the GPP is the annual growing season GPP (gC·m^{-2}·mm^{-1}). The spatiotemporal variations in CUE in the growing season, spring, summer, and autumn were analyzed by employing the raster calculation function in ArcGIS to compute the CUE for each grid cell from 2000 to 2018.

2.3.2. Carnegie–Ames–Stanford Approach (CASA) model

The estimation of the vegetation NPP on the Mongolian Plateau was conducted utilizing the CASA model, which incorporates the physiological and ecological traits of vegetation, along with growth-related environmental factors (Li et al., 2019). The parameters required by the CASA model include the TA, PPT, RAD, NDVI, and vegetation cover type. NPP can be expressed by two factors: the Absorbed Photosynthetic Active Radiation (APAR) and the light energy conversion rate, ε,

calculated as follows; see Potter et al. (1993) for details.

$$NPP_{(i,j)} = APAR_{(i,j)} \times \varepsilon_{(i,j)}, \tag{2}$$

$$APAR_{(i,j)} = PAR_{(i,j)} \times FPAR_{(i,j)}, \tag{3}$$

$$PAR_{(i,j)} = SOL_{(i,j)} \times 0.5, \tag{4}$$

and

$$\varepsilon_{(ij)} = T_{\varepsilon1(ij)} \times T_{\varepsilon2(ij)} \times W_{\varepsilon(ij)} \times \varepsilon_{max}, \tag{5}$$

where $SOL_{(i,j)}$ is the total RAD of pixel i in month j (MJ·m^{-2}), PAR is the incident photosynthetically active radiation (MJ·m^{-2}) per month, and $FPAR_{(i,j)}$ is the fraction of PAR absorbed by the vegetation canopy. The solar effective radiation ratio (400–700 nm) that vegetation can utilize is represented by the constant 0.5. Furthermore, $T_{\varepsilon1(i,j)}$ and $T_{\varepsilon2(i,j)}$ are the temperature stress factors, $W_{\varepsilon(i,j)}$ is the water stress factor, and ε_{max} is the maximum light energy use efficiency (gC·MJ^{-2}) of vegetation under ideal conditions; its value varies significantly depending on the vegetation type (Bao et al., 2016; Zhu et al., 2006).

$$T_{\varepsilon1(i,j)} = 0.8 + 0.02 \times T_{opt(i,j)} - 0.0005 \times \left[T_{opt(i,j)}\right]^2, \tag{6}$$

$$T_{\varepsilon2(i,j)} = \frac{1.184}{\{1 + exp\left[0.2 \times \left(T_{opt(i,j)} - 10 - T_{(i,j)}\right)\right]\}} \\ \times 1/\{1 + exp\left[0.3 \times \left(-T_{opt(i,j)} - 10 + T_{(i,j)}\right)\right]\}, \tag{7}$$

and

$$W_{\varepsilon(i,j)} = 0.5 + 0.5 \times EET_{(i,j)} / PET_{(i,j)}, \tag{8}$$

where $T_{(i,j)}$ is the average temperature of pixel i in month j (°C). $T_{opt(i,j)}$ indicates the optimum temperature for vegetation growth, it is the average temperature when the NDVI value reaches the highest value in a growing season. When $T_{(i,j)}$ is 10 °C higher or 13 °C lower than the $T_{opt(i,j)}$, the $T_{\varepsilon2(i,j)}$ is equal to the $T_{(i,j)}$, which is half of the $T_{\varepsilon2(i,j)}$ value at the $T_{opt(i,j)}$. $EET_{(i,j)}$ is the actual evapotranspiration (mm), and $PET_{(i,j)}$ is the potential evapotranspiration (mm).

The CASA model was initially developed for estimating NPP in North American vegetation and required parameter adjustments when applied elsewhere. Zhu et al. (2006) improved the model by taking into account the characteristics of various typical vegetation types in northern China. This included refinements in land use/cover type, determining the maximum light use efficiency, selecting high-precision meteorological data and remote sensing data. These led to higher accuracy in the simulated NPP, making it more suitable for temperate grassland areas. This improved CASA model is particularly valuable for exploring carbon quantification methods in arid and semi-arid ecosystems. The traditional CASA model involves multiple parameter formulas and is computationally intensive. In contrast, the improved model has developed a mature ENVI plug-in, enabling rapid and precise NPP predictions with the input of key parameters and remote sensing data. Zhu et al. (2006) simulated the maximum light energy use efficiency of each vegetation type using measured NPP data in China. These results have been widely used in the CASA model to estimate NPP in Inner Mongolia and the Mongolian Plateau (Bao et al., 2016; Long et al., 2010; Mu et al., 2014). The values for each vegetation type were as follows: needleleaf forest, 0.485 gC·MJ^{-2}; broadleaf forest, 0.985 gC·MJ^{-2}; shrub, 0.429 gC·MJ^{-2}; cropland, 0.604 gC·MJ^{-2}; grassland and other, 0.542 gC·MJ^{-2}. We used the ENVI plug-in of this model to calculate the NPP data for the Mongolian Plateau. For more details, refer to Zhu et al. (2006).

2.3.3. Statistical analyses

A one-way analysis of variance (ANOVA) was conducted in SPSS (v26.0) software to determine whether there were significant differences in CUE among various biomes, with a significance level of $p < 0.05$. Pearson's correlation coefficients were employed to assess the sensitivity of CUE to the climatic (TA, PPT, IWA, VPD, RAD, SSD, and CO_2) and soil variables (Sand, Clay, SOC, PH, and CEC).

2.3.4. Geodetector

Geodetectors, developed by Wang and Xu (2017), are designed to detect spatial variation and reveal its underlying driving factors. This method has no linear hypothesis, ensuring that it is immune to the collinearity of multiple independent variables. The method utilizes the Q-statistic to assess stratified spatial heterogeneity, identify explanatory factors, and analyze interactive relationships between variables. In this study, three detectors, i.e., the factor, interaction, and ecological detectors, were employed to gain insights into the relative importance of the climatic and soil characteristics and their interactive relationships in influencing CUE. The factor detector Q-statistic measures the extent to which a single factor, X, explains the spatial stratified heterogeneity of the variable Y. The range of Q values is [0, 1]. The larger the Q-value, the stronger the determinant power of the independent variable X on the dependent variable Y, and vice versa. The interaction detector identifies interactions between two explanatory variables ($Q_{X1 \cap X2}$). It assesses whether the combined effect of these two factors $X1$ and $X2$ enhances or diminishes their influence on the dependent variable Y, or if their effects on Y are independent of each other. Additionally, the ecological detector examines whether the interaction between the two explanatory factors, $X1$ and $X2$, significantly impacts the spatial distribution of Y, with statistical significance typically defined at $p < 0.05$. The detail of the Geodetectors can be found in the study of Wang and Xu (2017).

2.3.5. Generalized additive model (GAM) and residual analysis

The GAM is a non-parametric extension of the linear model, which can analyze the nonlinear effects of various factors on dependent variables (Benedetti and Abrahamowicz, 2004; Souza et al., 2018). In this study, GAM was used to improve the traditional residual analysis method. The four most influential factors identified by the Geodetectors with the largest Q values ($p < 0.05$), were incorporated as independent variables in the GAM model to predict CUE caused by climate change. Subsequently, residual analysis was employed to separate the nonlinear effects of climate change and human activities on CUE changes across the Mongolian Plateau from 2000 to 2018:

$$g(CUE_c) = \beta_0 + \beta_1(X_1) + \beta_2(X_2) + \beta_3(X_3) + \cdots + \beta_4(X_4) \tag{9}$$

where CUE_c is the predictive CUE caused by climate change, g is the link function; β_0 is the intercept; and $\beta_1, \beta_2, \beta_3$, and β_4 are the fitting functions for the four most influential factors of X_1, X_2, X_3, and X_4, respectively. The available link functions encompass identity, logit, log, negative reciprocal, and squared reciprocal. The selection of link function depends on the response data type for the independent and dependent variables. When using the *mgcv* package in RStudio to build the GAM model, it automatically optimizes parameters based on the response data type to determine the most suitable link function (Wood, 2017). Furthermore, it is assumed that the actual CUE changes result from the combined influence of climate change and human activities. Therefore, we obtained CUE_h as follows:

$$CUE_h = CUE_a - CUE_c \tag{10}$$

where CUE_a is the actual calculated CUE value based on Eq. (1). CUE_h is the residual value of CUE, which represents the effect of human activities on vegetation CUE.

Sen's slope is a robust non-parametric statistical trend calculation method. This method has high computational efficiency, is insensitive to measurement errors and outlier data, and is suitable for trend analysis of long-term series data (Sen, 1968). It was applied to evaluate the relative contribution of climate change and human activities on CUE, as listed in Table 1 (Wen et al., 2017; Liu et al., 2019).

3. Results

3.1. Spatiotemporal distribution of CUE across the Mongolian Plateau

As depicted in Fig. 3, the CUE of the Mongolian Plateau showed a declining trend between 2000 and 2018. spring CUE values were generally higher, with inter-annual variation ranging from 0.46 to 0.75. In comparison, the autumn CUE values were lower, with a relatively small range of 0.33–0.39. The summer CUE range was the closest to the

Table 1
Methods for evaluating the relative contributions of climate change and human activities.

| Slope	Predictions and residuals		Relative contribution
	S (CUE_c)	S (CUE_h)	
S (CUE_a) > 0	>0	<0	Climate change with higher positive effects (CCP)
	<0	>0	Human activities with higher positive effects (HAP)
	>0	>0	Climate change and human activities with higher positive effects (CHP)
S (CUE_a) < 0	<0	>0	Climate change with higher negative effects (CCN)
	>0	<0	Human activities with higher negative effects (HAN)
	<0	<0	Climate change and human activities with higher negative effects (CHN)
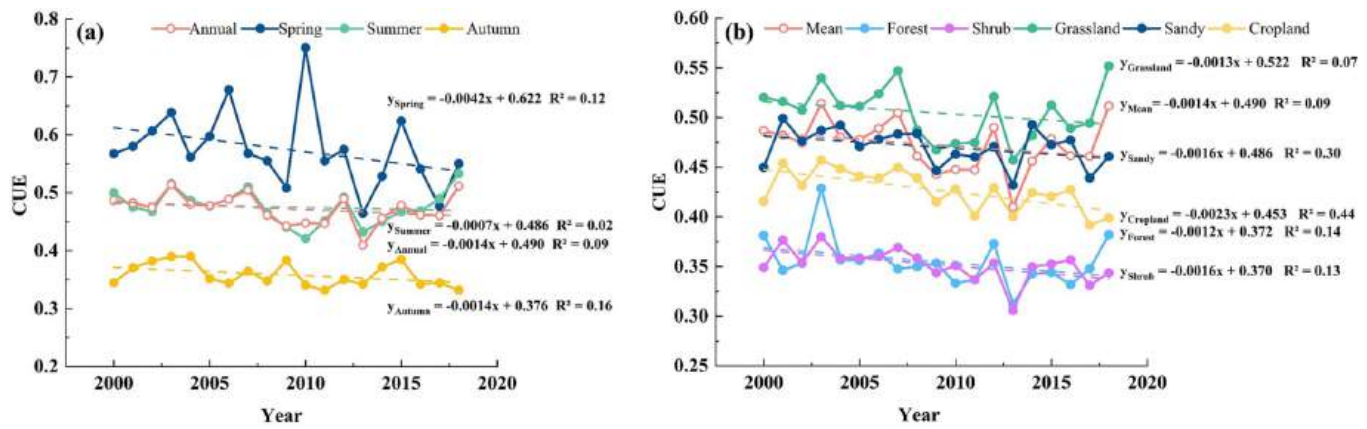
Fig. 3. Inter-annual variability of the average CUE in different (a) seasons and (b) main vegetation types across the Mongolian Plateau from 2000 to 2018.

Mongolian Plateau's mean range (0.42–0.53). Among the five main vegetation types, the CUE indicated a slight declining trend, among which, cropland showed the most significant decrease ($Slope_{cropland}$ = −0.0023, R^2 = 0.44). Additionally, the CUE of sandy vegetation was the closest to the average. Higher CUE values were observed in grasslands, whereas forests and shrubs exhibited relatively lower CUE values. Generally, high and low CUE values appeared alternately during the study period on the Mongolian Plateau; the lowest CUE values mainly appeared in 2013.

Fig. 4 depicts the spatial patterns of the average CUE throughout the entire growing season, spring, summer, and autumn from 2000 to 2018. Notably, the distribution of CUE throughout the growing season exhibited spatial heterogeneity across the Mongolian Plateau, characterized by a stepwise gradient from southwest to northeast (Fig. 4a). The CUE values varied from <0.3 to >0.6, with a mean of 0.48. Higher CUE values were observed in arid regions, whereas lower values were observed in semi-humid regions. The areas with the highest CUE values were primarily concentrated in the DRS region of the Central Gobi and the ALM region of the Altai Mountains, whereas the forest ecosystems neighboring the Greater Xing'an and Khangai-Khentei mountains
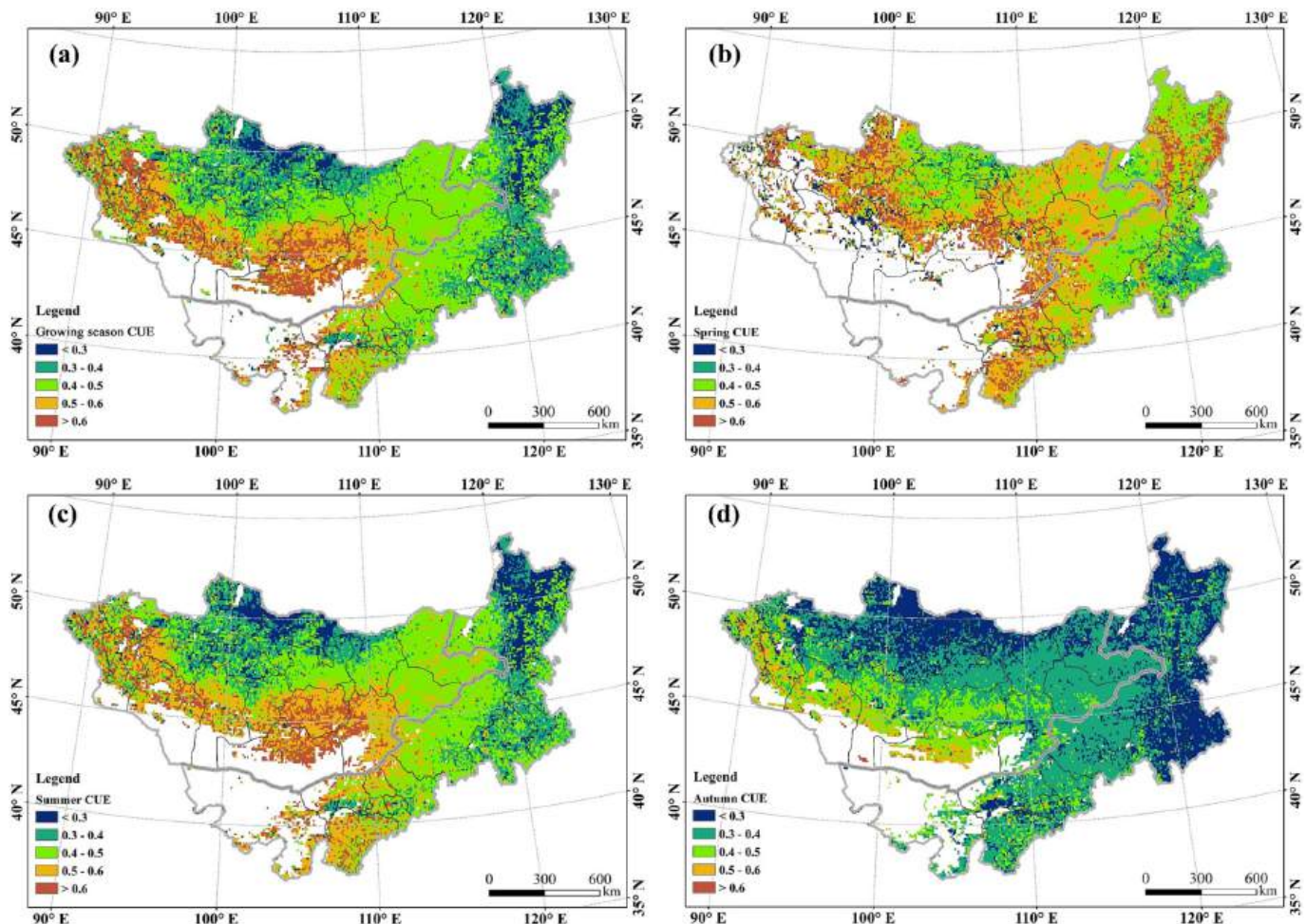

Fig. 4. Spatial distribution of the average CUE in the (a) growing season, (b) spring, (c) summer, and (d) autumn across the Mongolian Plateau from 2000 to 2018.

exhibited the lowest CUE values. The CUE values in spring were generally higher, with an average value of 0.57 (Fig. 4b). More than 55 % of the regional CUE values were >0.5; missing values appeared in the arid regions of the southwest. There was a robust spatial agreement between the overall growing season and summer CUE, with a mean of 0.48 (Fig. 4c). CUE decreased in most regions with the arrival of autumn, especially in the TYG, CRO, and SVG regions. The average CUE in autumn was 0.36, which was significantly lower than that in spring and summer (Fig. 4d).

3.2. Differences in CUE among various biomes

Fig. 5 shows the average growing season CUE of several ecosystems in the Mongolian Plateau from 2000 to 2018. The one-way ANOVA demonstrated large differences between the CUE of the five main vegetation types ($p < 0.05$). Grassland ecosystems exhibited the highest CUE (0.51), followed by SVG, CRO, and SHR; the lowest value (0.34) was observed in forests. Further analysis showed significant differences among the different forest and grassland subtypes. The CUE of the DRS was the highest among grasslands (0.63), whereas that of the MEG was the lowest (0.39). TYG had the largest area (40.90 %); its CUE was the closest to the average. Although ALM had a small proportion of the area, its CUE was relatively high (0.55). Additionally, broadleaf forests generally had a higher CUE and occupied smaller areas, whereas needleleaf forests exhibited the opposite patterns.

3.3. Identification of dominant factors and their underlying mechanisms

3.3.1. Influence of climatic and soil factors on CUE

Fig. 6 shows the effects of climatic factors and soil variables on CUE in different Mongolian Plateau ecosystems from 2000 to 2018. Correlation coefficients revealed varying responses among diverse ecosystems. Compared to soil factors, climatic factors substantially affected CUE more, except in the ALM ecosystem. CUE generally had negative correlations with the PPT, IWA, and SOC, but was positively correlated with other factors in the majority of the study area. For the climatic factors, the correlation coefficient between CUE and IWA was higher than that with other climatic variables. Furthermore, CUE was
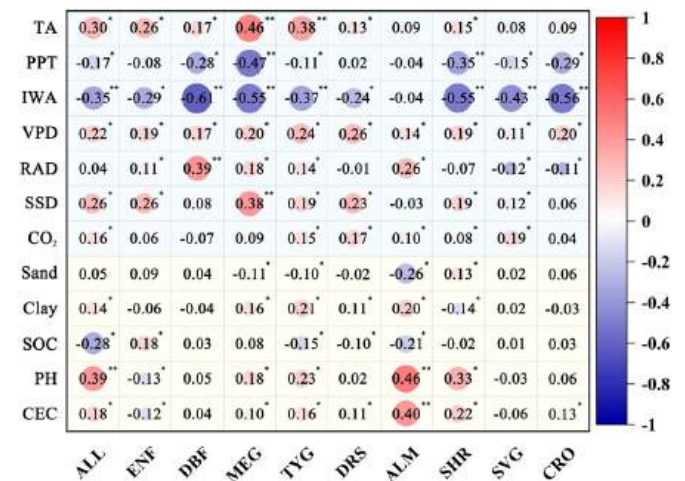

Fig. 6. Responses of multiple factors to CUE in different vegetation types. Light blue and pale-yellow backgrounds represent the climatic and soil factors, respectively. Significance: *$p < 0.05$, **$p < 0.01$. TA: air temperature; PPT: precipitation; IWA: index of water availability; VPD: vapor pressure deficit; RAD: solar radiation; SSD: sunshine duration; CO_2: atmospheric CO_2 concentration; Sand: fraction of sand; Clay: fraction of clay; SOC: soil organic content; PH: soil pH; CEC: cationic exchange capacity; ALL: all vegetation types; ENF: needleleaf forest; DBF: broadleaf forest; MEG: meadow grassland; TYG: typical grassland; DRS: desert steppe; ALM: alpine meadow; SHR: shrubs; SVG: sandy vegetation; and CRO: cropland.

extremely significantly negatively correlated with IWA ($p < 0.01$), indicating that IWA can better control CUE variation over the entire Mongolian Plateau. Notably, the relationship between CUE and PPT was similar to that between CUE and IWA; however, the correlation was relatively weak. The correlations were the lowest in the arid DRS and high-altitude ALM ecosystems. Additionally, VPD was significantly positively correlated with CUE ($p < 0.05$) in most of the ecosystems. Similarly, TA had a low positive effect on CUE in some relatively dry ecosystems, whereas stronger relationships were found in semi-humid forest ecosystems and semi-arid grassland ecosystems. Regarding the
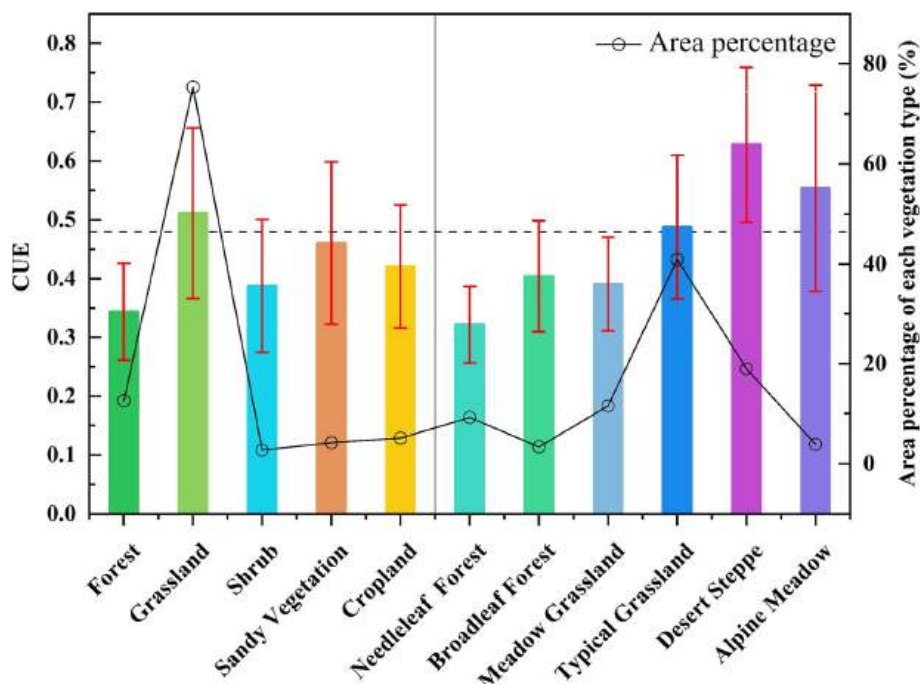

Fig. 5. Average CUE of the different main vegetation types and subtypes across the Mongolia Plateau from 2000 to 2018.

soil factors, soil pH showed a more decisive influence than other soil factors and was significantly positively correlated with CUE ($p < 0.05$). Although soil clay percentage and CEC have relatively weak correlations with CUE, they also partially affect the variation in CUE in many ecosystems.

3.3.2. Contributions of climatic and soil factors to CUE

Fig. 7 shows the individual contributions of various factors and their control mechanisms on CUE dynamics across the Mongolian Plateau. The factor detector q-statistic results showed that PPT ($Q_{PPT} = 0.487$) and IWA ($Q_{IWA} = 0.444$) were the two climatic factors with great explanatory power for the CUE of the entire study area. Meanwhile, pH ($Q_{PH} = 0.397$) and SOC ($Q_{SOC} = 0.372$) were the main contributing soil factors (Fig. 7a), corresponding to the correlation coefficient results. However, the effects varied across ecosystems. There were no large differences in the responses to various factors in the ENF (Fig. 7b). TA and atmospheric CO_2 substantially contributed to CUE in the DBF (Fig. 7c). In grassland ecosystems (Fig. 7d–g), the contribution of SSD to CUE was prominent among the climate variables. Particularly, in the TYG (Fig. 7e), SSD exceeded PPT and became the dominant factor. The determinant power of soil pH in the meadow grassland was insignificant ($p > 0.05$, Fig. 7d). The contribution of soil clay and sand fractions alternated, depending on the grassland type, indicating that soil texture significantly controls CUE. Additionally, the contribution of RAD to CUE in SHR, SVG, and CRO ecosystems increased (Fig. 7h–j), while the role of soil factors relatively weakened. Notably, PPT and SOC did not control CUE variation in CRO; all soil factors had an insignificant effect on the SVG.

In the natural environment, the spatial distribution of CUE is jointly affected by multiple influencing factors; a single factor rarely determines the variation in CUE. Fig. 8 shows the interactive contributions of the various factors and their significance. There were large differences in the interactions between influencing factors depending on the ecosystems. The influencing factors in the entire study area were mainly bio-synergistic and nonlinear synergistic; there were no independent factors (Fig. 8a). The maximum Q value was observed between IWA and PPT ($Q_{IWA \cap PPT} = 0.604$), indicating that the synergy of moisture factors enhanced the explanation of CUE. However, the determinant powers between TA and RAD, VPD and CEC, and pH and SOC were insignificant. In most ecosystems, the joint effect of various influencing factors was primarily bio-enhancement or nonlinear enhancement; a uni-weakening relationship was rare. The weakened effect mainly appeared between IWA and RAD, VPD and CO_2, RAD and CO_2, SSD and CO_2, and SAND and CO_2 in the DBF ecosystem, implying that the increase in the atmospheric CO_2 concentration and other factors jointly led to the decreased control of CUE (Fig. 8c). Additionally, the SVG had a marked contribution decline to CUE under the interaction between VPD and RAD ($Q_{VPD \cap RAD} = 0.434$; Fig. 8i). The maximum joint effects were generally shared by the IWA and other climatic factors; however, soil elements were equally important. Soil factors in the DBF ($Q_{SOC \cap TA} = 0.347$; Fig. 8c), SHR ($Q_{SOC \cap RAD} = 0.717$; Fig. 8h), and SVG ($Q_{PH \cap RAD} = 0.587$; Fig. 8i) can effectively enhance the explanation of climate factors on CUE. This finding further illustrates that soil features strongly impact the spatial variation in CUE, which is consistent with the correlation coefficient results. The CRO exerted the greatest contribution under the joint effect of VPD and TA ($Q_{VPD \cap TA} = 0.443$; Fig. 8j), which may be due to the temperature dependence of crops.

3.3.3. Effects of climate change and human activities on CUE

Based on the trend results and identification criteria (Table 1), the spatial pattern of the drivers of CUE change (climate change or human activities) was revealed, and an attribution analysis of CUE change in different vegetation types was performed. Overall, climate change and human activities negatively affected CUE in >90 % of the study area from 2000 to 2018 (Fig. 9a). Among them, the combination of climate change and human activities had the largest negative effect on CUE

(CHN = 68 %), followed by the negative effect caused by climate change (CCN = 17 %), as well as the negative effect caused by human activities (HAN = 8 %). Only a few areas had positive effects, generally no more than 10 %. Fig. 9b shows that different vegetation types respond differently to climate change and human activities. The reduction in CUE in the ENF, TYG, and SHR regions due to climate change was more prominent, with relative contributions of 18, 33 and 27 %, respectively, which spatially corresponded to the mixed forest-shrub regions of the Greater Xing'an Mountains and the Eastern Mongolia-Hulunbuir-Xilin Gol Grassland. Meanwhile, human activities had significantly reduced the CUE in the ENF, TYG, and SVG regions, reaching 21, 12 and 18 %, respectively, corresponding to the mixed forest-grass regions of the Khangai Mountains, Horqin Sandy Land, and Mu Us Sandy Land.

4. Discussion

4.1. Variations in CUE across the Mongolian Plateau

Spatiotemporal variation in CUE has been extensively studied at various scales (Adingo et al., 2021; Tucker et al., 2013). Previous studies estimated the global average CUE using remote sensing methods and process models at 0.52 and 0.45, respectively (He et al., 2018; Tang et al., 2019). This suggests that estimating the NPP and GPP using different methods can result in a wide range of CUE values (0.201–0.822) (Tang et al., 2019). MODIS data have been employed in studies to calculate an average CUE of 0.54 ± 0.01 for terrestrial ecosystems in China (Chen and Yu, 2019), 0.51 ± 0.04 for Northwest China and Inner Mongolia (NWIM) (Gang et al., 2019), and 0.57 for the arid and semi-arid desert/grassland biome transition zone (Du et al., 2021). Our findings show that the average CUE for the Mongolian Plateau is 0.48, with a range of 0.26 to 0.75, which is roughly within the acceptable accuracy range for the NWIM CUE. This difference may be attributed to the spatial scales used in previous studies.

The overall trend of CUE for the Mongolian Plateau, however, is consistent with that of preceding study areas, showing a slow decrease each year (Du et al., 2021; Gang et al., 2019). Generally, the Mongolian Plateau CUE decreased gradually from southwest to northeast and was primarily influenced by climate characteristics. CUE was higher in relatively dry and cool climates and lower in relatively humid and warm climates. This could be explained by the relatively moist heat environment causing more carbon release and thus lowering CUE (El Masri et al., 2021; Zhang et al., 2009). In spring (April–May), leaf and stem biomass increase rapidly, more photosynthesis is used for NPP accumulation, and CUE is generally higher (Du et al., 2021). Vegetation activities in the southwest near the Gobi Desert recovered slowly, resulting in missing CUE values. The CUE was lower in the summer (June–August) than in the spring. This phenomenon could be attributed to the intense autotrophic respiration consumption of the vegetation, resulting in the reduction of NPP accumulation at the same photosynthetic rate (Gang et al., 2019; Maseyk et al., 2008). The CUE decline in autumn (September–October) was primarily concentrated in the TYG, CRO, and SVG, which was attributed to the rapid decrease in the aboveground NPP due to crop and pasture harvesting in autumn, resulting in the lowest CUE values (Albrizio and Steduto, 2003; Li et al., 2019). Additionally, the recent implementation of "Grain for Green" ecological environment restoration projects has resulted in the most significant decline in the CRO CUE (Du et al., 2021).

Previous studies have pointed out that the CUE between ecosystems is not constant at 0.5. Climate, vegetation type, stand age, and soil nutrient conditions all influence CUE (Chen and Yu, 2019; Zhang et al., 2009; Li et al., 2019). Grasslands had the highest CUE among the five main vegetation types, followed by the SVG and CRO, and SHR and forests had the lowest values. As previously reported, dry and cool grasslands had higher CUE values than did moist and warm forests, whereas the CRO had intermediate CUE values (El Masri et al., 2021; Kim et al., 2018). The grassland ecosystem had the highest CUE due to
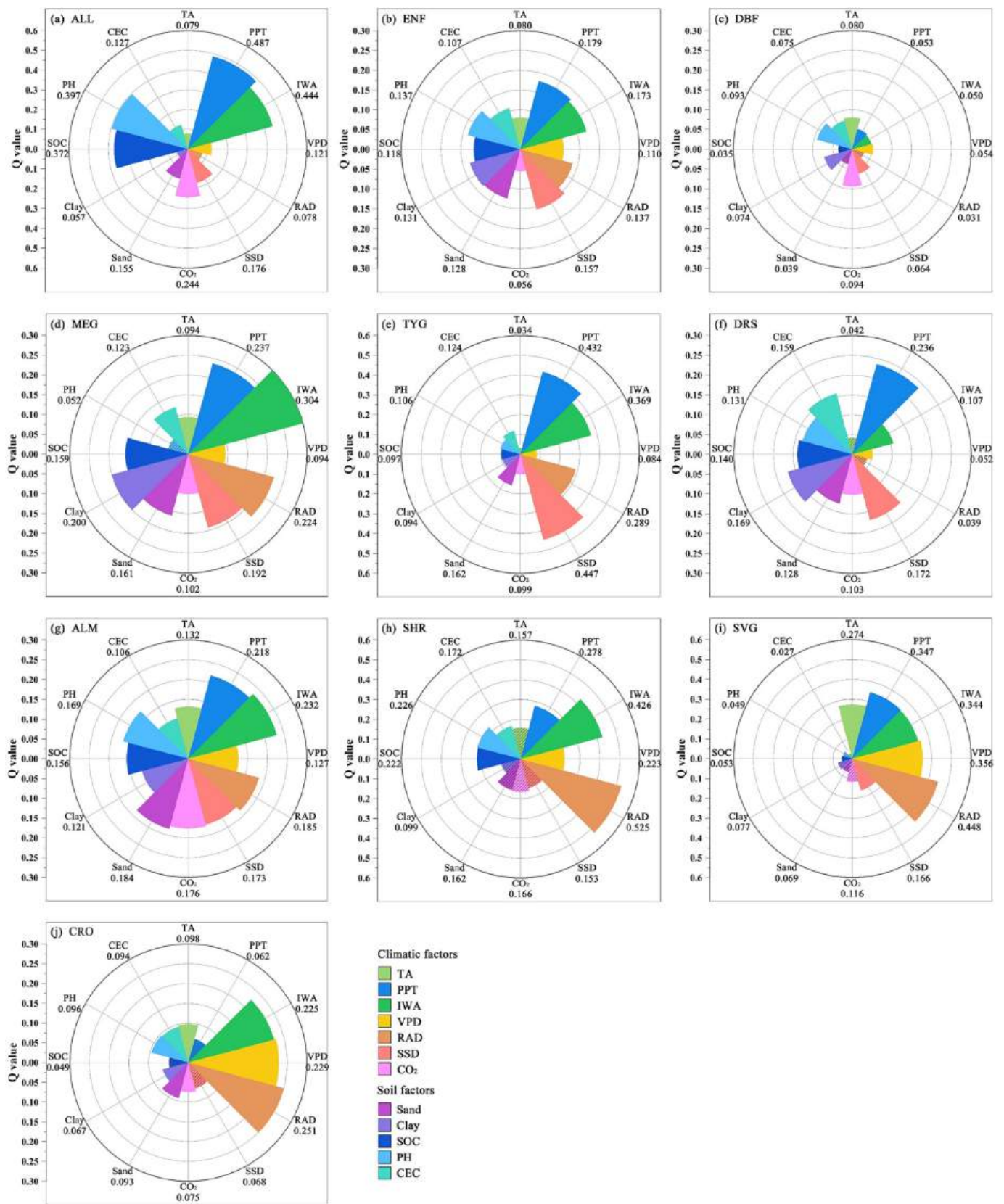
Fig. 7. Factor detector q-statistic between multiple factors and CUE for different vegetation types (sectors with hatches represent nonsignificant relationships). TA: air temperature; PPT: precipitation; IWA: index of water availability; VPD: vapor pressure deficit; RAD: solar radiation; SSD: sunshine duration; CO2: atmospheric CO2 concentration; Sand: fraction of sand; Clay: fraction of clay; SOC: soil organic content; PH: soil pH; CEC: cationic exchange capacity; ALL: all vegetation types; ENF: needleleaf forest; DBF: broadleaf forest; MEG: meadow grassland; TYG: typical grassland; DRS: desert steppe; ALM: alpine meadow; SHR: shrubs; SVG: sandy vegetation; and CRO: cropland.
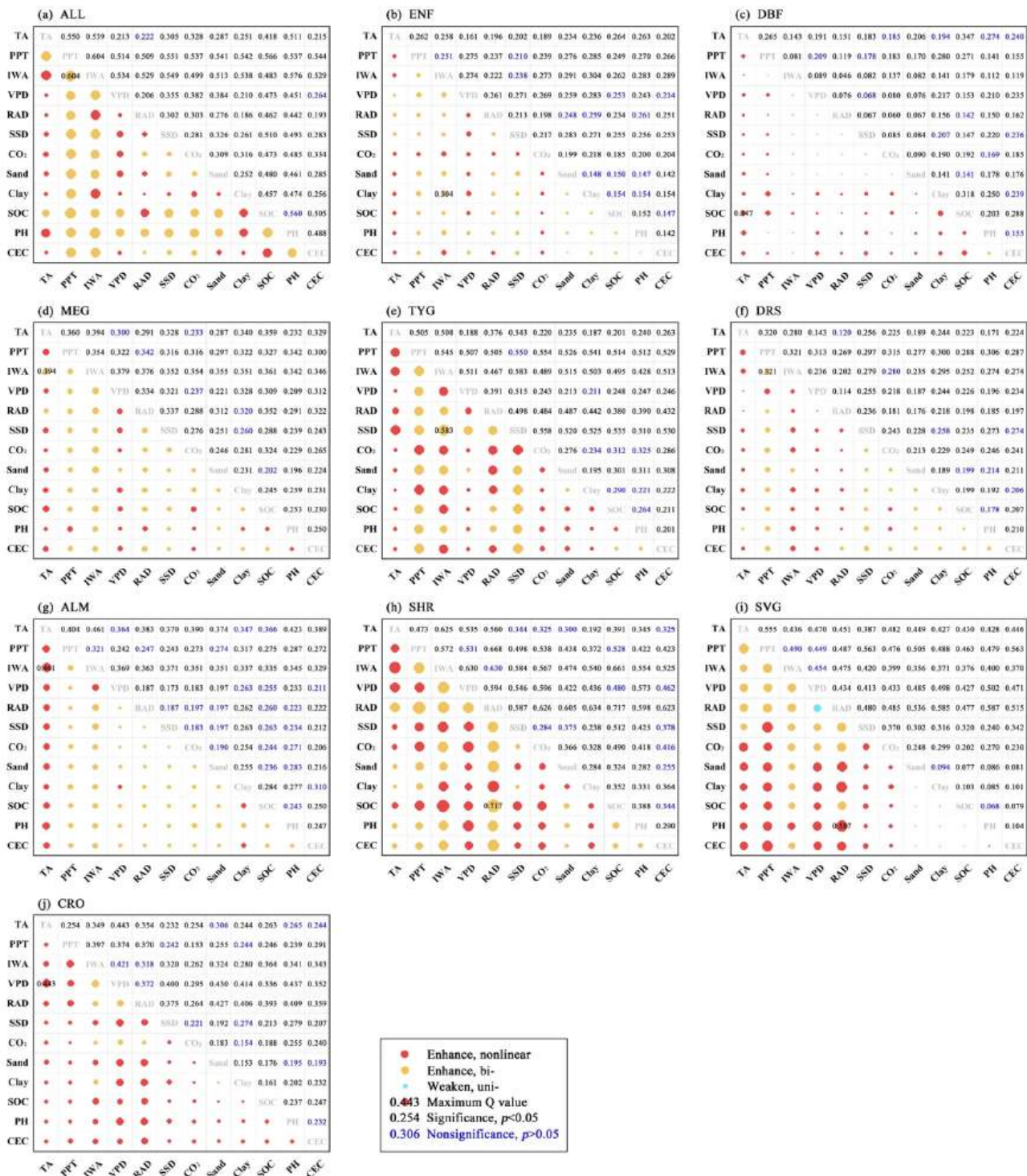
Fig. 8. Q-statistic of the interaction and ecological detectors between the pairwise factors and CUE for different vegetation types. TA: air temperature; PPT: precipitation; IWA: index of water availability; VPD: vapor pressure deficit; RAD: solar radiation; SSD: sunshine duration; CO_2: atmospheric CO_2 concentration; Sand: fraction of sand; Clay: fraction of clay; SOC: soil organic content; PH: soil pH; CEC: cationic exchange capacity; ALL: all vegetation types; ENF: needleleaf forest; DBF: broadleaf forest; MEG: meadow grassland; TYG: typical grassland; DRS: desert steppe; ALM: alpine meadow; SHR: shrubs; SVG: sandy vegetation; and CRO: cropland.
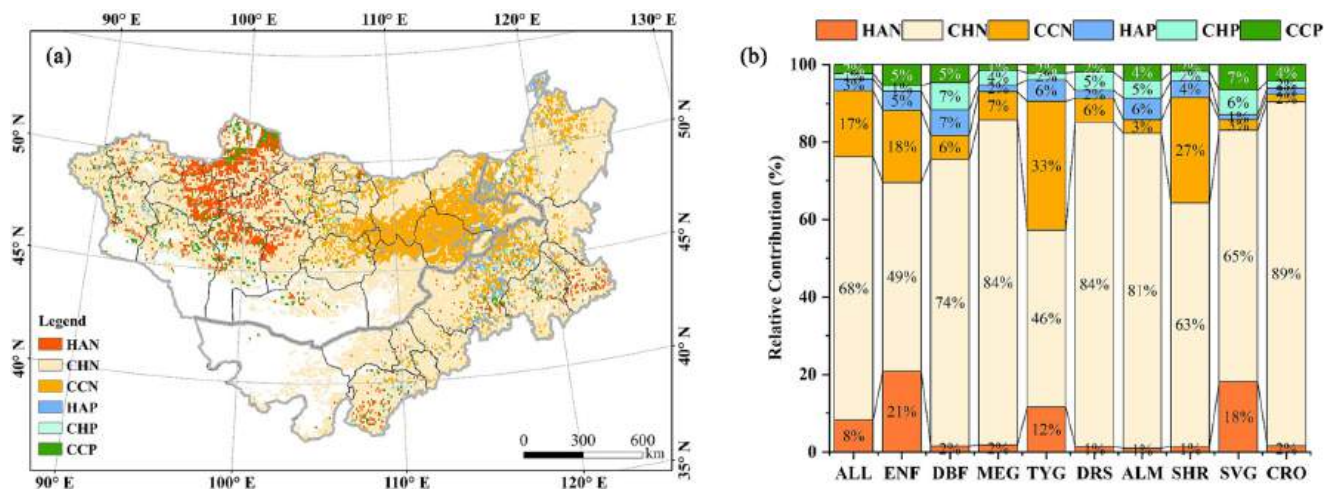
the lower autotrophic respiration consumption; the accumulated NPP was higher than that of other ecosystems with the same GPP (Kim et al., 2018). A comparison of the grassland ecosystem subtypes revealed that the CUE in the low-coverage DRS subtype was greater than that in the medium-high coverage TYG and MEG subtypes. This discrepancy can be attributed to the varying levels of water availability within the grassland ecosystem (Choudhury, 2000; Du et al., 2021).

In the same ecosystem, unfavorable vegetation growth conditions, including lower canopy density and water stress, may lead to an increased CUE (Du et al., 2021; Gang et al., 2019). TA had a greater impact on alpine vegetation respiration than the GPP. In cooler ALM regions, vegetation requires a relatively low capacity to sustain living tissues, resulting in lower respiration costs and a higher CUE (Chen et al., 2021; Ganjurjav et al., 2022). Similarly, differences in CUE among

Fig. 9. Relative contributions of climate change and human activities to CUE variations for different vegetation types. HAN: human activities with higher negative effects; CHN: climate change and human activities with higher negative effects; CCN: climate change with higher negative effects; HAP: human activities with higher positive effects; CHP: climate change and human activities with higher positive effects; and CCP: climate change with higher positive effects.

the SVG, SHR, and forests were determined by vegetation coverage and water stress.

Collalti and Prentice (2019) found that the ENF has a lower global CUE than that of the DBF. This difference could be attributed to forest management and stand age (Collalti and Prentice, 2019; Zhang et al., 2009). Younger forests tend to have a higher CUE because they allocate more carbon to growth than to respiration, whereas mature forests use more photosynthetic products to maintain respiration (Delucia et al., 2007; Giardina et al., 2003). Anthropogenic disturbances (timber harvesting) reduce biomass stocks and competition for light, water, and nutrients, which are the primary explanations for the decline in CUE with stand age (Collalti and Prentice, 2019; Du et al., 2021; Giardina et al., 2003). Crops can use more photosynthetic products for biomass accumulation than natural vegetation owing to the favorable climatic conditions, soil nutrient supply (fertilization, soil loosening, weeding), and other measures, resulting in a higher CUE for the CRO (El Masri et al., 2021; Kim et al., 2018).

4.2. CUE control mechanisms

Many studies have shown that fluctuations in CUE are significantly influenced by climatic and soil factors (Zhang et al., 2014; Allison et al., 2010). Our conclusion that climatic factors have a greater impact on CUE than soil variables is supported by a study on CUE management in terrestrial ecosystems in China (Chen and Yu, 2019). The ALM had the opposite response, which could be attributed to their soil properties (fertile and nutrient-rich soil), as has been discovered in the Tibet Plateau, Northern Europe, and North American grasslands (Chen et al., 2021; Ganjurjav et al., 2022). Alpine vegetation with high nutrient availability can allocate more photosynthetic products to biomass with a higher CUE (El Masri et al., 2021). These studies confirmed our findings.

Precipitation and temperature can directly affect various vegetation life activities, thereby affecting CUE (Choudhury, 2000; Zhang et al., 2014). However, in arid/semi-arid areas, PPT has a significantly greater impact on CUE than that of TA (Gang et al., 2019; Du et al., 2021). Studies conducted in the past have demonstrated that in regions with an annual PPT below 2300 mm/year, a negative correlation exists between PPT and CUE. This may be related to factors such as decreased radiation, increased nutrient leaching, insufficient soil oxygen, accelerated organic matter decomposition, and decreased nutrient availability (Zhang et al., 2009). When PPT is low (<200 mm/year) in an arid or unfavorable growth environment, vegetation increases the carbon conversion efficiency by reducing autotrophic respiration consumption and the

demand for water (Gang et al., 2019; Mu et al., 2017). This aids in explaining the weak correlation between CUE and PPT in the arid DRS and ALM at high altitudes.

As previously documented, CUE has a parabolic relationship with temperature (Zhang et al., 2014; Pold et al., 2020). The findings in those studies are consistent with the findings here, i.e., CUE increases with an increasing temperature between −10 and 20 °C (He et al., 2018). The combined effects of hydrothermal conditions, in addition to temperature and PPT, should significantly affect the carbon cycle. IWA has been shown to primarily mediate the spatial variation in CUE as a comprehensive alternative to individual variables (PPT and TA) (Reichstein et al., 2007; Chen and Yu, 2019). As a result, the significant negative correlation between IWA and CUE is stronger than that between PPT and CUE. Additionally, Jones et al. (2019) observed that the soil pH was significantly correlated with CUE. When the soil pH > 5.5, the CUE values increased with an increasing pH, supporting our results.

Factors that are highly correlated with CUE also strongly explain CUE, but the effects vary depending on the ecosystem. According to Reichstein et al. (2007), the IWA primarily controls spatial variation in the European forest carbon composition, whereas the PPT is slightly weaker. This confirms that the IWA and PPT are the two main climatic elements that contribute to CUE. Thus, IWA and other climatic elements have the greatest overall joint effects in most ecosystems. Additionally, changes in the soil pH have an impact on the ability of soil minerals to adsorb and bind with organic substances, which subsequently affects the SOC stability and soil carbon sequestration process (Jones et al., 2019; Liang and Zhu, 2021). Therefore, the soil pH and SOC are the two main soil elements that contribute to CUE.

Other areas with different responses merit further discussion. The contribution of SSD to CUE in the grasslands becomes gradually prominent, especially in the TYG ecosystem, which may be due to the fact that warm climatic conditions can increase grassland biomass and quality. A longer SSD leads to more favorable pasture photosynthesis, flowering, and pollination, and inhibits pests and diseases (Geor, 2010; McCarroll and Pawellek, 2001). TYG is the main source of forage grass across the Mongolian Plateau, where SSD contributes the most to the TYG CUE. However, the control of soil pH in the MEG was insignificant, most likely because changing the soil pH did not affect MEG community stability. This was demonstrated in a study on the acidification and alkalinization treatment of three types of grasslands (DRS, TYG, and MEG) in northern China (Liu et al., 2022a, 2022b). The SHR, SVG, and CRO are heavily influenced by RAD, which can be explained by greater solar radiation, sufficient light, and strong photosynthesis favoring agro-pastoral

ecotone production (Dong et al., 2021; Geor, 2010). However, PPT and SOC did not control the CUE of CRO (*p* > 0.05), which may be attributed to the fact that artificial fertilization, irrigation, and other measures greatly reduced the dependence of crops on PPT and soil SOC (Du et al., 2021; Ganjurjav et al., 2022).

Evidence suggests that both climate change and anthropogenic activities are the major drivers of vegetation dynamics (Wen et al., 2017; Liu et al., 2019). The dynamic changes in CUE of different vegetation types may be caused by anthropogenic disturbances, including overgrazing, intensive deforestation, policy-driven land use change, and ecological restoration projects (Dong et al., 2021; Liu et al., 2022a, 2022b; Liu et al., 2019). Overgrazing greatly affects vegetation growth, especially in the grassland pastures on the southern slope of Khangai Mountain, which subsequently causes changes in CUE (Liu et al., 2019). In contrast, there are many coniferous forests on the north slope of Khangai Mountain. The recent rapid development of tourism has led to changes in vegetation habitats (Walther et al., 2020). Additionally, due to insufficient cropland resources, the pressure of population growth on land is the direct cause of desertification in sandy land, resulting in a reduction in vegetation productivity and CUE (Yu et al., 2018; Yang et al., 2017).

4.3. Limitations and future implications

A few uncertainties remain concerning the study of CUE control on the Mongolian Plateau. First, errors may be introduced when converting source datasets of different resolutions into a single long-term series with uniform resolution. Second, NPP and GPP data from different sources may introduce deviations in CUE (He et al., 2018; Tang et al., 2019). Third, although the most important meteorological and soil variables were selected, many other important influencing factors could not be quantified (Fernández-Martínez et al., 2016; Reichstein et al., 2007).

Moreover, one of the focus areas of this study was the interactive control mechanisms of CUE. Our results indicated that the joint effects of all factors were mostly bio-enhancement or nonlinear enhancement, rarely a uni-weakened relationship, suggesting that the interaction of two factors can effectively improve the explanation of CUE. Although the application of geodetectors and generalized additive models can effectively separate the nonlinear effects of various factors on CUE, there have been few studies on this topic. The interactive control mechanism for CUE is still in its infancy, and our findings require further investigation and validation. Therefore, future studies on CUE control should focus on the interactions between multiple factors and their effects on the relevant physiological and ecological mechanisms.

5. Conclusions

This study investigated CUE in the Mongolian Plateau, an ecologically sensitive arid and semi-arid region. Utilizing multi-source remote sensing data, we analyzed the spatiotemporal patterns and control mechanisms influencing CUE. Our findings led to the following conclusions: (1) The CUE of the Mongolian Plateau showed a slow decline each year, with an average of 0.48. Notably, the CUE was higher in spring and lower in autumn. There was a robust spatial agreement between the CUE during the growing season and summer, which gradually decreased from southwest to northeast and was mainly affected by climatic characteristics. CUE was higher in relatively dry and cool climates and lower in relatively humid and warm climates. (2) CUE exhibited significant variations across different ecosystem types. The order of CUE at the biome level was grassland > SVG > CRO > SHR > forest. This progression was mainly due to differences in climatic characteristics, vegetation coverage, water stress, stand age, and management practices. DRS and ALM had low productivity but a high CUE compared with that of the other grassland types. (3) Climatic factors had a greater impact on CUE than that of soil variables, whereas the ALM had the opposite effect

because of its unique soil properties (fertile soil, rich in nutrients). CUE showed negative correlations with PPT, IWA, and SOC, but positive correlations with other factors. The IWA and PPT were the two climatic elements that contributed the most to CUE. PPT strongly controlled CUE in the TYG and DRS, whereas CUE was mainly controlled by the IWA in other ecosystems. Soil pH and SOC were the two soil elements that contributed the most to CUE. Soil pH strongly controlled the CUE in most ecosystems, except for the MEG. (4) The joint effects of all the factors were enhanced and rarely weakened the relationships. Generally, the interaction of the IWA with other climatic factors effectively enhanced the explanation of CUE. Additionally, the combination of climate change and anthropogenic activities largely explained the higher negative impact of CUE (68 %), followed by climate change (17 %), and anthropogenic activity-induced reduction in CUE (8 %). Only a few positive effects generally did not exceed 10 %. However, as the interactive control mechanism of CUE has rarely been studied, our results require further investigation and validation.

This study improves our understanding of the changes and responses of CUE to environmental drivers on the Mongolian Plateau. Grassland ecosystems have a higher CUE and greater variability than mature forest ecosystems. Focusing on the ecological construction of typical grasslands and sandy lands (after grassland degradation) is conducive to balancing carbon absorption and emissions in East Asia. Further studies on effective management and conservation strategies are required to improve CUE and promote the construction of sustainable multi-vegetation ecosystems on the Mongolian Plateau.

CRediT authorship contribution statement

Xinyi Liu: Conceptualization, Methodology, Software, Validation, Formal analysis, Writing – original draft. **Quan Lai:** Resources, Data curation, Methodology, Software, Writing – review & editing. **Shan Yin:** Conceptualization, Investigation, Validation, Writing – review & editing. **Yuhai Bao:** Supervision, Investigation, Project administration, Funding acquisition. **Siqin Tong:** Investigation, Validation, Software. **Zolzaya Adiya:** Investigation, Software, Data curation. **Amarjargal Sanjjav:** Data curation, Software, Investigation. **Rihe Gao:** Validation, Data curation, Investigation.

Declaration of competing interest

The authors declare that they have no known competing financial interests or personal relationships that could have appeared to influence the work reported in this paper.

Data availability

Data will be made available on request.

References

Adingo, S., Yu, J., Xuelu, L., Li, X., Jing, S., Xiaong, Z., 2021. Variation of soil microbial carbon use efficiency (CUE) and its influence mechanism in the context of global environmental change: a review. PeerJ 9, e12131.

Albrizio, R., Steduto, P., 2003. Photosynthesis, respiration and conservative carbon use efficiency of four field grown crops. Agric. For. Meteorol. 116, 19–36.

Allison, S.D., Wallenstein, M.D., Bradford, M.A., 2010. Soil-carbon response to warming dependent on microbial physiology. Nat. Geosci. 3, 336–340.

Bao, G., Qin, Z., Bao, Y., Zhou, Y., Li, W., Sanjjav, A., 2014. NDVI-based long-term vegetation dynamics and its response to climatic change in the Mongolian Plateau. Remote Sens. 6, 8337–8358.

Bao, G., Bao, Y., Qin, Z., Xin, X., Bao, Y., Bayarsaikan, S., Zhou, Y., Chuntai, B., 2016. Modeling net primary productivity of terrestrial ecosystems in the semi-arid climate of the Mongolian Plateau using LSWI-based CASA ecosystem model. Int. J. Appl. Earth Obs. Geoinf. 46, 84–93.

Benedetti, A., Abrahamowicz, M., 2004. Using generalized additive models to reduce residual confounding. Stat. Med. 23, 3781–3801.

Bradford, M.A., Crowther, T.W., 2013. Carbon use efficiency and storage in terrestrial ecosystems. New Phytol. 199, 7–9.

Chen, Z., Yu, G., 2019. Spatial variations and controls of carbon use efficiency in China's terrestrial ecosystems. Sci. Rep. 9, 19516.

Chen, N., Zhang, Y., Zhu, J., Cong, N., Zhao, G., Zu, J., Wang, Z., Huang, K., Wang, L., Liu, Y., 2021. Multiple-scale negative impacts of warming on ecosystem carbon use efficiency across the Tibetan Plateau grasslands. Glob. Ecol. Biogeogr. 30, 398–413.

Choudhury, B.J., 2000. Carbon use efficiency, and net primary productivity of terrestrial vegetation. Adv. Space Res. 26, 1105–1108.

Collalti, A., Prentice, I.C., 2019. Is NPP proportional to GPP? Waring's hypothesis 20 years on. Tree Physiol. 39, 1473–1483.

Cox, P.M., Betts, R.A., Jones, C.D., Spall, S.A., Totterdell, I.J., 2000. Acceleration of global warming due to carbon-cycle feedbacks in a coupled climate model. NATURE 408, 184–187.

Delucia, E.H., Drake, J.E., Thomas, R.B., Gonzalez Meler, M., 2007. Forest carbon use efficiency: is respiration a constant fraction of gross primary production? Glob. Chang. Biol. 13, 1157–1167.

Dillaway, D.N., Kruger, E.L., 2014. Trends in seedling growth and carbon-use efficiency vary among broadleaf tree species along a latitudinal transect in eastern North America. Glob. Chang. Biol. 20, 908–922.

Dong, G., Zhao, F., Chen, J., Zhang, Y., Qu, L., Jiang, S., Ochirbat, B., Chen, J., Xin, X., Shao, C., 2020. Non-climatic component provoked substantial spatiotemporal changes of carbon and water use efficiency on the Mongolian Plateau. Environ. Res. Lett. 15, 95009.

Dong, G., Zhao, F., Chen, J., Qu, L., Jiang, S., Chen, J., Xin, X., Shao, C., 2021. Land uses changed the dynamics and controls of carbon-water exchanges in alkali-saline Songnen Plain of Northeast China. Ecol. Indic. 133, 108353.

Du, L., Gong, F., Zeng, Y., Ma, L., Qiao, C., Wu, H., 2021. Carbon use efficiency of terrestrial ecosystems in desert/grassland biome transition zone: a case in Ningxia province, Northwest China. Ecol. Indic. 120, 106971.

El Masri, B., Stinchcomb, G.E., Cetin, H., Ferguson, B., Kim, S.L., Xiao, J., Fisher, J.B., 2021. Linking remotely sensed carbon and water use efficiencies with in situ soil properties. Remote Sens. 13, 2593.

Falkowski, P., Scholes, R.J., Boyle, E., Canadell, J., Canfield, D., Elser, J., Gruber, N., Hibbard, K., Högberg, P., Linder, S., 2000. The global carbon cycle: a test of our knowledge of earth as a system. Science 290, 291–296.

Feng, J., Zeng, X., Zhang, Q., Zhou, X., Liu, Y., Huang, Q., 2021. Soil microbial trait-based strategies drive metabolic efficiency along an altitude gradient. ISME Commun. 1, 71.

Fernández-Martínez, M., Vicca, S., Janssens, I.A., Campioli, M., Penuelas, J., 2016. Nutrient availability and climate as the main determinants of the ratio of biomass to NPP in woody and non-woody forest compartments. Trees 30, 775–783.

Gang, C., Zhang, Y., Guo, L., Gao, X., Peng, S., Chen, M., Wen, Z., 2019. Drought-induced carbon and water use efficiency responses in dryland vegetation of northern China. Front. Plant Sci. 10, 224.

Ganjurjav, H., Hu, G., Zhang, Y., Gornish, E.S., Yu, T., Gao, Q., 2022. Warming tends to decrease ecosystem carbon and water use efficiency in dissimilar ways in an alpine meadow and a cultivated grassland in the Tibetan Plateau. Agric. For. Meteorol. 323, 109079.

Geor, R.J., 2010. Current concepts on the pathophysiology of pasture-associated laminitis. Vet. Clin. N. Am. Equine Pract. 26, 265–276.

Giardina, C.P., Ryan, M.G., Binkley, D., Fownes, J.H., 2003. Primary production and carbon allocation in relation to nutrient supply in a tropical experimental forest. Glob. Chang. Biol. 9, 1438–1450.

He, Y., Piao, S., Li, X., Chen, A., Qin, D., 2018. Global patterns of vegetation carbon use efficiency and their climate drivers deduced from MODIS satellite data and process-based models. Agric. For. Meteorol. 256, 150–158.

Ise, T., Litton, C.M., Giardina, C.P., Ito, A., 2010. Comparison of modeling approaches for carbon partitioning: impact on estimates of global net primary production and equilibrium biomass of woody vegetation from MODIS GPP. J. Geophys. Res. Biogeosci. 115.

Jones, D.L., Cooledge, E.C., Hoyle, F.C., Griffiths, R.I., Murphy, D.V., 2019. pH and exchangeable aluminum are major regulators of microbial energy flow and carbon use efficiency in soil microbial communities. Soil Biol. Biochem. 138, 107584.

Khalifa, M., Elagib, N.A., Ribbe, L., Schneider, K., 2018. Spatio-temporal variations in climate, primary productivity and efficiency of water and carbon use of the land cover types in Sudan and Ethiopia. Sci. Total Environ. 624, 790–806.

Kim, D., Lee, M., Jeong, S., Im, J., Cha, D.H., Lee, S., 2018. Intercomparison of terrestrial carbon fluxes and carbon use efficiency simulated by CMIP5 earth system models. Asia-Pac. J. Atmos. Sci. 54, 145–163.

Kwon, Y., Larsen, C.P., 2013. Effects of forest type and environmental factors on forest carbon use efficiency assessed using MODIS and FIA data across the eastern USA. Int. J. Remote Sens. 34, 8425–8448.

Li, X., Xiao, J., 2019. A global, 0.05-degree product of solar-induced chlorophyll fluorescence derived from OCO-2, MODIS, and reanalysis data. Remote Sens. 11, 517.

Li, B., Huang, F., Qin, L., Qi, H., Sun, N., 2019. Spatio-temporal variations of carbon use efficiency in natural terrestrial ecosystems and the relationship with climatic factors in the Songnen Plain, China. Remote Sens. 11, 2513.

Liang, C., Zhu, X., 2021. The soil microbial carbon pump as a new concept for terrestrial carbon sequestration. Sci. China Earth Sci. 64, 545–558.

Liu, Y., Zhang, Z., Tong, L., Khalifa, M., Wang, Q., Gang, C., Wang, Z., Li, J., Sun, Z., 2019. Assessing the effects of climate variation and human activities on grassland degradation and restoration across the globe. Ecol. Indic. 106, 105504.

Liu, X., Lai, Q., Yin, S., Bao, Y., Qing, S., Bayarsaikhan, S., Bu, L., Mei, L., Li, Z., Niu, J., 2022a. Exploring grassland ecosystem water use efficiency using indicators of precipitation and soil moisture across the Mongolian Plateau. Ecol. Indic. 142, 109207.

Liu, K., Liu, Z., Zhou, N., Shi, X., Lock, T.R., Kallenbach, R.L., Yuan, Z., 2022b. Diversity-stability relationships in temperate grasslands as a function of soil pH. Land Degrad. Dev. 33, 1704–1717.

Long, H.L., Li, X.B., Wang, H., Wei, D.D., Zhang, C., 2010. Net primary productivity (NPP) of grassland ecosystem and its relationship with climate in Inner Mongolia. Acta Ecol. Sin. 30, 1367–1378.

Manzoni, S., Taylor, P., Richter, A., Porporato, A., Ågren, G.I., 2012. Environmental and stoichiometric controls on microbial carbon-use efficiency in soils. New Phytol. 196, 79–91.

Maseyk, K., Grünzweig, J.M., Rotenberg, E., Yakir, D., 2008. Respiration acclimation contributes to high carbon-use efficiency in a seasonally dry pine forest. Glob. Chang. Biol. 14, 1553–1567.

McCarroll, D., Pawellek, F., 2001. Stable carbon isotope ratios of Pinus sylvestris from northern Finland and the potential for extracting a climate signal from long Fennoscandian chronologies. The Holocene 11, 517–526.

Mu, S., Zhou, K., Qi, Y., Chen, Y., Fang, Y., Zhu, C., 2014. Spatio-temporal patterns of precipitation-use efficiency of vegetation and their controlling factors in Inner Mongolia. Chin. J. Plant Ecol. 38, 1.

Mu, S., You, Y., Zhu, C., Zhou, K., 2017. Spatio-temporal patterns of precipitation-use efficiency of grassland in northwestern China. Acta Ecol. Sin. 37, 1458–1471.

NJ, T.D.M., 1992. World atlas of desertification. In: United Nations Environment Programme. Edward Arnold, London (69 pp.).

Pold, G., Domeignoz-Horta, L.A., Morrison, E.W., Frey, S.D., Sistla, S.A., DeAngelis, K.M., 2020. Carbon use efficiency and its temperature sensitivity covary in soil bacteria. mBio 11, e2219–e2293.

Potter, C.S., Randerson, J.T., Field, C.B., Matson, P.A., Vitousek, P.M., Mooney, H.A., Klooster, S.A., 1993. Terrestrial ecosystem production: a process model based on global satellite and surface data. Glob. Biogeochem. Cycles 7, 811–841.

Reichstein, M., Papale, D., Valentini, R., Aubinet, M., Bernhofer, C., Knohl, A., Laurila, T., Lindroth, A., Moors, E., Pilegaard, K., 2007. Determinants of terrestrial ecosystem carbon balance inferred from European eddy covariance flux sites. Geophys. Res. Lett. 34.

Saurer, M., Siegwolf, R.T., Schweingruber, F.H., 2004. Carbon isotope discrimination indicates improving water-use efficiency of trees in northern Eurasia over the last 100 years. Glob. Chang. Biol. 10, 2109–2120.

Sen, P.K., 1968. Estimates of the regression coefficient based on Kendall's tau. J. Am. Stat. Assoc. 63, 1379–1389.

Souza, J.B., Reisen, V.A., Franco, G.C., Ispány, M., Bondon, P., Santos, J.M., 2018. Generalized additive models with principal component analysis: an application to time series of respiratory disease and air pollution data. J. R. Stat. Soc.: Ser. C: Appl. Stat. 67, 453–480.

Tang, X., Carvalhais, N., Moura, C., Ahrens, B., Koirala, S., Fan, S., Guan, F., Zhang, W., Gao, S., Magliulo, V., 2019. Global variability of carbon use efficiency in terrestrial ecosystems. Biogeosci. Discuss. 1–19.

Tucker, C.L., Bell, J., Pendall, E., Ogle, K., 2013. Does declining carbon-use efficiency explain thermal acclimation of soil respiration with warming? Glob. Chang. Biol. 19, 252–263.

Walther, M., Horn, W., Dashtseren, A., 2020. Uvs Nuur: a sentinel for climate change in eastern Central Asia. In: Large Asian Lakes in a Changing World: Natural State and Human Impact, pp. 235–257.

Wang, J., Xu, C., 2017. Geodetector: principle and prospective. Acta Geograph. Sin. 72, 116–134.

Waring, R.H., Landsberg, J.J., Williams, M., 1998. Net primary production of forests: a constant fraction of gross primary production? Tree Physiol. 18, 129–134.

Wen, Z., Wu, S., Chen, J., Lü, M., 2017. NDVI indicated long-term interannual changes in vegetation activities and their responses to climatic and anthropogenic factors in the Three Gorges Reservoir Region, China. Sci. Total Environ. 574, 947–959.

Wood, S.N., 2017. Generalized Additive Models: An Introduction With R. CRC press.

Yang, T., Cao, J., Wang, Y., Liu, Y., 2017. Soil moisture influences vegetation distribution patterns in sand dunes of the Horqin Sandy Land, Northeast China. Ecol. Eng. 105, 95–101.

Yu, X., Huang, Y., Li, E., Li, X., Guo, W., 2018. Effects of rainfall and vegetation to soil water input and output processes in the Mu Us Sandy Land, northwest China. Catena 161, 96–103.

Zhang, Y., Xu, M., Chen, H., Adams, J., 2009. Global pattern of NPP to GPP ratio derived from MODIS data: effects of ecosystem type, geographical location and climate. Glob. Ecol. Biogeogr. 18, 280–290.

Zhang, Y., Yu, G., Yang, J., Wimberly, M.C., Zhang, X., Tao, J., Jiang, Y., Zhu, J., 2014. Climate-driven global changes in carbon use efficiency. Glob. Ecol. Biogeogr. 23, 144–155.

Zhu, W., Pan, Y., He, H., Yu, D., Hu, H., 2006. Simulation of maximum light use efficiency for some typical vegetation types in China. Chin. Sci. Bull. 51, 457–463.

所属一级学科	项目编号
地理学	CXJJB21020

内蒙古师范大学研究生科研创新基金项目

结 题 报 告 书

项目名称：<u>基于叶绿素荧光遥感的内蒙古植</u>

<u>被生长对气候变化的响应</u>

主 持 人：<u>　　　刘心怡　　　</u>

导 　　师：<u>　　　银山　　　</u>

所学专业：<u>　　　地理学　　　</u>

研究方向：<u>　土地覆被与生态修复　</u>

内蒙古师范大学研究生院

二〇一八年十月制

一、简表

项目编号	CXJJB21020	项目名称	基于叶绿素荧光遥感的内蒙古植被生长对气候变化的响应
项目负责人	刘心怡	参加人	美丽、元志辉、叶志刚、卜灵心、塔娜

研究经费	资助总额	2000 元	研究期限	计划完成年月	2022 年 11 月
	支出总额	2000 元		实际完成年月	2022 年 02 月

二、研究工作总结

主要内容提示：1．完成的研究内容及所采用的研究方法、技术路线；2．主要的研究结果，特别要说明主要的科学发现和创新之处，此项研究的科学意义和应用前景；3．与预期计划和目标比较，说明完成情况及存在问题（是否按照原计划进行、哪些内容进行了必要调整和改动）

1．完成的研究内容及所采用的研究方法、技术路线：

（1）研究内容：

　　①内蒙古四大沙地植被生产力时空分布特征与变化趋势。

　　基于 MODIS EVI、MODIS GPP、GOSIF 数据，通过 Anomaly 趋势分析法和 MK 突变检测方法，在时间和空间尺度上对突变年前后生长季内蒙古四大沙地植被生产力的时间变化特征、空间分布特征和变化趋势进行分析探讨。

　　②内蒙古四大沙地气温、降水、地表水及地下水储量时空变化特征分析。

　　选用一元线性回归方法和 IDW 插值法分别对内蒙古自治区及其周边 110 个气象站点 2003-2016 年生长季的平均气温、累积降水量进行了空间插值，并在四大沙地研究了近 14 年生长季气温、降水、地表水及地下水储量的时空分异特征与变化趋势。

　　③内蒙古四大沙地植被生长对水成分因子的响应及时滞效应。

　　利用多种相关分析法计算植被生产力对不同时序水成分因子的相关系数，通过相关系数值大小讨论植被生产力对水成分要素的滞后响应时间。

　　④内蒙古四大沙地植被生产力对气候变化的响应。

　　基于滞后响应结果，分析内蒙古 2003-2016 年生长季植被生产力与水成分因子的相关关系。通过植被生长变化驱动力规则，进一步揭示内蒙古沙地植被生产力与水成分因子间的关系，探讨不同水成分因子对植被生长的驱动情况及敏感性分析。

（2）研究方法：

　　①数据预处理：

　　采用 z-score 标准化分析、d-trend 去趋势分析、13-month 平滑处理等方法，对原始时间序列 GOSIF、MODIS EVI、MODIS GPP、REA-5 SM、GRACE TWS 等数据进行平滑及重构处理，降低由传感器性能、数据传输误差、地形与大气条件因时而导致的噪声。提高四大沙地植被生产力和水成分因子的时空表征能力，以提高数据质量及研究结果的可信度。

　　②数据分析：

　　Anomaly 趋势分析和 Mann-Kendall 检验方法应用于植被生产力变化趋势分析和气候突变分析；IDW 空间插值用于气象数据的空间插值；皮尔森相关系数、数学统计方法等应用于定性定量化分析；自相关系数分析植被生产力及水成分因子的时滞效应；偏相关系数等分析植被生产力及水成分因子对气候变化的响应。
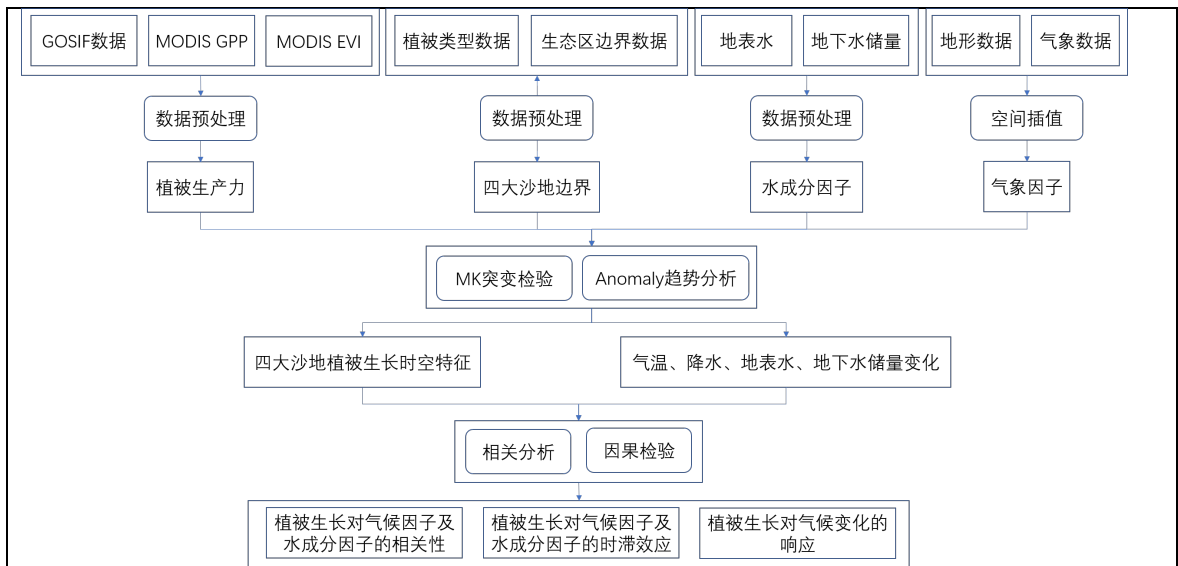
（3）技术路线：

图 1. 技术路线图

2．主要的研究结果，特别要说明主要的科学发现和创新之处，此项研究的科学意义和应用前景：

（1）内蒙古四大沙地植被生长条件及蓄水成分的空间变化

2003—2016 年，四大沙地的植被生长总体呈增长趋势。虽然浑善达克沙地和科尔沁沙地的植被生长在 2010 年之前有所退化，但 2010 年后有所改善。四大沙地的植被生长和土壤水分(SM)均普遍增加，科尔沁沙地的 SM 显著增加（84% anomaly > $1.4×10^{-2}$ cm^3/cm^3）。除呼伦贝尔沙地外，其他沙地陆地水储量（TWS）均呈下降趋势，其中毛乌素沙地下降幅度最大（97% anomaly < -40mm）。
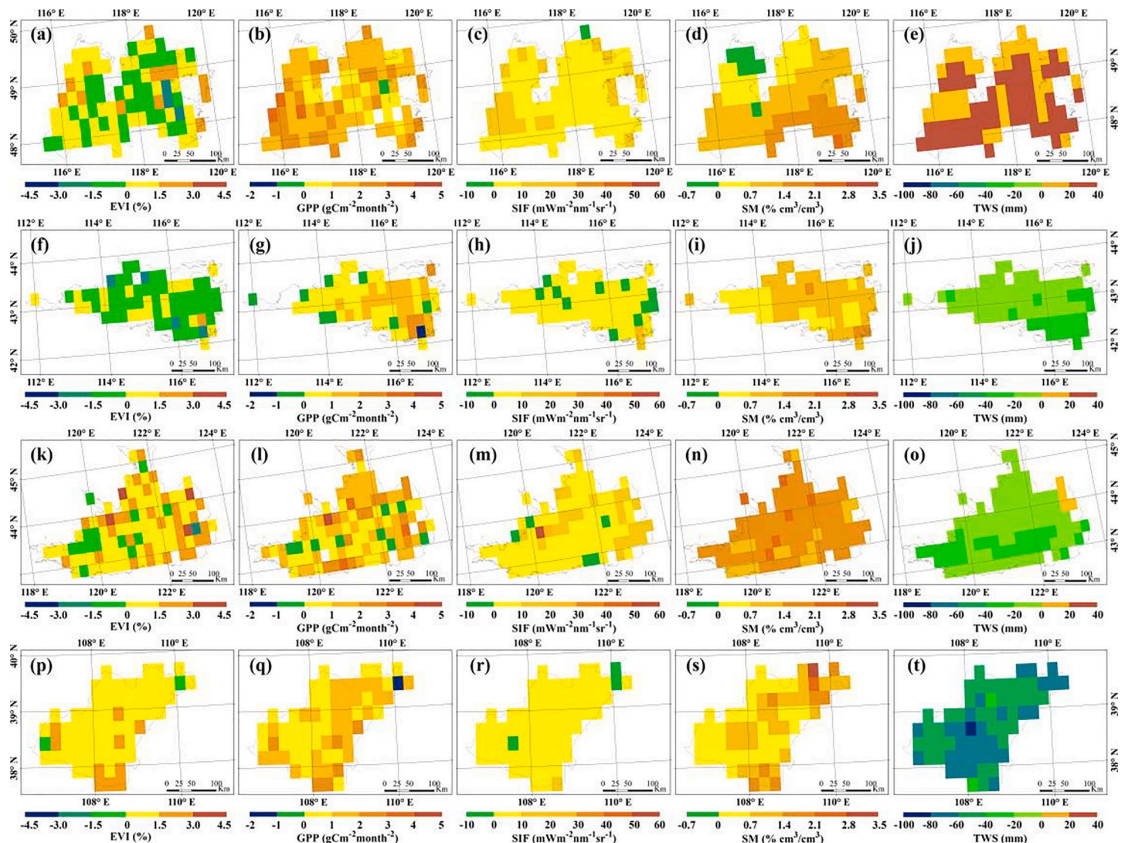

图 2. 四大沙地 EVI、GPP、SIF、SM、TWS 的距平数

（2）内蒙古四大沙地植被-水分相关性

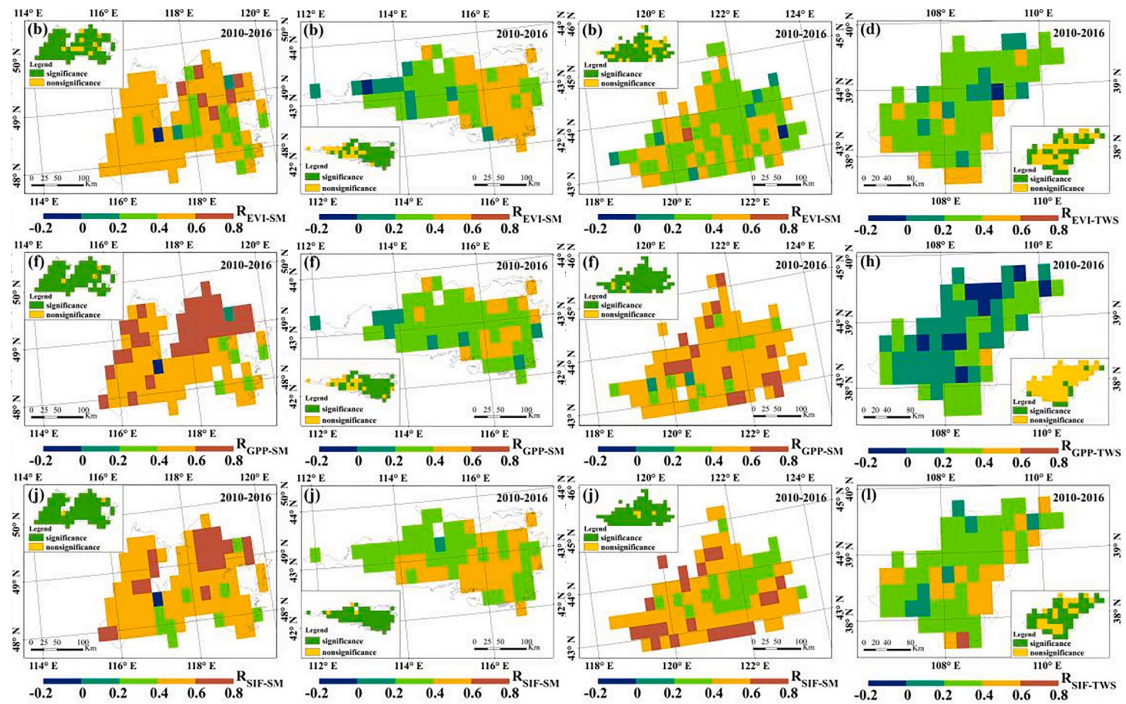与植被指数（EVI）或总初级生产力（GPP）相比，太阳诱导叶绿素荧光（SIF）对沙地降水梯度和植被类型的变化更加敏感。因此，SIF 对于表征沙地植被生产力和捕捉水分变化具有明显的优势。

图 3. 四大沙地植被-水分关系图

（3）2003-2016 年内蒙古四大沙地植被水分动态

植被-水分关系的空间格局遵循年平均降水量的梯度，这表明降水量（或地表 SM）为植被生长提供了有利的自然条件，并与植被生产力呈正相关。同时，由于地下水的不断减少，植被对地下水的依赖逐渐降低。因此，植被生长变化与 SM 和 TWS 具有一定程度的一致性，但植被生长对地表 SM 变化的敏感性强于整体 TWS（$R_{SM} > R_{TWS}$，$p < 0.05$）。
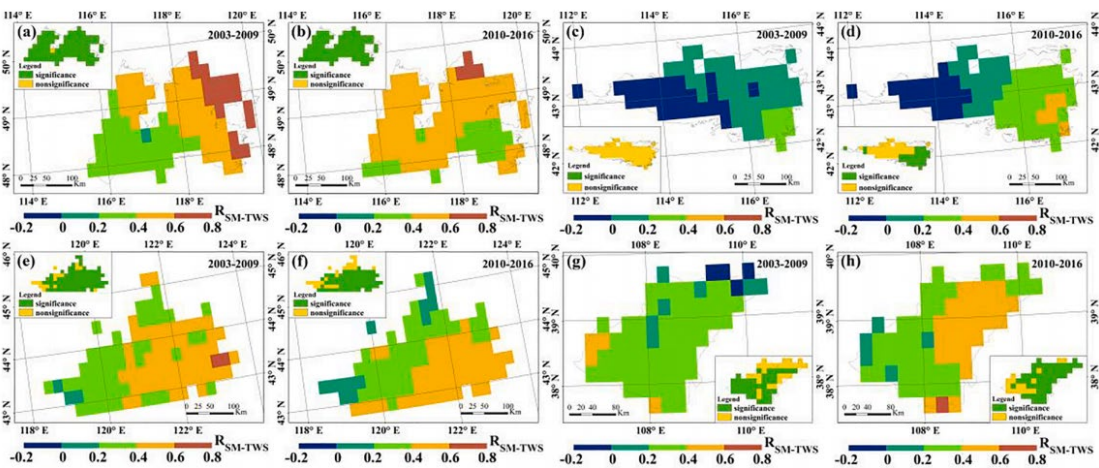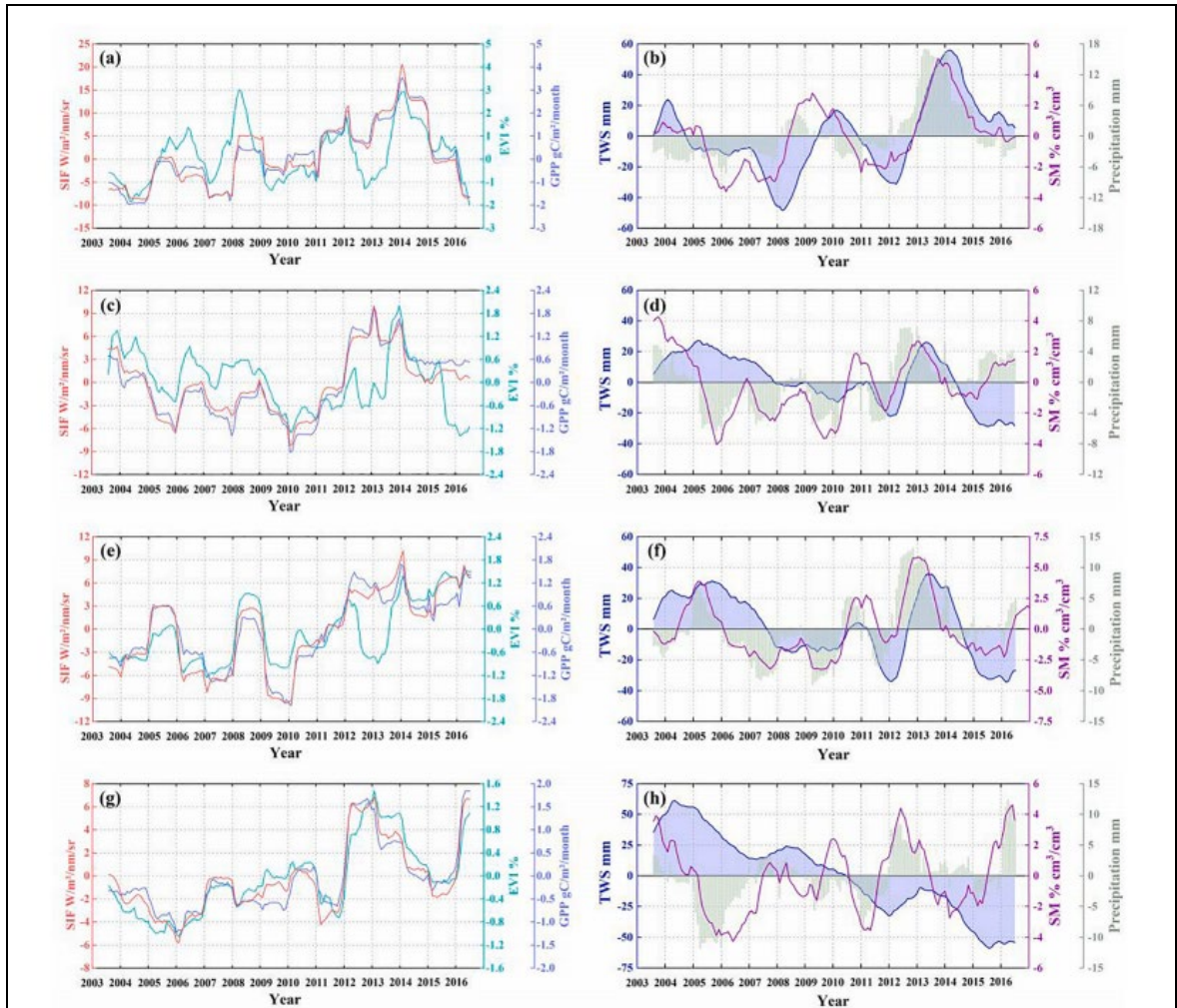

图 4. 四大沙地 SM-TWS 关系图

图 5. 四大沙地植被水分动态

（4）内蒙古四大沙地 SM 和 TWS 的时滞效应及对气候变化的响应

四大沙地中 SM 和 TWS 的持久性或时滞效应普遍存在 1 个月左右的滞后，特别是毛乌素沙地的持久性最长（0.94 个月和 1.1 个月）。前期的持续时间普遍长于后期，这表明沙地植被需要更多或更持久的补水来弥补前期的供水不足。随着内蒙古由旱季转入雨季，水分恢复时间相对缩短，对植被生长的制约也会减弱。因此，后期四沙地植被生长明显恢复。
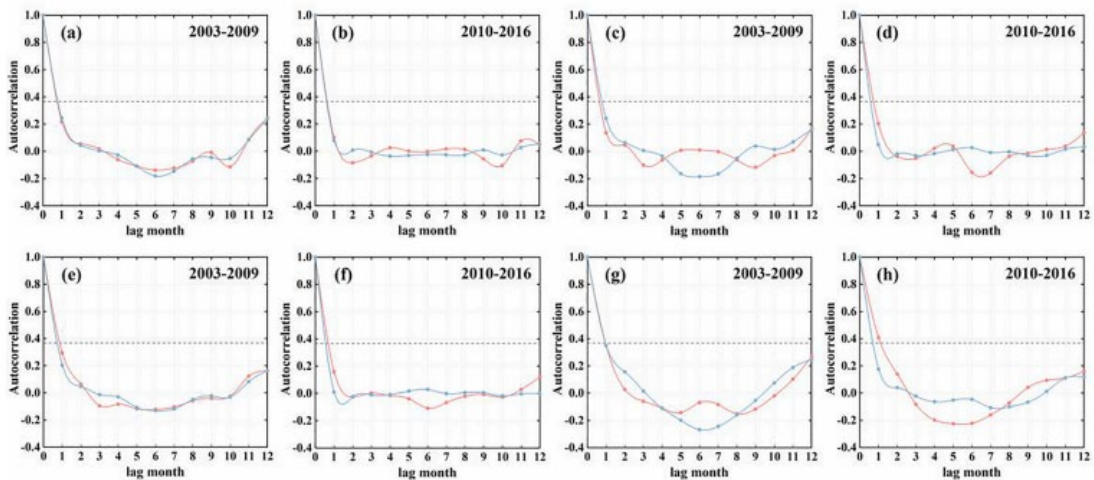

图 6. 四大沙地 SM 和 TWS 的时滞效应

本研究为气候变化背景下的沙地管理和恢复提供科学依据。建议针对内蒙古干旱/半干旱地区四大沙地的具体水分条件，制定不同的植被恢复和保护策略，包括提高水分利用效率、保持土壤湿度和减少地下水的过度使用。

3．与预期计划和目标比较，说明完成情况及存在问题（是否按照原计划进行、哪些内容进行了必要调整和改动）：

已根据申请题目发表一篇 SCI 论文，提前完成了预期计划，并无调整或改动原计划的情况。

三、项目成果一览表

序号	作　者	出版或发表题目	成果形式	出版或发表单位及时间
1	Xinyi Liu, Quan Lai, Shan Yin, Yuhai Bao, Song Qing, Li Mei, Lingxin Bu（刘心怡，来全，银山，包玉海等）	Exploring sandy vegetation sensitivities to water storage in China's arid and semi-arid regions（探讨内蒙古干旱半干旱地区沙地植被对蓄水条件的敏感性）	SCI 论文	Ecological Indicators，2022 年 2 月 20 日

四、审核意见

导师审核意见：

研究成果符合基金预期目标，同意结题。

导师（签章）：银山　　2023 年 8 月 28 日

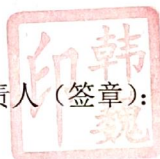学院学术分委员会审核意见：

同意结题

负责人（签章）：　　（单位公章）

2023 年 9 月 28 日

研究生院核准意见：

负责人（签章）：　　（单位公章）

　　年　　月　　日

注：本表一式二份，一份留研究生处备案，一份由主持人留存。

结 题 证 明

项目类别：内蒙古师范大学研究生科研创新基金项目

项目名称：基于叶绿素荧光遥感的内蒙古植被生长对气候变化的响应

项目编号：CXJJB21020

负责人：刘心怡

参与人：美丽、元志辉、叶志刚、卜灵心、塔娜

特此证明

内蒙古师范大学研究生院

2023 年 月 6 日